SYNTHESIS AND CHARACTERISATION OF PHOSPHORESCENT COPPER (I) COMPLEXES FOR LIGHT EMITTING DEVICES

A thesis submitted for the degree of

Doctor of Philosophy

by

María Inmaculada Andrés-Tomé

Wolfson Centre for Material Processing

Brunel University

June 2013

Abstract

Over the last decade, many significant developments have been made to improve the active materials in a new generation of organic light emitting devices (OLEDs). Current OLED technology is focused on organo-transition metal complexes, which emit from the triplet excited state and exhibit bright phosphorescence. Efficient in devices have been reported using these luminescent materials, such as iridium and platinum complexes, however, rare metal abundance concerns, high price and toxicology have inspired the study of alternative phosphorescent materials, such as copper or silver complexes.

In this research, novel copper complexes have been synthesized, such as trinuclear and mononuclear copper (I) complexes, using a range of ligands, such as alkynyl, phosphine alkynyl and pyridine ligands. The synthesised complexes have been characterised by with a range of techniques, such as UV/Vis absorption and emission spectroscopy, nuclear magnetic resonance (NMR), thermogravimetric analysis (TGA), differential scanning calorimetry (DSC), cyclic voltammetry (CV) and scanning electron microscopy (SEM).

Most of the copper complexes have shown very interesting luminescent properties in solution and solid state and some of them were studied for future application in a device.

Agradecimientos

En primer lugar me gustaría dar las gracias a mis supervisores de doctorado, Dr. Paolo Coppo y Prof. P. Kathirgamanathan por haberme dado la oportunidad de trabajar on llos en este proyecto,por todos sus conocimientos y ayuda. También quisiera dar mi más sentido agradecimiento a Researcg Council de Reino Unido por la financiación de mi proyecto y a la coordinadora de Wolfson Centre Dr. Fiona Cotterill.

Durante estos más de tres años de investigación he recibido el apoyo y la ayuda desinteresada de muchísimos científicos, entre los que se encuentran mienbros de diferentes universidades, compañías, etc. Por todo ello quisiera agradecer a Dr. Peter Meadows, Dr. Naoyuki Fuji y Dr. Hiroaki Sasakawa de JEOL por sus analisis de RMN, Prof. Andy P. Monkman, Dr. Fernando Baiao Dias y Khalid Abdullah del Departamento de Ciencias Físicas de la Universidad de Durham por su ayuda incondicional en mis análisis de días intesos en Durham, Dr. Giuliano Jacobellis, Dr. Gianluca Farinola de la Universidad de Bari y NMSS de Swansea, por sus análisis de RMN de Masas. Siempre habrá dos personas muy especiales que nunca olvidaré por toda su ayuda, conociminetos cintíficos e impagable experiencia, Prof. Chris Winscom y John Fyson, sin estos dos grandiosos científicos esta investigación no hubiera sido possible.

Al igual que todo el conocimento y ayuda científica, yo no hubiera podido terminar esta investigación sin la maravillosa ayuda de Dr. Diego Lanzarot Zúñiga, desde pasar tardes ayudandome con a bioquímica de tercero de carrera, ayudarme con mi ingles de principiante, hasta terminar leyendo mi tesis doctoral y lo que siempre es más importante para mí, tu consejo. Quisiera destacar la gran ayuda desde Graduate School, especialmente Dr. Tina Ramkalawan, Dr. Senthila Quirke y la que fue mi jefa y ahora es mi gran amiga Mrs. Charlotte Zittel.

Durante todos estos años de soñar con la química, investigación y finalmente con un doctorado he conocido a muchísima gente de differentes nacionalidades. Mis amigas de España, con las que siempre he contado Rebeca (gracias por esas intensas conversaciones telefónicas y tu apoyo), Laura y Lara (mis dos ELES y las mejores "compis" de Universidad). A mi gran grupo de chicos de Wolfson Alex, Xiao

y Myles, nunca me lo podría haber pasado mejor en el despacho, gracias por vuestro apoyo y ayuda cuando rompía el ordenador.

Quisiera especialmente dar las gracias a Nishan, quien me ha ayudado desde el principio de mi aventura inglesa, quien me enseñó el divertido mundo de los OLEDs y quien siempre me ayudado en los buenos y tantísimos malos momentos. Gracias por aguantar.

Y finalmente, quisiera agradecer a las personas más importantes de mi vida, nada de lo que tengo lo hubiera conseguido sin vosotros, mi familia, mi gran familia. Mis hermanas, Ana por sus collejas ya que hora podemos ver los resultados y por recordarme que yo pudo hacer lo que me propogan, Marise,por enseñarme que las ciencias no es cosa de hombres. A mis tias Manoli e Ino, o major dicho a mis "titas" Moli y Fefa, gracias por haber sido mas que unas titas. A mi abuela, y también mejor dicho a mi Yaya, todo lo que soy empezó contigo y nunca se irá. Y por supuesto a mis padres, José e Isi, gracias por enseñarme lo más importante. Nunca podré expresar por escrito a mi familia lo agradecida que estoy a todos ellos. Gracias por escucharme siempre.

A todos vosotros gracias por creer en mi.

Acknowledgements

I would like to thank all my friends, from Spain especially Rebeca, Laura and Lara; from England and other parts of the world, Olivier and my group of friends from Wolfson Centre. I want to say the biggest thanks to Nishan, who showed me the fantastic world of devices and who has supported me from the beginning of my life in the UK.

And finally, thanks to the most important people in my life, all of this could not be possible without the support and help from my family, my sisters Ana and Marise, my aunties Manoli and Ino, my Yaya and my parents Isi and Jose. I will never be able to express by writing how thankful I am. Thanks for always listening to me.

Thanks for believing in me!

Table of Contents

List of Figures

List of Graphs

Tables

Chapter 1: Introduction to emitting materials for OLEDs

Esta tesis está dedicada a mis sobrinos, Miguel, Diego, Manuel y mi sobrina María. Esta tesis es un ejemplo que si quieres algo de verdad, lo puedes conseguir.

1.1. Next generation of light emitting devices

Since the 1970s there has been scientific curiosity about organic electroluminescencent devices [1]. During the last two decades, organic light emitting diodes (OLEDs) have attracted considerable interest [2]. In 1987, Tang and Van Slyke, from Kodak, first reported efficient high-performance OLEDs [3, 4]. This new technology is based on the use of organic fluorescent dyes as emitters, which can provide an array of different colour [5, 6]. In the 1990s OLEDs based on phosphorescent transition metal complexes were proposed as a more efficient way to harvest light from electrically generated excited states [7, 8]. Research in these particular type of emitters has grown exponentially over the past decade.

The growth of OLED technology has been doomed by scepticism whether OLEDs could progress into commercial products, as organic material are known to be unstable to oxygen and unstable undo operational conditions [9]. In addition, the manufacturability of these devices, which require the deposition of many different layers of materials was in question. However, significant progresses in OLED technology has been achieved since the 1990s in device fabrication and encapsulation, which can eliminate water and oxygen from the device, extending the operational lifetime by many orders of magnitude and making the technology competitive with liquid crystal displays and inorganic LEDs [10, 11].

OLEDs received significant attention due to their promising applications in low voltage flat-panel displays [12] to replace existing liquid crystal displays technology (LCD) [2]. OLEDs are also promising candidates for interior lighting. The conversion of the electricity into light is now competitive with fluorescent bulbs and tubes and inorganic light emitting diodes (LEDs) (efficacy 100 lmW^{-1}) [13].For lighting purposes, LED technology is limited by the geometry of the device which dictates the use of diffusers to usefull redirect the light. OLEDs are flat devices, which offers a significant advantage for lighting applications, with an active emissive layer of 100-200nm [8] and a total thickness of only a few millimetres.

When compared with existing LCD technology, OLEDs offer a better viewing angle, a more vivid colour contrast and improved power consumption, as there is no need for a back light, as each individual pixel can be switched on and off.

Mechanically, OLEDs can be made significantly lighter than existing displays and if printed on plastic, they also offer a limited degree of flexibility. [14, 15].

1.1.1. Structure of OLEDs

A basic structure of organic light emitting diodes (OLEDs) consists of multi semiconducting organic layers which are either solution-processed or vacuum-deposited (Figure 1). The first layer above the glass substrate is a transparent conducting anode, typically indium tin oxide (ITO). The layer deposited on the anode is a hole transporting layer (HTL). Similarly, the organic layer in contact with the cathode is the optimized electron transporting layer (ETL).
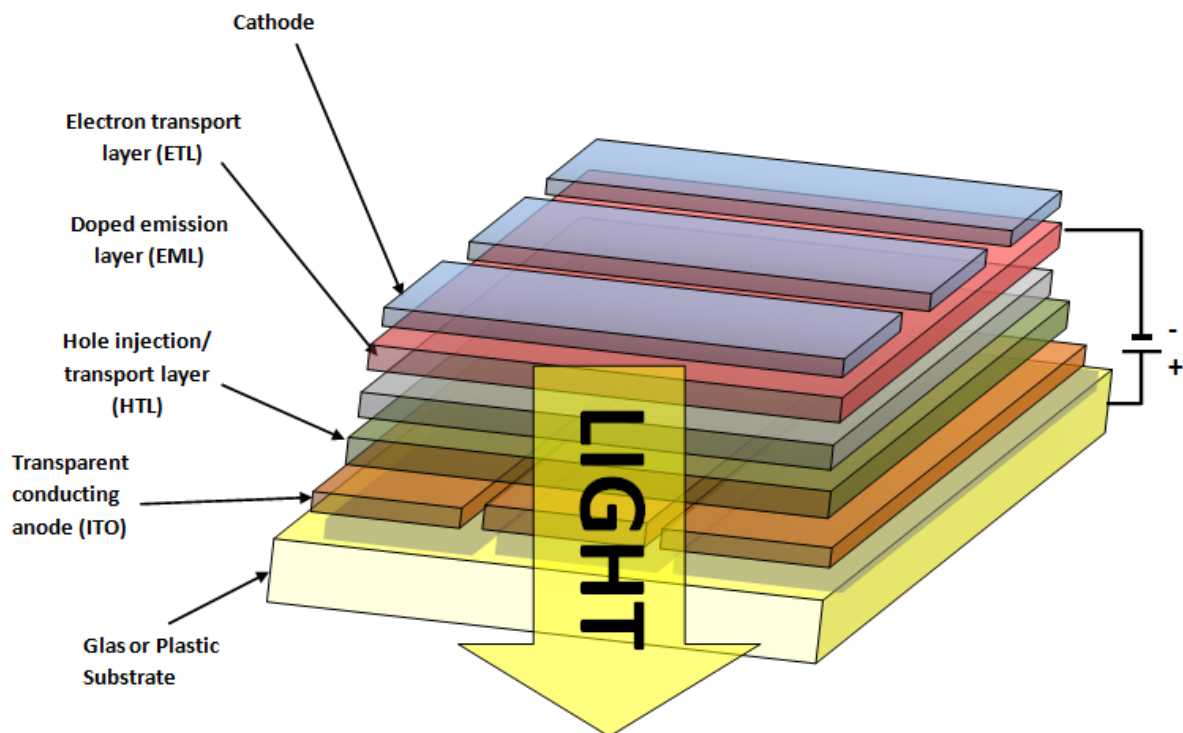
Figure 1. *Basic structure of an OLED [16].*

During operation, a voltage is applied across the device such that the anode is positive with respect to the cathode. Electrons migrate through the semiconducting layer, towards the anode and holes migrate towards the cathode. As holes and electrons meet in the emitting layer, the electron, travelling in the conduction band, decays by emission of a photon of light.

The number and type of layers depend upon the chosen materials and fabrication methodology. In general, an optimised multilayer structure increases the performance of the device by lowering the barrier for the hole injection from the

anode and by allowing control over the electron-hole recombination region (Figure 2) [17].
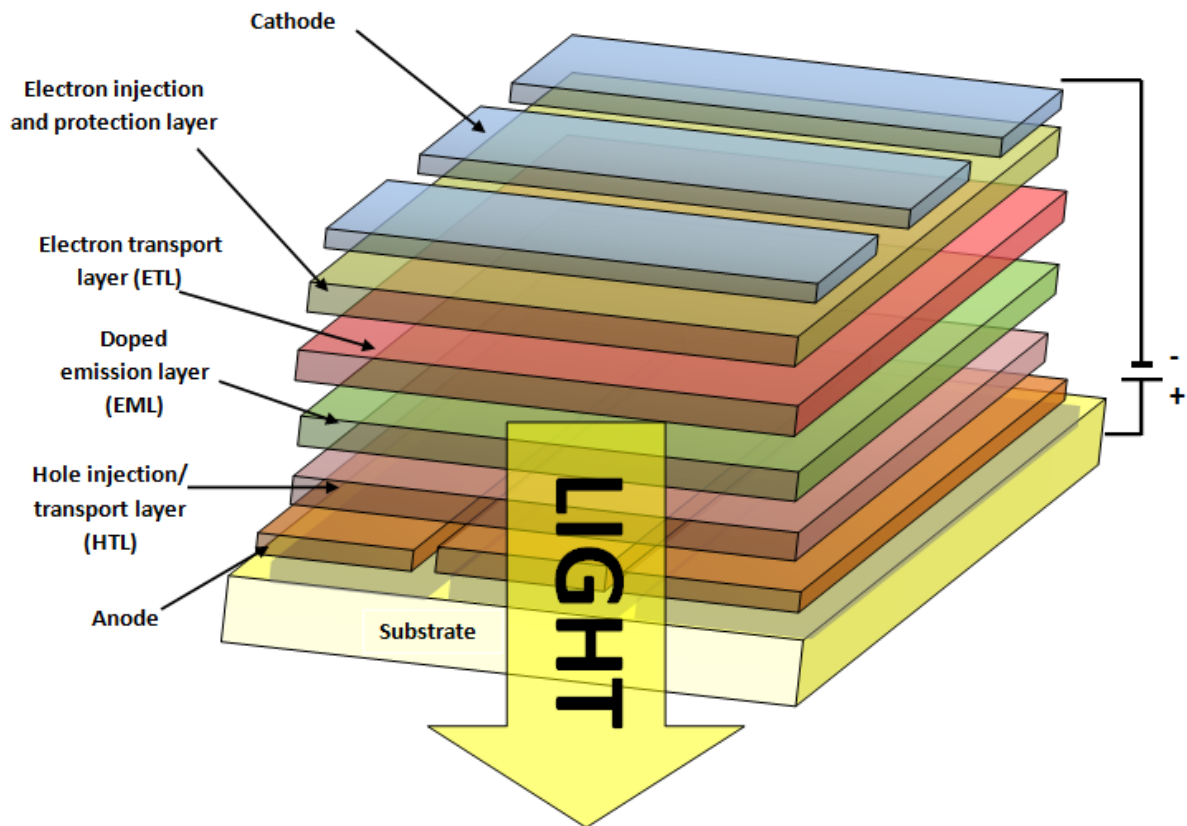
Figure 2. *Multilayer structure of an OLED [17].*

The multilayer structure is shown in Figure 2, with a new layer, which is the doped emission layer (EML). This layer is the basic principle of an OLED as it possess the doped organic material which with the necessary energy provided by the recombination of the holes and electrons, emit light. This new layer, provide the most important property to OLED since it can be processed in many more ways than LED.

1.1.1.1. Anode

The anode material, in general, requires the following properties [18]:

   i.   Highly conductive so as to reduce contact resistance.

  ii.   High work function (WF > 4.1 eV) to promote efficient hole injection.

 iii.   Good film forming and wetting properties of applied organic materials so as to guarantee good contact with the adjacent organic layers.

 iv.   Good stability, both thermal and chemical.

v. Transparent, or highly reflective material.

The structure of OLEDs, which is displayed in the figure 2, shows clearly that the light must go through the layers and escape from the device, this is typically achieved by using an anode made of indium-tin-oxide (ITO). ITO is a stable anode for devices on rigid supports, possesses high optical transmission, low sheet resistance, high work function, excellent adhesion to the substrates, chemical stability and good surface morphology [15].

In addition, the anode must be capable of reducing the ambient light reflection from the reflective cathode to intensify the contrast of the device [18]. The anode may also be made using a stack of layers with graded refractive indexes to minimize the total reflection of the ambient light from the conventional OLEDs. The thickness and the refractive index of ITO can be varied with a desired gradient to form an optically absorbing and electronically conducting anode for high contrast OLEDs by developed lithographic techniques for device fabrication.

There are other transparent and conductive electrode materials, such as fluorine doped tin oxide (FTO) [19], aluminium doped zinc oxide (AZO) [20], indium doped zinc oxide, magnesium indium oxide, nickel tungsten oxide or other transparent conductive oxide materials.

Polyaniline, or PANI, is one of the most studied conducting polymers of the past 50 years [21]. It is due to its high electrical conductivity, light weight, mechanical flexibility and low cost. All these properties make PANI an attractive alternative to the use of ceramic oxides. Some of its applications are as a hole injection layer, transparent conductor, an ITO replacement and as chemical vapours and solution based sensor.

Platinum has a high work function (5.6 eV) and it contributes to increase hole injection. However, as the anode must be very thin and transparent, it would be deposited on the conventional ITO. Malliaras and co-workers have shown that a thin layer (≤ 10 Å or ≤ 1nm) of platinum on ITO increases hole injection by up to a factor of 100 with respect to uncoated ITO [22].

1.1.1.2. Cathode

The cathode material requirements are usually lower than anode materials, as they do not need transparency, combined with electrical conductivity. In some case, the cathode is transparent when a completely transparent OLED is needed. The requisites for cathode materials are the following [18]:

1. High conductivity.
2. Low work function to promote electron injection.
3. Good film-forming and wetting properties to guarantee good contact with adjacent organic layers.
4. Good stability.
5. Highly reflective or transparent if used in top-emitting OLEDs.

Usually, cathode materials are pure metals or metal alloys. Sometimes, ITO could be used as the cathode with suitable modifications.

Magnesium (Mg), calcium (Ca), barium (Ba) or aluminium (Al) are used as cathode because they possess a low work function. This character promotes the electron injection into the lowest unoccupied molecular orbital (LUMO) level of the ETL material. However, this characteristic implies high chemical reactivity. The reactivity between the cathode metals and the external environment happens frequently, requiring encapsulation of the device.

1.1.1.3. Hole transport layer (HTL)

The main function of the hole transport layer is to provide the positive charge carrier holes a pathway to migrate from the anode into the electron transport layer. It is common within small-molecule-based OLED devices, however it is less common in polymer-based devices as conjugated polymers are good conductors themselves [18].

The materials for HTL are easy to oxidise and moderately stable in the one-electron oxidised (radical-cation) form. The materials possess low energy HOMO and LUMO. These properties lead into the following chemical classes of materials for HTL: triarylamine, triphenylmethanes and phenylazomethines.

Triarylamines are the most common material for HTL as they possess a good electrochemical and thermal stability, adequate hole mobility and can be prepared in

high purity. Two of the most used are N,N'-(3-methylphenyl)-1,1'-biphenyl-4,4'-diamine (TPD) and 4,4'-bis[N-(1-naphthyl-1)-N-phenyl-amino]-biphenyl (α-NPD). These materials possess high hole drift mobilities. In theory, it is believed that a good hole transition layer material should have a low energy barrier from the anode to HTL and a relatively high glass transition temperature (T_g).

The triphenylmethanes were first developed for photoconductor applications [23]. They show one of the highest hole mobility known for amorphous organic material, in the range of 10^{-3} to 10^{-4} cm^2/Vs [24].

A series of diphenylamine-substituted phenylazomethine dendrimers were synthesised by Yamamoto and co-workers [25, 26]. These materials show high thermal stability. When a metal ion-complex and this kind of material were used in a device, the luminescence and electroluminescence efficiency were increased. They are promising materials for highly efficienty OLEDs [27, 28].

1.1.1.4. Electron transport layer (ETL)

The electron transport materials help to move electrons from the cathode into the organic layers of the device, via hopping mechanism, including transitory production of anion radicals in the molecules involved [18].

The requirement for a good electron transport material are following:
1. High electron affinity (EA), < 3.2 eV. This value need to suit the work function of the cathode and reduce the energy barrier difference between the cathode and the emitter.
2. Good electron transport mobility (μ_e > 10^{-5} cm^2/Vs). This property will help to transport electrons to the emitter layer and efficiently enclose the exciton in the emission layer.
3. High thermal stability (T_g>120 ^{o}C).
4. Stable electrochemistry and electric field stability. In other words, it needs to have a reversible one-electron reduction.
5. Suit the optical band gap of the emitters. In order to increase the efficiency, the materials should be transparent in the visible region.
6. The materials should be processable and compatible with neighbouring materials to get uniform films.

1.1.2. Device fabrication

One of the most important aspect in the manufacture of OLEDs is the total thickness of the layers. The organic layer is in general limited to 80 to 100 nm (800 Å to 10^3 Å) to obtain efficient charge transport at suitable driving voltages [29]. As a consequence, light is generated very close to the metallic cathode and the proximity of the metal electrode causes severe optical absorption losses. In order to minimise these quenching image force losses, a possible strategy is to increase the thickness of the organic layers.

Before the deposition of the organic layers, HTL or ETL, an insulating layer of 100nm SiO_2 is deposited by sputtering (Figure 3). The analysis of the device performance was qualitatively confirmed by numerical simulations [29].
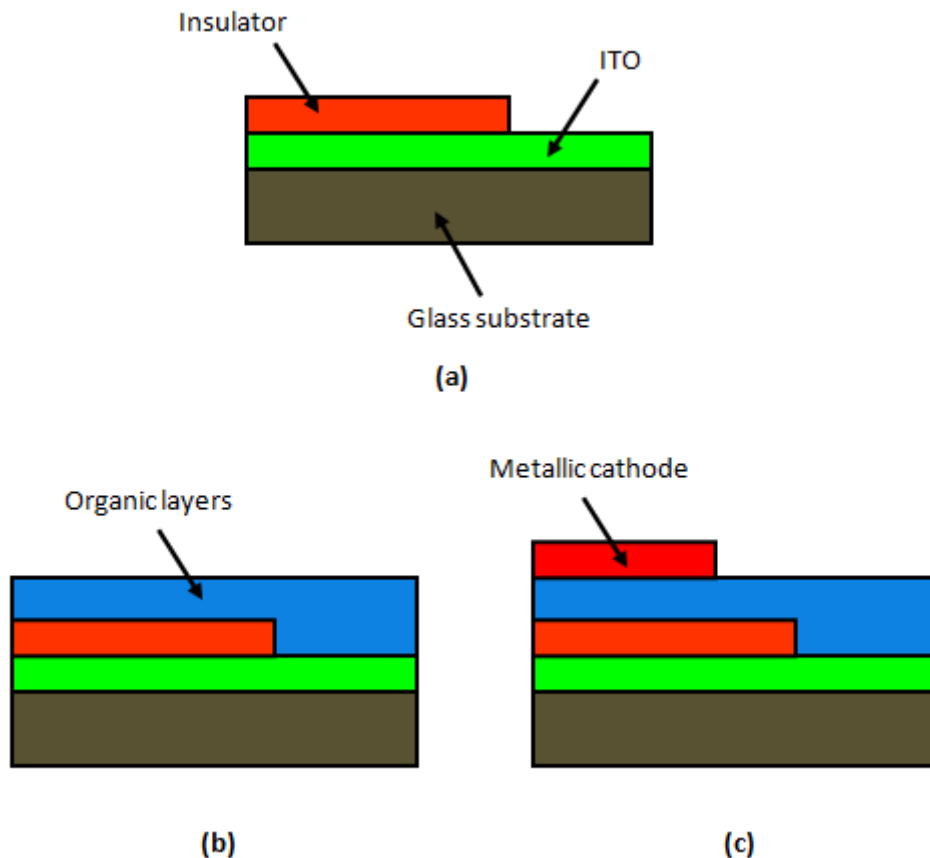
Figure 3. *Schematic description of the processing sequence for the fabrication of the light-emitting field-effect device structure: (a) situation before the deposition of the organic layers with the insulator; (b) deposition of the organic layers; (c) deposition of the metal cathode [29].*

Over the last 20 years there have been significant improvements in the manufacturing of organic light emitting diodes. There are different methods, such as vapour-deposition and solution processing of polymeric materials and inks. Some of these improvements in device performance have made commercial display OLEDs viable. These methods are competing with liquid crystal displays (LCDs) in an expanding flat panel display marketplace [18]. Moreover, some researchers are exploring the use of vapour-deposited organic materials in devices such as photovoltaics [30], organic lasers [31] and organic thin-film transistors (TFTs) [32].

1.2.   Organic light-emitting diode operating mechanism

In the light generating mechanism, holes are injected from the anode and electrons from the cathode into the organic layers (Figure 4). There is a barrier for both holes (h^+) and electrons (e^-) for both holes penetration in the HTL and electron penetration of the ETL [16].
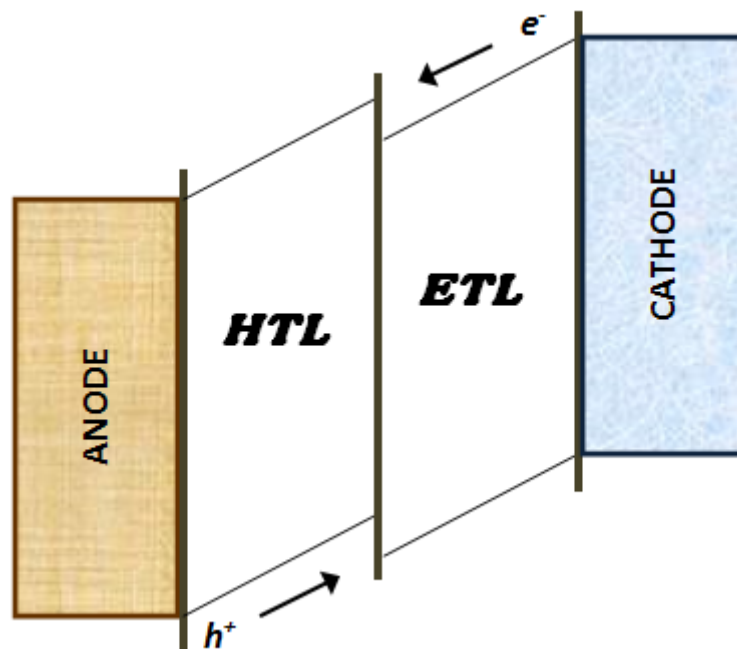
Figure 4. *Basic operation of an OLED [16].*

With a suitable suitable energy barrier between the electron and the hole injection layers (EILs and HILs) and the cathode and the anode, electrons and holes are injected in the ETL and HTL.

Once the electrons and holes have been injected, they move through the ETL and HTL and into the doped emission layer (EML), where the charges meet and recombine. The electron migrate with an external potential, ΔV, through the host material towards the anode. Normally, this process requires thermal activation energy not to be quenched, due to inhomogeneities and to host reorganisation effects related to the polaronic properties of the electrons.

1.2.1. Charge transport in organic materials

Charge transport in organic semiconductors is similar to inorganic semiconductors, it exists via drift and diffusion. However, transport in organic material is much more complicated due to their complex molecular nature. The charge transport is impeded due to polarisation effects, the larger intermolecular distances and smaller intermolecular orbital overlaps compared with inorganic semiconductors. There are numerous theories which describe charge transport in organic semiconductor materials, but none of them can explain all experimental studies [33, 34].

1.2.2. Band transport model

Band transport occurs in delocalised states and is limited by scattering of lattice vibrations. However, the lattice vibrations are reduced at low temperature, which suggests that the charge carrier mobility increases with decreasing temperature. Most organic semiconductors are characterised by a high degree of disorder and low electronic coupling; these electronic couplings are Van der Waals and dipole-dipole interactions. The weak electronic coupling between different molecules can be broken, producing localised states. As a result, band transport is generally not the preferred transport mechanism in organic semiconductors, being limited to highly ordered molecular crystals such as naphthalene [35], anthracene [36], rubrene [37] and pentacene [38].

1.2.3. Multiple trapping and release model

The multiple trapping and release model (MTR) describes charge transport in hydrogenated amorphous silicon [39], but sometimes it has been used to explain the transport in disordered organic materials [40]. This model of transport implies that

charge transport occurs through delocalised states. However, this transport is hampered by impurities, defects and grain boundaries, which generate a distribution of traps near the transport band. During the transport, charge carriers can be trapped. These trapped carriers may be thermally liberated to reach the transport band, where they can end up trapped again. The MTR has been used successfully to describe transport in organic semiconductor films [41], where the energy levels below the LUMO or HOMO is to a large extent due to disorder.

1.2.4. Hopping transport model

Charge carriers in disordered organic semiconductor materials move along the lattice via a hopping mechanism, as they possess weak intermolecular coupling. It means that the states for charge carriers in these materials are considered as localised [42, 43]. The transport is thermally activated tunnelling of carriers between localised states.

The mobility of the charge carriers depends on the energy within the density of states distribution and increases if the density of the near neighbouring states is large, or if there are states available at lower energy. As organic disordered semiconductors are influenced by polarisation effects, the movements of the charges can be limited. Charge transport in this kind of materials is described as a series of carrier hopping from one site to the next, followed by polaronic relaxation.

The electron experiences a Coulomb attraction and the charges recombine, an exciton is formed and, depending upon the nature of the emitting material (EMs) and depending on the selection rules, light emission from a singlet (fluorescence) or from a triplet excited (phosphorescence) state results. The process of hole trapping as a first step can occur, if the oxidation potential of the emitter material compares favourably with the HOMO energy of the HTL (Figure 5).
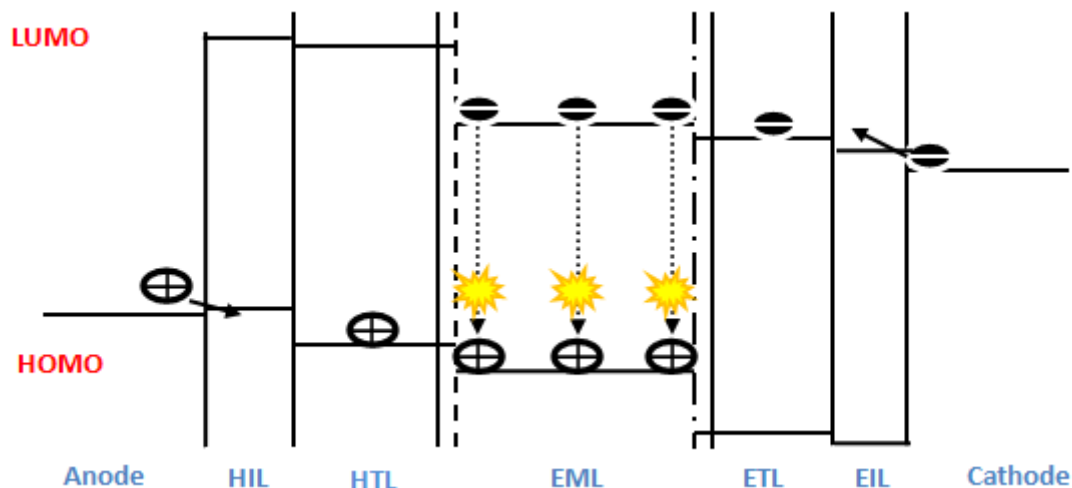
Figure 5. *The light generating mechanism of OLEDs.*

1.3. Light emitting materials

The materials which generate light, are in many cases a mixture of two or more materials. At least, one of them is an electroluminescent emissive material, often combined with a charge transporting host material. In general, the guest-host system is common in the different kind of OLEDs, such as SMOLED, whereas in polymeric LED (PLED) is usually composed of a single conjugated polymer.

Light-emitting materials need to possess many properties and they must be effectively combined. These properties are: the layer must be able to transport charges, both holes and electrons, in order that the charge carriers move through the layer and find each other; the recombination charge must create an excited state in the material and the mixture of materials. If they are used for long –lived devices, must be uniformly dispersed (good film forming properties as a solid solution) and not be affected by material migration under an applied electric field (no electrophoresis).

The chemical and photo-physical properties of the emissive material itself lead to a classification of OLEDs. They are two main types:

1. SMOLEDs: they contain small-molecule emissive materials which could be processed by vacuum deposition techniques or solution coating (spin coating or ink jet printing).
2. PLEDs: they contain polymeric emissive materials, which are almost exclusively processed by solution coating.

23

1.3.1. Luminescence

Luminescence can be classified into two categories: luminescence from electronically excited singlet (S_1) or triplet (T_1) states. Emission from singlet state is called *fluorescence* and emission from triplet state is called *phosphorescence* [44]. This last process is intrinsically spin-forbidden and the timescale is much longer than in fluorescent process, in the order of micro- to milliseconds.

A typical molecule shows different transitions between singlet states, singlet and triplet state or triplet states, all those transitions are shown in the Jablonski diagram (Figure 6).
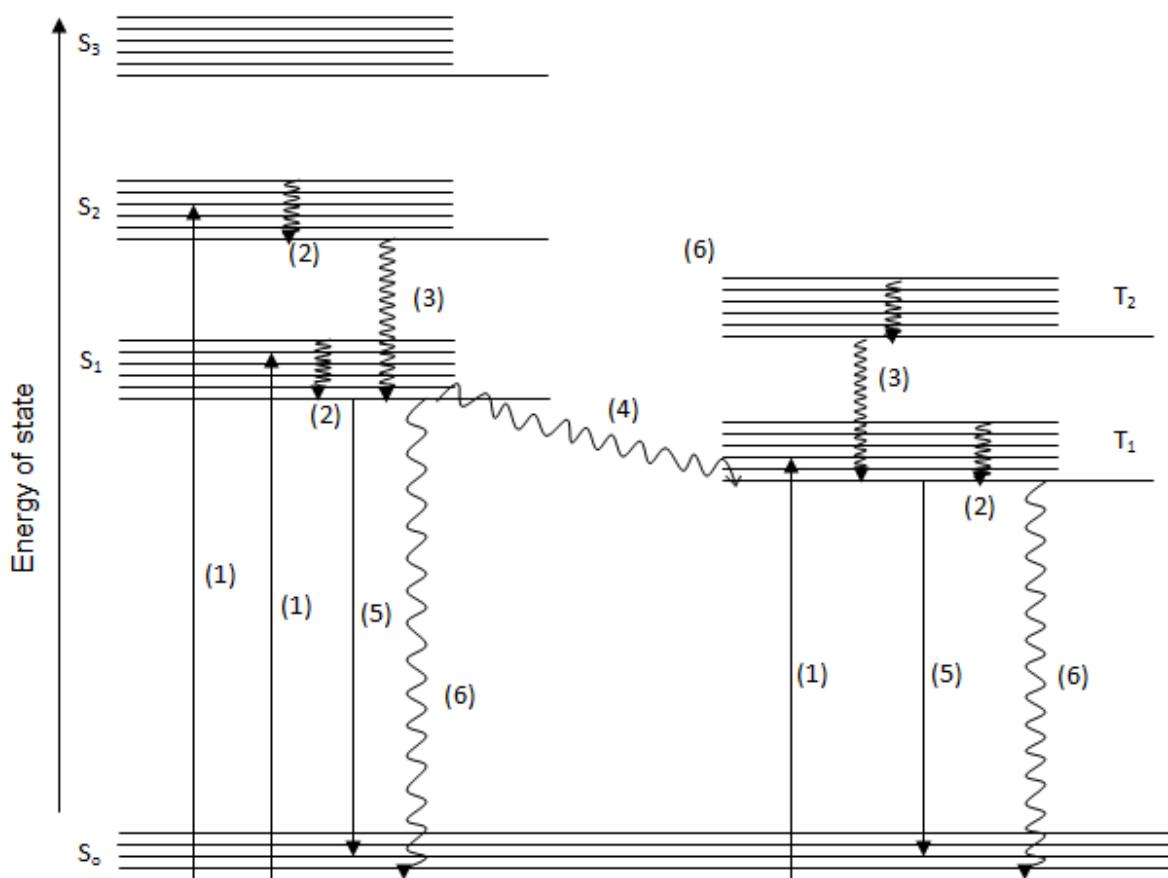
Figure 6. *The Jablonski diagram shows the photophysical processes in a typical molecule A-B. The processes, which are shown in the molecular system, are: (1) light absorption, (2) vibrational relaxation, (3) internal conversion (IC), (4) intersystem crossing (ISC), (5) radiative transition and (6) nonradiative transition [44].*

In the diagram, S_0 represents the ground state energy. The ground state is the non-excited state [45]. S_1 and S_2 are the excited singlet states where the

electrons sit as pairs with opposite spins (+½ or -½) in a single orbital. On the right end of the diagram the triplet states are represented by T_1 and T_2, where the nonbonding electrons may occupy this level in two separate orbitals with the electron spins parallel to each other.

In a molecule, there is a difference of energy, or energy gap, between the highest occupied molecular orbital (HOMO) and the lowest unoccupied molecular orbital (LUMO). If the absorbed energy is larger than the HOMO-LUMO energy gap of a molecule, the transition from the ground state (S_0) to the lowest energy level of S_1 is allowed. The molecule may also experience a change in vibration, rotation and/or go into the higher electronic state (S_2). These processes are labelled (1) in the Figure 3. The time it takes a molecule to experience the transition from the ground state to the excited state is extremely short, in the order of femtoseconds (10^{-15} s).

The relaxation of an electron from the excited state to a lower energy level can be radiative or non radiative (2). An electron in the highest single state S_1, S_2 or S_3, relaxes to the lowest vibrational state of them via non radiative, vibrational relaxation (3). An electron can change spin from a singlet excited state (S_1) to the triplet excited state (T_1) via an intersystem crossing process (ISC) (4), this happens when the triplet state vibrational energy levels overlap with the lowest energy level in S_1. This process is followed by internal conversion to the lowest energy of T_1. Typically ISC is forbidden in most systems.

The other kinds of processes are called radiative processes, which result in the emission of light (5). The emission of light can be produced by the processes of fluorescence and phosphorescence. Fluorescence is the electronic transition from the singlet excited state (S_1) to the singlet ground state (S_0). This process occurs within nanoseconds after the absorption of light which is at shorter wavelength. Organic molecules with conjugated double bonds, such as compounds with aromatic rings, show fluorescent emission because the energy differences between excited state and ground state orbitals are small enough to give photons in the visible part of the electromagnetic spectrum.

In order to obtain an effective guest-host system, between the electroluminescent emissive material and the transporting host material , there are

several factors which must be considered, such as the phase compatibility of the host and guest, the aggregation of the molecules and the host-guest energy level and orbital alignment. Efficient electroluminescent host-guest system have been studied by Thom and co-workers, using computational methods, predicting suitable host carbazole molecules for phosphorescent iridium guest complexes [46]. In this study , the band gap of the guest falls within the band gap of the host to help transport of electrons and holes from the host to the guest, where they recombine (Figure 7). This applies to singlet and triplet excited states of the host and the guest.
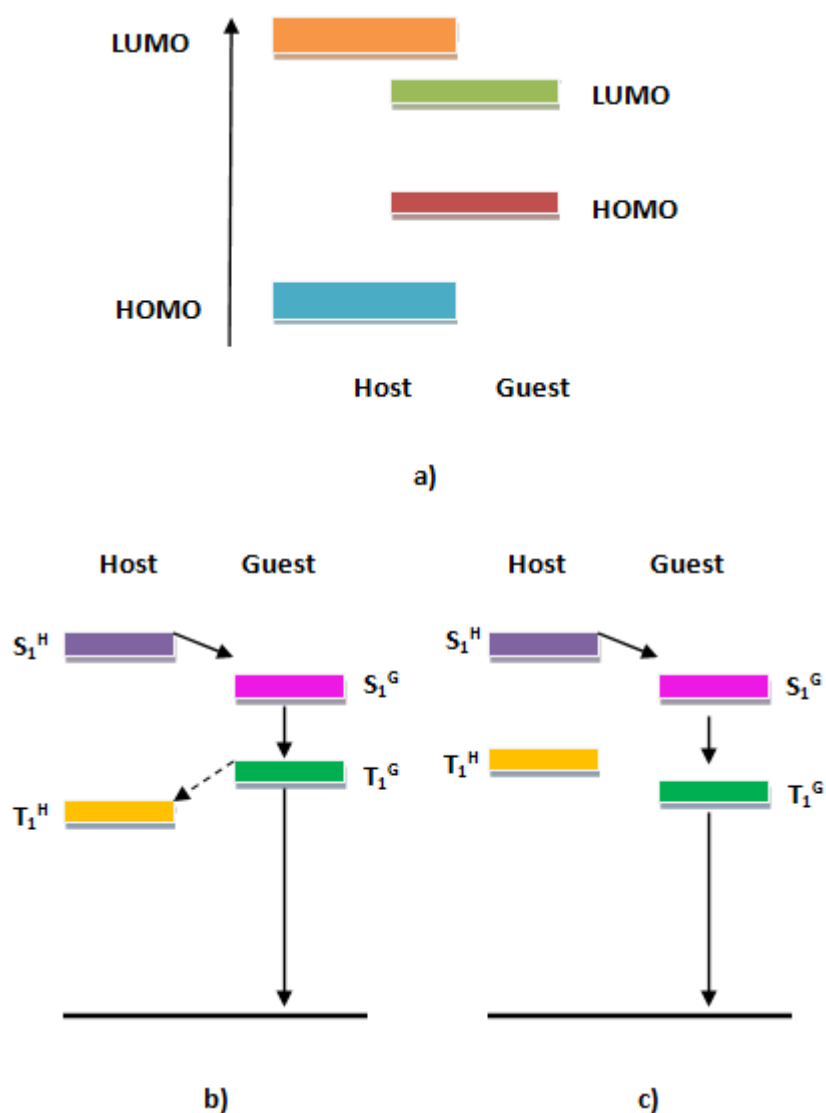
Figure 7. *Energy level relationship in a phosphorescent guest-host system, where: a) relationship between the band gap of the guest and the host; b) poor energy transfer between guest-host system; c) efficient energy transfer between guest-host system. The ground state was taken as zero.*

As we can see in Figure 7, for an efficient energy transfer from the host to the guest in the triplet state, which means there will be phosphorescence, the excited triplet state of the host must be higher than that of the guest.

1.3.1.1. Factors influencing luminescence

One of the requirements for fluorescence and phosphorescence is a molecular structure which absorbs ultraviolet or visible radiation [47]. We can say the stronger the absorption of a molecule, the more intense its luminescence will be. Molecules which contain conjugated double bonds, especially those with a high degree of resonance stability, show efficient luminescence, as they show intense electronic absorption in the ultraviolet to the visible region of the electromagnetic spectrum.

Transition metal complexes can be optically active because of their symmetrical configuration or because they are attached to optically active ligands [48]. Their spectral band shape and transition energy is the consequence of their specific electronic structure [44]. The presence of metal atoms enhances the intersystem crossing, as they show a strong spin orbit coupling. Phosphorescence is therefore allowed in metal complexes.

The nature of the solvent plays an important role in the absorption and emission spectra, as the intermolecular solvent-solute interaction results in molecular geometry variations [49]. However, the interpretation of solvent effects is difficult because its magnitude is small on the spectra and is not easy to calculate precisely [50]. Some of the significant factors, which are worth considering, are the dipole moment, the size of the solute molecules and the difference between the dipole moment in the ground and excited state. The quantum yield of luminescence is higher in dense solutions, as opposed to a liquid because the viscosity of the solution increases and, as a consequence, the probability of the loss of the excitation energy by non radiative decay becomes lower.

The temperature influences the magnitude of luminescence. A rise in temperature increases the frequency of collisions between the molecules and the probability non-radiative decay increases as well. In general, we can say that a temperature increase produces a decrease in luminescence [51].

1.3.2. Optical properties of transition metal complexes

Electronic transitions are frequently considered in metal complex as *d-d* transitions as they involve the molecular orbitals which have mainly metal d character [52]. However, it is necessary to mention that not all electronic transitions, in the visible and ultraviolet spectral region are produced as *d-d* transitions; charge transfer absorption, in which electrons are transferred from ligand to metal or vice versa, can appear in this region too and they are much more intense than *d-d* absorptions [53]. The complexes colours are determined by the magnitude of the spacing between these levels and this spacing depends on factors such as the geometry of the complexes, the nature of the bonding ligands and the oxidation state of the metal ion.

Electron-electron repulsion has been so far ignored. However, this effect will make a significant contribution to the electron energy in any complex which has more than one electron or more than one *d*-level vacancy.

For metal complexes, the electronic configuration follows the same configuration as for organic molecules [54]. By a molecular orbital (MO) diagram of an octahedral transition metal complex, which can be applied to complex of Co (III), Ru (II) and other d^6 metal ions, we will define the different types of electronic transitions. They are shown in Figure 8.
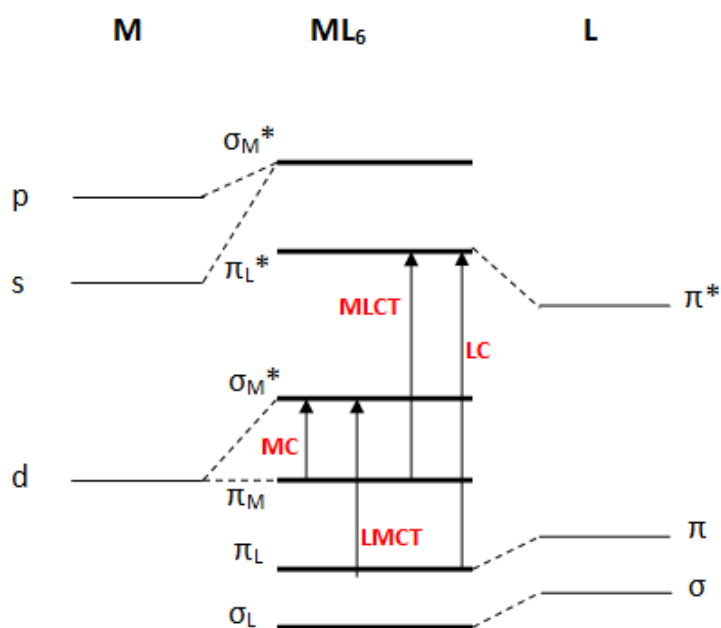
Figure 8. *Molecular orbital (MO) diagram for an octahedral complex of a transition metal.*

For organic molecules, excited configurations can take place from the ground configuration, by promoting one electron from occupied to vacant MOs. There are electronic transitions which can be expected at relatively low energies:

i. *Metal-centered* (MC): transition from nonbonding orbitals (π_M), of t_{2g} symmetry, to antibonding orbitals (σ_M^*), of e_g symmetry.

ii. *Ligand-centered* (LC): transition from bonding orbitals (π_L) to antibonding orbitals (π_L^*).

iii. *Ligand-to-metal charger-transfer* (LMCT): transition from bonding orbitals (π_L) to antibonding orbitals (σ_M^*).

iv. *Metal-to-ligand charge-transfer* (MLCT): transition from nonbonding orbitals (π_M) to antibonding orbitals (π_L^*).

The relative energy of these electronic transitions depends on the nature of the metal and the ligands in predictable ways. In other words, low-energy metal-centered (MC) transitions are expected for transition metals of the first row, low-energy ligand-to-metal charge-transfer (LMCT) transitions are expected for complexes which carry at least one ligand that is easy to oxidise and a metal which is to reduce. Low-energy metal-to-ligand charge-transfer (MLCT) transitions are expected when the complex carries a metal which is easy to oxidise and a ligand easy to reduce and low-energy ligand-centered (LC) transitions are expected for aromatic ligands with extended π and π^* orbitals.

In the following schemes, we will compare the possible electronic transitions in a tetrahedral complex to those of an octahedral complex (Figure 9 and 10).

In any tetrahedral complex, the lowest energy σ-bonding orbitals will be filled and be primarily ligand in character. Next, there are two states of σ-nonbonding molecular orbitals, one ligand-centred and one metal-centred.
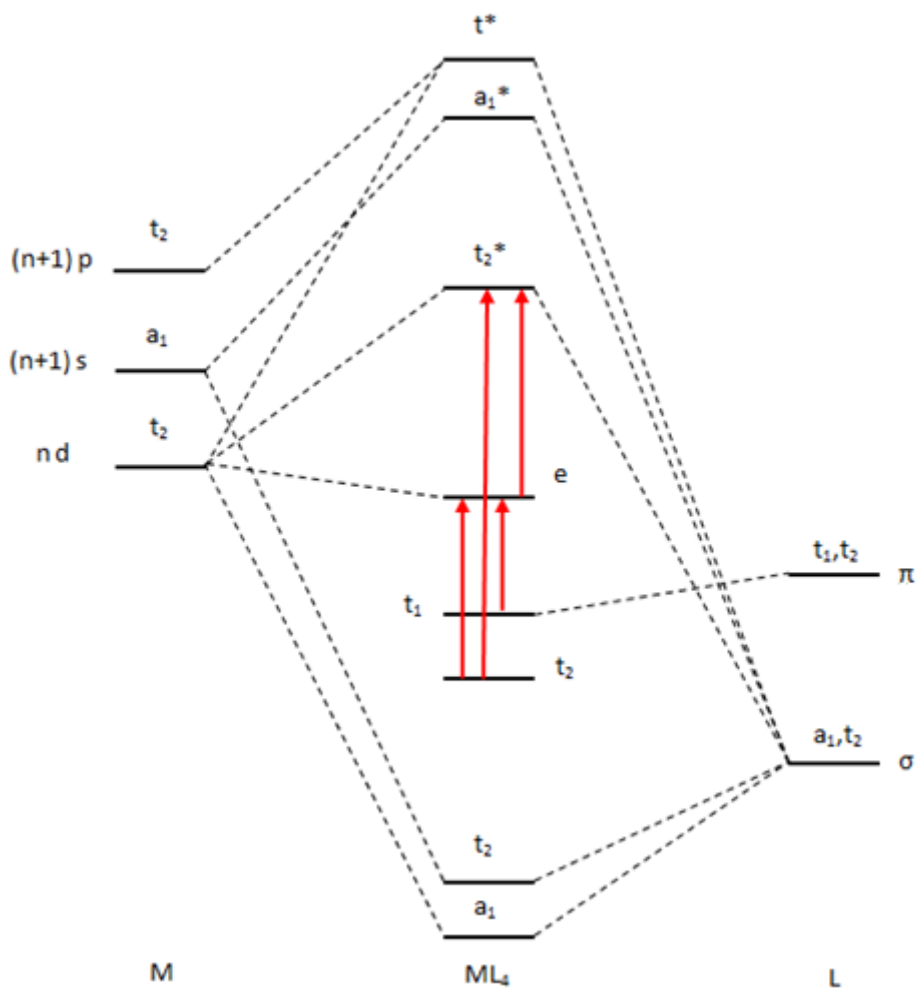
Figure 9. *Molecular orbital diagram for a tetrahedral ML$_4$ complex [52].The possible ligand to metal charge transferences (LMCT) are showing by red arrows.*
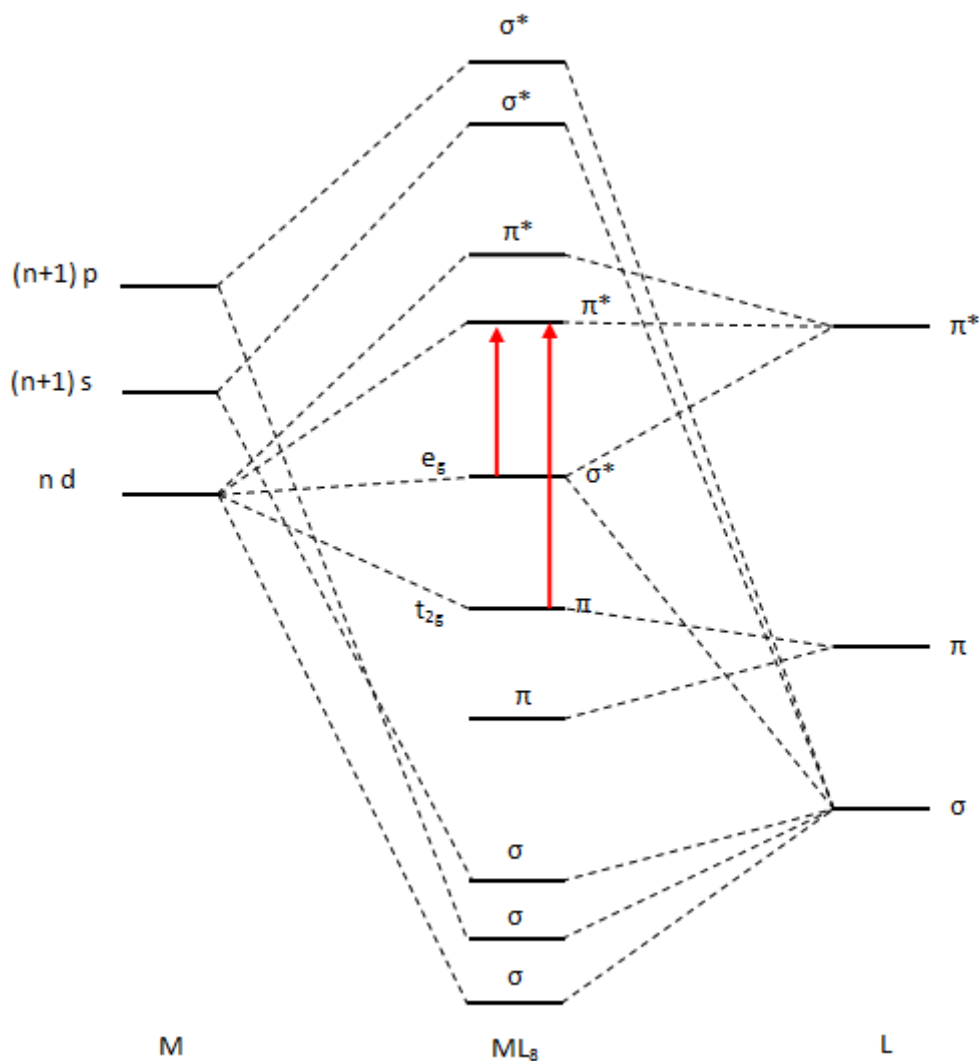
Figure 10. *Molecular orbital diagram for octahedral ML8 complex [52]. The possible metal to ligand charge transferences (MLCT) are shown by red arrows.*

In Figure 10, we can see the MLCT transitions for an octahedral complex, which have occupied the t_{2g} and e_g* orbitals.

1.3.2.1. Ruthenium complexes

Ruthenium complexes and more specifically Ru (II) polypyridine complexes, have been investigated in detail as they have important photochemical properties. Some of their extraordinary properties are high chemical stability, reversible redox activity, phosphorescent emission and long excited state lifetime [55, 56].

Ruthenium (II) is a d^6 system and the polypyridine ligands have σ donor orbital localised on the nitrogen atoms and π donor and π* acceptor orbital more or less delocalised on aromatic rings (Figure 11).
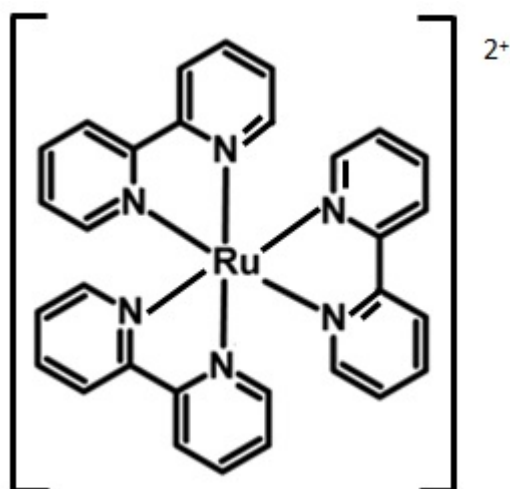
Figure 11. *Molecular structure formula of [Ru(bpy)$_3$]$^{2+}$.*

Ruthenium complexes follow a single-configuration one-electron description of the excited state in octahedral symmetry. In this symmetry, the complexes show the three types of electronic transitions at low energy. As we can see in Figure 12, the promotion of an electron from π_M metal orbital to the π_L* ligand orbitals gives rise to metal-to-ligand charge transfer (MLCT) excited state, in contrast to the promotion of an electron from π_M to σ_M* orbitals, giving rise to metal-centered (MC) excited states. The transition ligand-centered (LC) excited states can be obtained by promoting an electron from π_L to π_L*. We must notice that all these excited states may have singlet or triplet multiplicity.
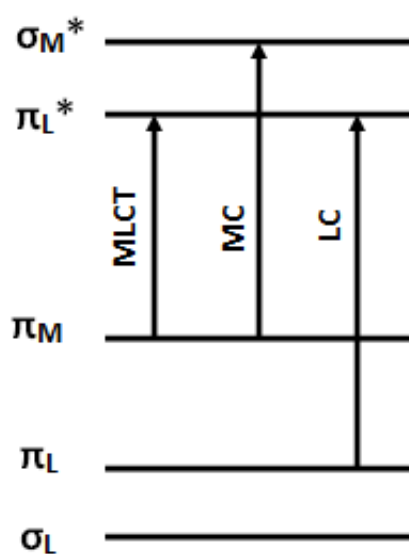
Figure 12. *Molecular orbital diagram for Ru (II) polypyridine complexes in octahedral symmetry.*

For most of Ru (II) polypyridine complexes the lowest excited state is a ^{3}MLCT level and thus exhibits relatively long lifetime and intense luminescent emission.

Several studies have shown the typical absorption bands of $[Ru(Bpy)_3]^{2+}$, in alcohol solution [57]; at 285 nm which is corresponding to a spin-allowed LC $\pi \rightarrow \pi^*$ transitions [58], at 240 and 450 nm corresponding to spin-allowed MLCT d$\rightarrow \pi^*$ transitions (Figure 13).
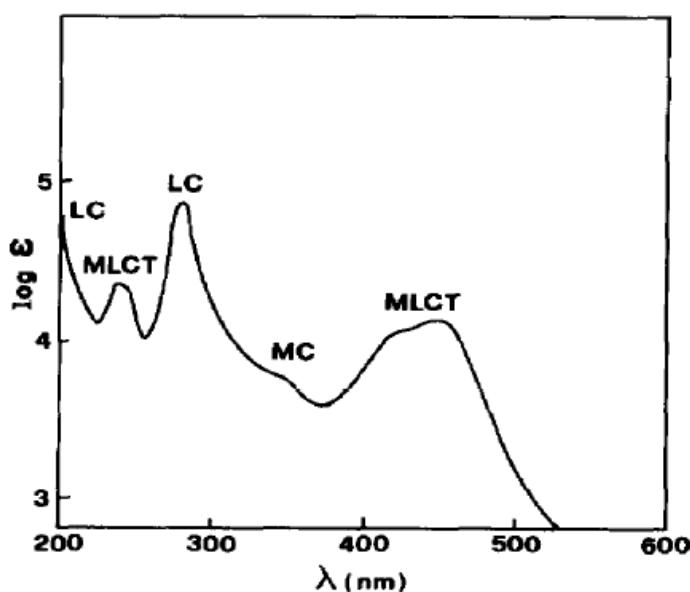
Figure 13. *Absorption spectrum of Ru(bpy)$_3^{2+}$ [57].*

Moreover, the intensity, lifetime and energy are temperature dependent: when the temperature was increased, the emission lifetime and the quantum yield decreased.

1.3.2.2. Osmium complexes.

Many reviews of osmium (II) complexes have been published during the past few years where the aspects of photophysics and photochemistry have been covered [59], especially those of osmium (II) imine complexes.

The photophysical properties of osmium complexes with 2,2'-bipyridine ligands, $[Os(bpy)_3]^{2+}$ have been investigated by Yersin and others in the 1980s [60-63]. Some of the ligands used in Os (II) complexes, are shown in figure 14.

The luminescence of Os (II) complexes is comparable with Ru (II) complexes, in general they have a lower energy than other metal complexes and is due to the

more negative one-electron oxidation potential of the osmium (II) complexes. Their excited state lifetimes are shorter due to the spin-orbit coupling and their energy gap.
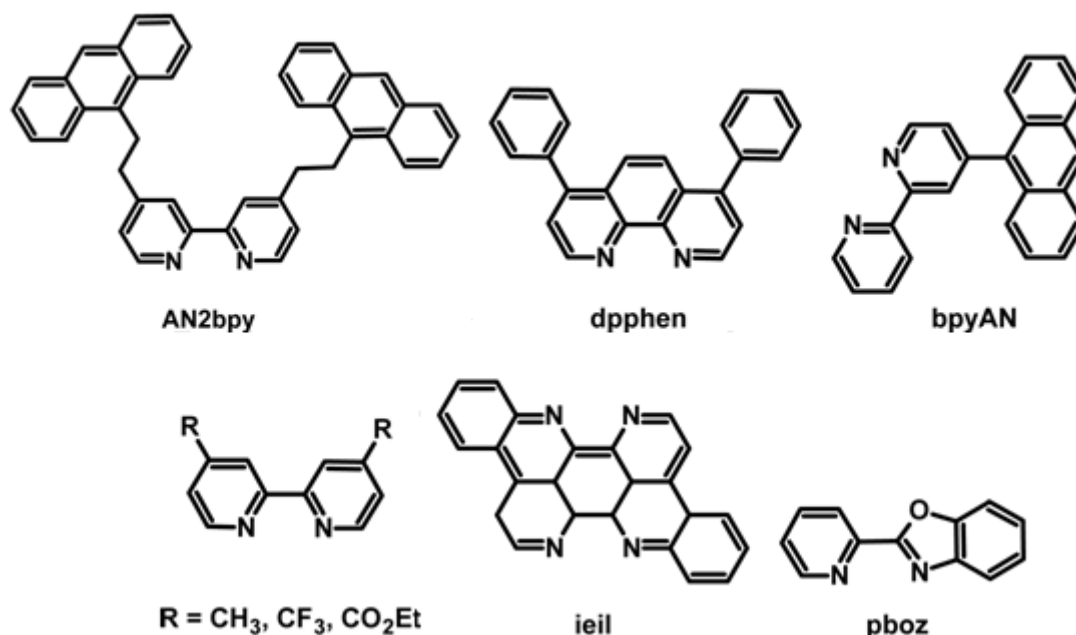
Figure 14. *Structures of some of the ligands used for osmium (II) complexes.*

In general, the absorption of these complexes is in the visible region of the spectrum and the emission has been detected in the near-infrared. For example, the emission of complexes with "ieil" ligands, such as $[Os(ieil)_3]^{2+}$ is centered at 1060nm with very low luminescence quantum yield [61, 64].

1.3.2.3. Rhodium complexes

Rhodium complexes and their properties have been studied. Since the 1970s, there are many reports on different rhodium complexes such as rhodium (III) polypyridine complexes and their cyclometalated analogues. Photophysics and photochemistry are determined by the interaction between ligand-centered (LC) and metal-centred (MC) excited states, with the relative energy depending on the metal coordination environment [65].

The tris (1,10-phenanthroline) rhodium (III) ion, $Rh(phen)_3^{3+}$ (Figure 15) was used to explain the typical photoluminescence behaviour of this class of complexes. The complex did not show emission at room temperature. However, at 77 K (-196.15 ^{o}C) high quantum yield and long lifetime were measured. The emissions at 465, 485,

524 and 571 nm were assigned to ligand-centred (LC) phosphorescence emission from a π-π* triplet state localized on the phenanthroline ligands [66-68].
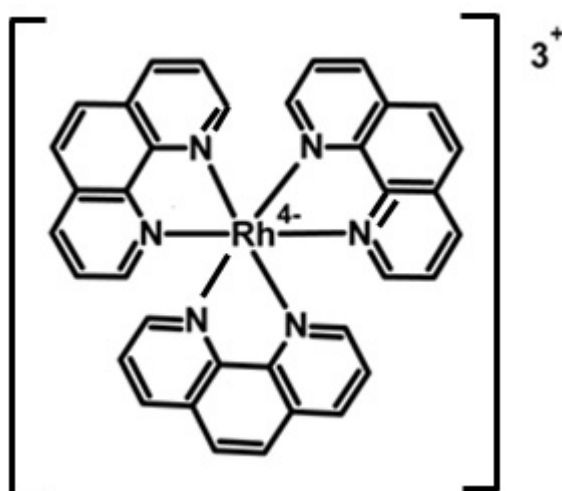
Figure 15. *Molecular structure formula of [Rh(phen)₃]³⁺.*

The temperature dependence can be explained on the basis of decay of the ligand-centred (LC) triplet via a thermally activated process involving an upper metal-centred (MC) state [59].

Binuclear rhodium complexes, which are both ligand-bridged species and bridged metal-metal, show long lifetimes of luminescence as typical of a MLCT excited state [56].

1.3.2.4. Platinum complexes

Platinum sits in group 10 of the periodic table, along with nickel and palladium. The electronic configuration is d^8, which by a simple ligand-field splitting diagram (Figure 16), indicates that these metal ions have a thermodynamic preference to form square planar complexes in the presence of strong-field ligands. This geometry forces a single unoccupied orbital to high energies, while allowing the stabilisation of three of the occupied orbitals [69]. Their square planar geometry influences directly their photochemical and photophysical properties [56].
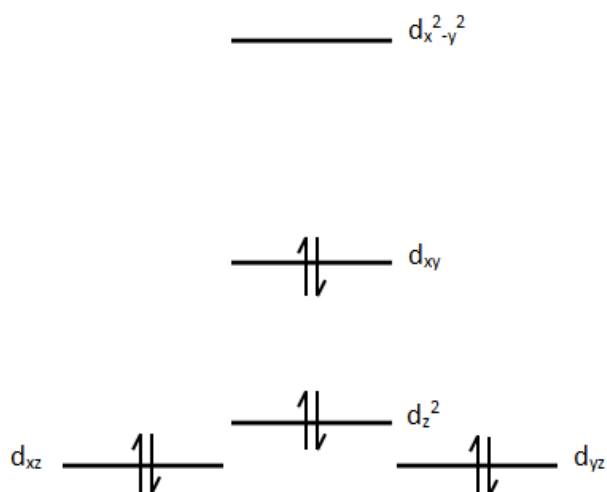
Figure 16. *Ligand field-splitting diagram for metal d orbitals in a square planar complex.*

Most of the metal ions, such as Ru (II), Os (II), Rh (II) and Ir (III), present an octahedral symmetry. However, in the case of Pt (II), the complexes have a square-planar geometry, which produces a very different photochemistry. The absorption or luminescence are influenced by this square-planar nature in Pt (II) complexes.

As we can see in figure 16, the $d_{x^2-y^2}$ orbital is strongly antibonding; however, if the orbital is populated with electrons by excitation, the molecule experiences a significant distortion in the conformation of the excited state and Pt-Ligand bond lengths increase. This is an unfavourable situation for luminescence from an excited state, where non-radiative internal conversion or intersystem crossing to the ground state can happen.

The 6-coordinate d^6 complexes present a spherical profile, while ligands of Pt (II) complexes are essentially flat and this allows close interactions, either with identical complexes or with other molecules. The planar nature of the complexes allow axial interactions, in other words interactions between the d_z^2 orbitals of two platinum ions [70, 71]. From the point of view of optical spectroscopy and excited states, this axial interaction implies that the highest occupied metal-based molecular orbital has increased in energy, compared with the isolated molecules, so that the lowest-energy optical transitions are shifted to even lower energies.

1.3.2.5. Iridium complexes

Iridium complexes were not very well known until twenty years ago. Today, there are numerous papers where Ir (III) complexes and their luminescent properties are discussed, as they present long lifetime and intense emission in the visible region [56].

Most of the reported iridium complexes have cyclometalated ligands. One of the main reason for iridium research is related to their use in organic light emitting diode (OLED) fabrication [72].

The Ir (III) is $5d^6$ centred and the complexes are octahedral, as are Fe (II) [65], Ru (II) [57], Os (II) [73] and Re (I) [74], whose metal centres are $3d^6$, $4d^6$, $5d^6$ and $5d^6$ respectively.

In Figure 17, we can see the orbital and state energy diagram for electronic transitions in a polyimine complex of d^6 metal centres.
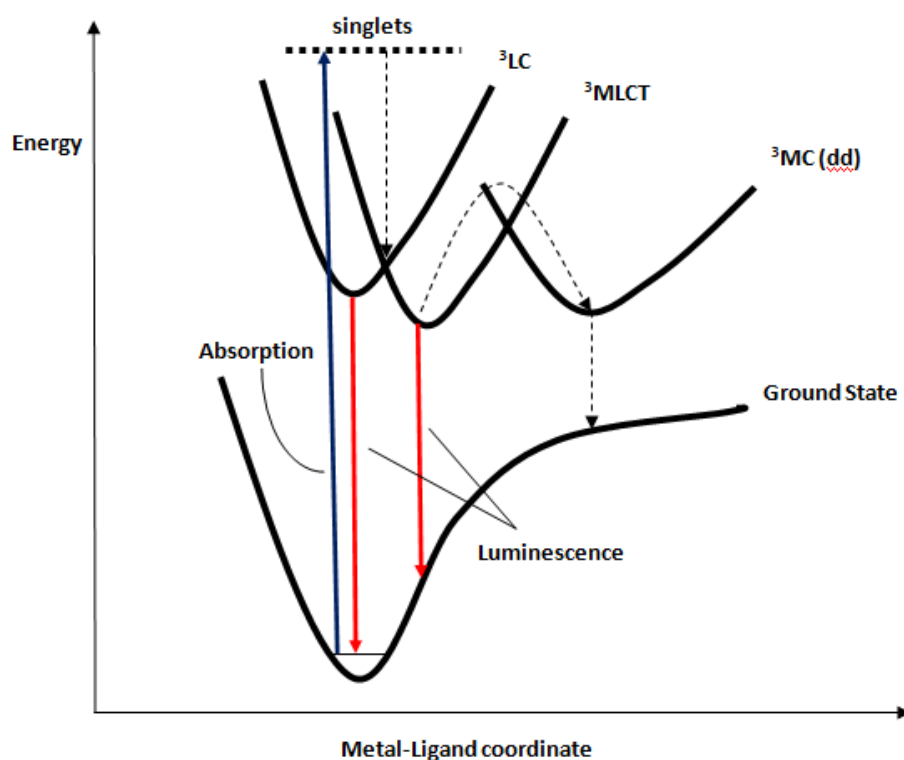
Figure 17. *Electronic transitions in a Ir (III) polyimine complexes [75]*.

The excitation is associated with electronic transitions from the ground state to singlet levels of various natures and electronic localizations, such as ligand centered (^{1}LC), metal-centered (^{1}MC) and metal to ligand charge transfer (^{1}MLCT). On the other hand, emission is from triplet levels, ^{3}MLCT or ^{3}LC [75]. This is a consequence

of the high spin-orbit coupling constant of the metal centres, which lead to a shift in their energy levels.

As mentioned, the Ir (III) complexes are characterized by octahedral geometry, where the ligand field splitting Δ (Figure 18) is very large and the MC levels are pushed so high in energy that normally they do not affect the emission properties and just the MLCT and LC levels are emissive.
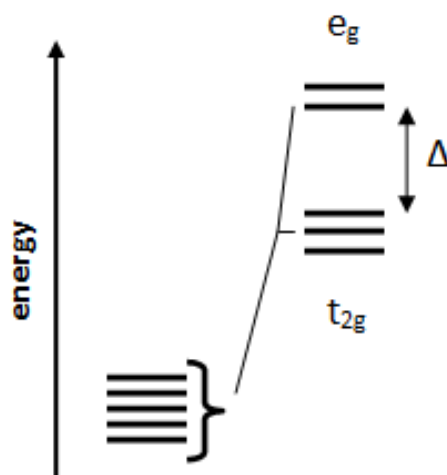
Figure 18. *d orbitals in octahedral field.*

1.3.2.6. Copper complexes

Copper metal has the advantage of wide availability. The abundance of the copper metal makes it an interesting material from the photochemical and photophysical point of view [54].

Copper is a d^9 element, like silver (Ag) and gold (Au). This element has two common oxidation states in solution: +1 and +2. The copper (I) complexes have superior photochemical and photophysical properties than copper (II) complexes, because the Cu (I) complexes have complete filling of *d* orbitals (d^{10}). This electronic configuration provides a symmetric localisation of the electronic charge and favours the tetrahedral disposition of the ligands around the metal centre.

There are numerous reported copper complexes, some of the most important, for their applications and properties, are the called heteroleptic diimine/diphosphine copper complexes [Cu(NN)(PP)]$^+$. These complexes contain N- and P- coordinating ligands and they have been studied since the late 1970s [60]. Copper complexes with two diimine ligands have been known as their luminescent properties [62],

however the substitution of one N-N ligand by one P-P ligand has improved the emission and has received tremendous interest in recent years [61, 63].

A group of copper complexes were reported by Armaroli and co-workers, $[Cu(dbp)(POP)]^+$ (dbp = 2,9-butyl-1,10-phenanthroline and POP = bis[2-(diphenylphosphino)phenyl]ether) (Figure 19), where the absorption spectra shows a band above 350 nm, which is attributed to ligand-centred transitions (LC) and another band between 350-450 nm, that is due to metal-ligand charge transfer (MLCT) (Figure 20) [76].

1. R = Phenethyl, R^1 = H
2. R = Bu, R^1 = H
3. R = Me, R^1 = Ph
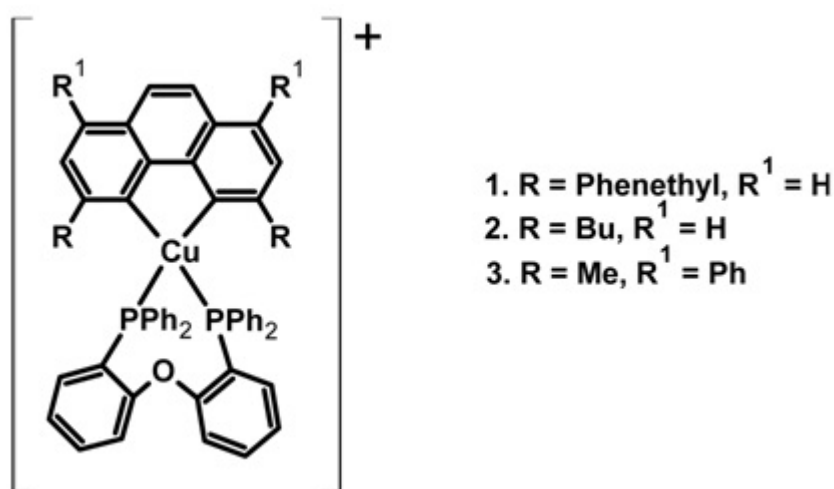
Figure 19. *Heteroleptic diimine/diphosphine copper complexes 1-3 [76].*
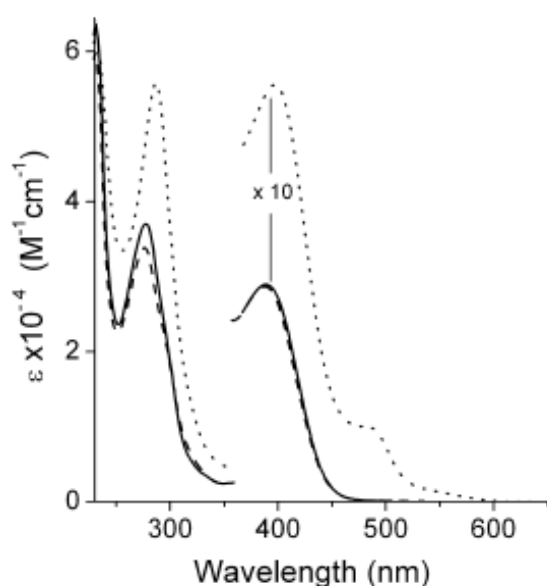
Figure 20. *Absorption spectra of copper complexes 1 (solid line), 2 (dashed line) and 3 (dotted line) at room temperature in a CH_2Cl_2 solution [76]*

The geometry and the strong dependency on solvent and oxygen is playing an important role in the study of the luminescence efficiency, as it can be decreased by exciplex quenching [64]. Blue-shifts of the lower-energy bands were observed compared to the spectra of the complexes with two diimine ligands $[Cu(NN)_2]^+$ (Figure 21) [61].
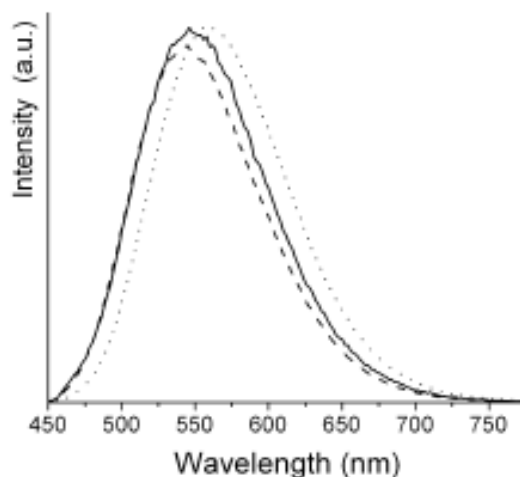
Figure 21. *Emission spectra of copper complexes 1 (solid line), 2 (dashed line) and 3 (dotted line) at room temperature in a CH$_2$Cl$_2$ solution [61].*

The intensive research for emission materials has produced numerous studies of organometallic triplet emitters [77]. Most of these studies are centered on the complexes of platinum (II) and iridium (III) as they have shown excellent properties as triplet emitters, especially for application in OLEDs. However, these materials are expensive and not sustainable for organic light emitting device applications [78]. Recently, research has focused on new materials with similar photoluminescence properties as iridium and platinum complexes. The d^{10} metals, copper, silver and gold, have shown important optical properties [78] and efficiency, such as the stable complexes of Cu(I) phenanthroline [79], Cu (I) acetylides [80], Cu(I) diethynylbenzene [81], trinuclear Ag(I) alkynyl [82], mononuclear Au(I) containing carbine, phosphine, thiolate and acetylide ligands [83] or dinuclear Au(I) diarylalkynyl [83] . Most of the copper and silver complexes have been made with acetylide ligands because these transition metals possess versatile reactivity and easily coordinate to them [84].

A collection of copper complexes has been prepared following different strategies in order to improve their photoluminescence quantum efficiency. These strategies have tried to involve suppressing non-radiative decay caused by distortion

of the excited states of the copper complexes [85-87]. The synthesised complexes have a variety of ligands in order to provide a range of colours of the emission [88]. Some of them are polynuclear complexes, that have been reported to have interesting optical properties which are due to their metal-metal interaction and their rigid structure, such as the pyridine and phosphine ligands [79, 89] which prevent structural relaxation, giving a stable structure and promote radiative decay. The fluoro substituents on the complexes have shown the ability to tune the colour of the emission in previous studies [90].

There is an increasing interest in the synthesis of alkynyl metal complexes because of their potential applications as nonlinear optical materials [91]. The interest in transition metal alkynyl complexes is based on two chemical aspects of the acetylide groups: their coordinated reactivity and their ability to coordinate to transition metals [84]. They have a linear geometry, where the *sp* hybridised carbons give increased linearity to the -C≡C- unit with an angle of 180° [72] and extended π-electrons delocalization [88]. The C≡C bonds are part of a reactivity study, because of the formation of cluster compounds, in which the alkynyl ligands bridges multiple metal centres and the ligand is transformed into a vinylidene, allenylidene or cummulenylidene [82]. Many alkynyl complexes have been reported over the past few years, such as $Au_2(dppm)_2(SO_3CF_3)_2$ (dppm: diphenylphosphino methane) [92], $[Pt_2(\mu\text{-}dppm)_2(\mu\text{-}C≡CR)(C≡CR)_2]^+$ [88], alkynyl polynuclear complexes with copper, rhenium, silver and platinum [81], $[Cu_3(\mu_3\text{-}\eta^1\text{-}C≡CPh)(\mu\text{-}dppm)_3](BF_4)_2$, $[Cu_3(\mu_3\text{-}\eta^1\text{-}C≡CPh_2)_2(\mu\text{-}dppm)_3]BF_4$, $[Cu_3(\mu_3\text{-}\eta^1\text{-}C≡CPh)(\mu_3\text{-}Cl)(\mu\text{-}dppm)_3]BF_4$ [84], $[Cu_3(\mu\text{-}PNP)_3(\mu_3\text{-}\eta^1\text{-}C≡CR')_2$ (PNP: bid(diphenylphosphino)-alkyl/-aryl amine) [91] and $[Au(C≡CR)L]$ (L:PPh_3, R:Me, Et, Ph, CF_3; L: $P(C_6H_4Me\text{-}p)_3$, R: Ph) [93].

In recent years, there has been an increasing need to extend this area of research, in order to produce novel mononuclear coordinated complexes that are able to exhibit long excited-state lifetimes, reversible redox behaviour and stability toward photodecomposition [72].

1.3.2.7. Gold complexes

In 1970, the first gold complex was reported [94], when the photoluminescence of the complex [Au(PPh$_3$)Cl] was studied. Since that publication,

the attention to gold (I) complexes has been growing, particularly the interaction of Au-Au and their photophysical properties.

The presence of the heavy metal in the complexes promotes the intersystem crossing. The heavy-atom effect contributes to the photo excitation of the singlet excited states and access to the spin-forbidden triplet states and as a result these complexes show phosphorescence.

In gold (I) complexes, such as $[Au_2(dmpm)_2](ClO_4)_2$ (dmpm = bis(dimethylphosphino)methane) and $[Au_3(dmmp)_2](ClO_4)_3$ (dmmp = bis(dimethylphosphinomethyl)phenylphosphine), the role of structure of the complexes is very important [95, 96]. Both complexes are phosphorescent, the bi-nuclear and tri-nuclear gold complexes show two main wavelength maximums that are in the emission spectrum, 455nm, τ_o = 1.2 µs and 467 nm, τ_o = 1.6 µs respectively, which was suggested to originate from an excited state of intraligand character, while at 555 nm, τ_o = 2.8 µs and 580 nm, τ_o = 7.0 µs respectively, which are phosphorescent but indicate reduced $d\sigma^*$-$p\sigma$ and $d\delta^*$-$p\sigma$ energy gaps, Figure 22. The effect of aurophilic distance on the HOMO-LUMO energy gap reduces the energy gap and as a consequence they shift their emission to red or longer wavelength.
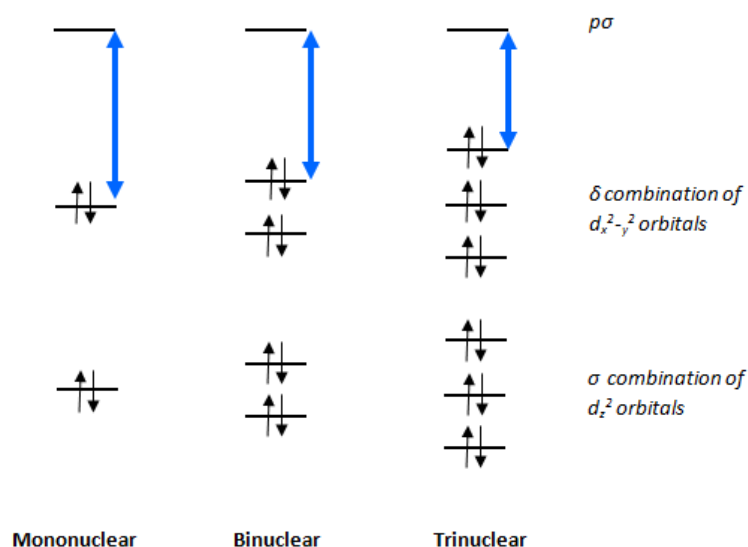
Figure 22. *Schematic molecular orbital diagram of gold (I) phosphine complexes [72].*

Another important group of gold complexes are those coordinated alkynyl ligands. It is due to the linear two-coordinate geometry of gold (I) [81].

Gold (I) alkynyl complexes are known to show interesting luminescence. They show an intramolecular Au-Au distance of 3.153 Å [97]. One of the first reported gold (I) alkynyl complexes was [Au_2(dppe)(C≡CPh) $_2$], with a phosphorescent emission at 420nm in dichloromethane at 298K and a solid-state emission at 550 nm at 298K (24.85 ^{o}C), which is characteristic to the [$(d\delta^*)^1(p\sigma)^1$] phosphorescence. While the related complex [Au_3(dppm)$_2$(C≡CPh)$_2$], which possesses an intramolecular Au-Au distances of 3.167 Å, shows a phosphorescent emission at 425 and 600 nm in MeCN at 298 K (24.85 ^{o}C) [98]. The aurophilic distances in the solid state structure of gold (I) complexes play an important role in perturbing the luminescence.

1.4. References

1. *Organic light emitting devices, synthesis, properties and applications*, ed. K.M.a.U. Scherf. 2006: Wiley-VCH pubs.

2. Geffroy, B., P. le Roy, and C. Prat, *Organic light-emitting diode (OLED) technology: materials, devices and display technologies.* Polymer International, 2006. **55**(6): p. 572-582.

3. Tang, C.W. and S.A. VanSlyke, *Organic electroluminescent diodes.* Applied Physics Letters, 1987. **51**(12): p. 913-915.

4. Lim, J.T., et al., *White-light-emitting devices based on organic multilayer structure.* Current Applied Physics, 2002. **2**(4): p. 295-298.

5. Yang, H., et al., *White organic light-emitting devices with non-doped-type structure.* Displays, 2006. **27**(4–5): p. 183-186.

6. Lee, Y.-J., et al., *Study of thermal degradation of organic light emitting device structures by X-ray scattering.* Thin Solid Films, 2007. **515**(14): p. 5674-5677.

7. Baldo, M.A., et al., *Highly efficient phosphorescent emission from organic electroluminescent devices.* Nature, 1998. **395**(6698): p. 151-154.

8. Pereira, L., *Organic light emitting diodes. The use of rare earth and transition metals*. 2012, USA: Pan Stanford Publishing Pte. Ltd. 364.

9. So, F. and D. Kondakov, *Degradation Mechanisms in Small-Molecule and Polymer Organic Light-Emitting Diodes.* Advanced Materials, 2010. **22**(34): p. 3762-3777.

10. Lee, T.W., et al., *Self-Organized Gradient Hole Injection to Improve the Performance of Polymer Electroluminescent Devices.* Advanced Functional Materials, 2007. **17**(3): p. 390-396.

11. Kuwabara, Y., et al., *Thermally stable multilared organic electroluminescent devices using novel starburst molecules, 4,4',4"-Tri(N-carbazolyl)triphenylamine (TCTA) and 4,4',4"-Tris(3-methylphenylphenylamino)triphenylamine (m-MTDATA), as hole-transport materials.* Advanced Materials, 1994. **6**(9): p. 677-679.

12. Huang, C.J., et al., *Improvement of color purity and electrical characteristics by co-doping method for flexible red-light organic light emitting devices.* Displays, 2009. **30**(4–5): p. 164-169.

13. P. Coppo, R.F., E. Galoppini, A. Maldotti, M.A. Miranda, K. Mizuno, J.S. Seixas de Melo, N. Serpone, T. Tsuno, *Photochemistry*, ed. A. Albini. 2009.

14. F. So, J.K.a.P.B., *Organic light-emitting devices for solid-state lighting.* MRS. Bulleting, 2008. **33**: p. 663-669.

15. Chiang, C.-J., et al., *Mechanical modeling of flexible OLED devices.* Organic Electronics, 2009. **10**(7): p. 1268-1274.

16. Shinar, J., *Organic light-emitting devices : a survey.* 2002, New York ; London: Springer.

17. *Highly efficient OLEDs with phosphorescent materials.*, ed. H. Yersin. 2008: Wiley-VCH pubs.

18. Li, Z.R. and H. Meng, *Organic light-emitting materials and devices.* 2007, Boca Raton, FL.: CRC Press ; London : Taylor & Francis [distributor].

19. Kawashima, T., H. Matsui, and N. Tanabe, *New transparent conductive films: FTO coated ITO.* Thin Solid Films, 2003. **445**(2): p. 241-244.

20. Schmidt, N.W., et al., *Effects of substrate temperature and near-substrate plasma density on the properties of dc magnetron sputtered aluminum doped zinc oxide.* Journal of Applied Physics, 2003. **94**(9): p. 5514-5521.

21. Okamoto, Y. and W. Brenner, *Organic semiconductors.* 1964, New York: Reinhold ; London : Chapman & Hall.

22. Kafafi, Z.H.E., *Organic light-emitting materials and devices IV.* 2001: SPIE.

23. Borsenberger, P.M., *Hole Transport in Bis (4-N,N-Diethylamino-2-Methylphenyl)-4-Methylphenylmethane Doped Polymers.* physica status solidi (b), 1992. **173**(2): p. 671-680.

24. P.M., B.W.T., Gruenbaum; E.H., Magin., *Hole Transport in Vapor-Deposited Triphenylmethane Glasses.* Jpn. J. Appl. Phys., 1996. **35**.

25. Higuchi, M., et al., *First Synthesis of Phenylazomethine Dendrimer Ligands and Structural Studies.* Journal of the American Chemical Society, 2001. **123**(19): p. 4414-4420.

26. Higuchi, M., et al., *Control of Stepwise Radial Complexation in Dendritic Polyphenylazomethines.* Journal of the American Chemical Society, 2003. **125**(33): p. 9988-9997.

27. Kimoto, A., et al., *Synthesis of Asymmetrically Arranged Dendrimers with a Carbazole Dendron and a Phenylazomethine Dendron.* Macromolecules, 2004. **37**(15): p. 5531-5537.

28.   Cho, J.-S., et al., *Synthesis of Diphenylamine-Substituted Phenylazomethine Dendrimers and the Performance of Organic Light-Emitting Diodes.* Macromolecular Chemistry and Physics, 2005. **206**(6): p. 635-641.

29.   Schols, S. and SpringerLink (Online service), *Device architecture and materials for organic light-emitting devices targeting high current densities and control of the triplet concentration.* 2011, Springer Science+Business Media B.V.: Dordrecht. p. xv, 154 p.

30.   Tang, C.W., *Two-layer organic photovoltaic cell.* Applied Physics Letters, 1986. **48**(2): p. 183-185.

31.   Kozlov, V.G., et al., *Laser action in organic semiconductor waveguide and double-heterostructure devices.* Nature, 1997. **389**(6649): p. 362-364.

32.   K. Kudi, M.Y., and T. Morisumi, *Field effect measurement of organic dye films.* Jpn. J. Appl. Phys., 1984. **23**: p. 130.

33.   Pope, M. and C.E. Swenberg, *Electronic processes in organic crystals and polymers.* 2nd ed. 1999, New York ; Oxford: Oxford University Press. xxix, 1328 p.

34.   Lanzani, G., *Photophysics of molecular materials : from single molecules to single crystals.* 2006, Weinheim: Wiley-VCH ; Chichester : John Wiley [distributor].

35.   Warta, W. and N. Karl, *Hot holes in naphthalene: High, electric-field-dependent mobilities.* Physical Review B, 1985. **32**(2): p. 1172-1182.

36.   Karl, N. and J. Marktanner, *Electron and Hole Mobilities in High Purity Anthracene Single Crystals.* Molecular Crystals and Liquid Crystals Science and Technology. Section A. Molecular Crystals and Liquid Crystals, 2001. **355**(1): p. 149-173.

37.   Podzorov, V., et al., *Hall Effect in the Accumulation Layers on the Surface of Organic Semiconductors.* Physical Review Letters, 2005. **95**(22): p. 226601.

38.   Ostroverkhova, O., et al., *Ultrafast carrier dynamics in pentacene, functionalized pentacene, tetracene, and rubrene single crystals.* Applied Physics Letters, 2006. **88**(16): p. 162101-162101-3.

39.   Le Comber, P.G. and W.E. Spear, *Electronic Transport in Amorphous Silicon Films.* Physical Review Letters, 1970. **25**(8): p. 509-511.

40. Horowitz, G., R. Hajlaoui, and P. Delannoy, *Temperature Dependence of the Field-Effect Mobility of Sexithiophene. Determination of the Density of Traps.* J. Phys. III France, 1995. **5**(4): p. 355-371.

41. Mottaghi, M. and G. Horowitz, *Field-induced mobility degradation in pentacene thin-film transistors.* Organic Electronics, 2006. **7**(6): p. 528-536.

42. Bässler, H., *Charge Transport in Disordered Organic Photoconductors a Monte Carlo Simulation Study.* physica status solidi (b), 1993. **175**(1): p. 15-56.

43. Vissenberg, M.C.J.M. and M. Matters, *Theory of the field-effect mobility in amorphous organic transistors.* Physical Review B, 1998. **57**(20): p. 12964-12967.

44. Yen, W.M., S. Shionoya, and H.F. Yamamoto, *Phosphor handbook*. 2nd ed. / edited by William M. Yen, Shigeo Shionoya, Hajime Yamamoto. ed. 2007, Boca Raton, Fla.: CRC ; London : Taylor & Francis [distributor].

45. Lichtman, J.W. and J.-A. Conchello, *Fluorescence microscopy.* Nat Meth, 2005. **2**(12): p. 910-919.

46. Thoms, T., et al., *Improved host material design for phosphorescent guest–host systems.* Thin Solid Films, 2003. **436**(2): p. 264-268.

47. Olsen, E.D., *Modern optical methods of analysis*. 1975, New York: McGraw-Hill. ix, 629 p.

48. *Coordination Chemistry : Vol. 1*. 1971, New York ; London: Van Nostrand Reinhold.

49. Krasovitskii, B.M. and B.M. Bolotin, *Organic luminescent materials*. 1988: VCH.

50. Rao, C.N.R., *Ultra-violet and visible spectroscopy : chemical applications*. 3rd ed. ed. 1975, London: Butterworth.

51. Hernandez-Hernandez, L., Gonzalez-Perez, C., *Introduccion al analisis instrumental*. 1st ed. 2002, Barcelona: Editorial Ariel S.A.

52. Lee, J.D., *Concise inorganic chemistry*. 5th ed. ed. 1996, London: Chapman & Hall.

53. Sharpe, A.G., *Inorganic chemistry*. 1981, London: Longman.

54. Balzani, V., S. Campagna, and G. Accorsi, *Photochemistry and photophysics of coordination compounds I*. 2007, Berlin: Springer.

55.   Balzani, V., et al., *Luminescent and Redox-Active Polynuclear Transition Metal Complexes†.* Chemical Reviews, 1996. **96**(2): p. 759-834.

56.   P. Coppo, R.F., E. Galoppini, A. Maldotti, M.A. Miranda, K. Mizuno, J.S. Seixas de Melo, N. Serpone, T. Tsuno, *Photochemistry.* 1st ed, ed. A. Albini. Vol. 37. 2009, Cambridge, UK: RSC Publishins.

57.   Juris, A., et al., *Ru(II) polypyridine complexes: photophysics, photochemistry, eletrochemistry, and chemiluminescence.* Coordination Chemistry Reviews, 1988. **84**(0): p. 85-277.

58.   Lytle, F.E. and D.M. Hercules, *Luminescence of tris(2,2'-bipyridine)ruthenium(II) dichloride.* Journal of the American Chemical Society, 1969. **91**(2): p. 253-257.

59.   Indelli, M.T., A. Carioli, and F. Scandola, *Excited-state absorption of tris(phenanthroline)rhodium(III). A handle on the excited-state behavior of a powerful photochemical oxidant.* The Journal of Physical Chemistry, 1984. **88**(13): p. 2685-2686.

60.   Buckner, M.T. and D.R. McMillin, *Photoluminescence from copper(I) complexes with low-lying metal-to-ligand charge transfer excited states.* Journal of the Chemical Society, Chemical Communications, 1978(17): p. 759-761.

61.   Cuttell, D.G., et al., *Simple Cu(I) Complexes with Unprecedented Excited-State Lifetimes.* Journal of the American Chemical Society, 2001. **124**(1): p. 6-7.

62.   Lowry, M.S. and S. Bernhard, *Synthetically Tailored Excited States: Phosphorescent, Cyclometalated Iridium(III) Complexes and Their Applications.* Chemistry – A European Journal, 2006. **12**(31): p. 7970-7977.

63.   McCormick, T., W.-L. Jia, and S. Wang, *Phosphorescent Cu(I) Complexes of 2-(2'-pyridylbenzimidazolyl)benzene: Impact of Phosphine Ancillary Ligands on Electronic and Photophysical Properties of the Cu(I) Complexes.* Inorganic Chemistry, 2005. **45**(1): p. 147-155.

64.   Palmer, C.E.A., et al., *Flash photolysis and quenching studies of copper(I) systems in the presence of Lewis bases: inorganic exciplexes?* Inorganic Chemistry, 1987. **26**(19): p. 3167-3170.

65.   Braterman, P.S., J.I. Song, and R.D. Peacock, *Electronic absorption spectra of the iron(II) complexes of 2,2'-bipyridine, 2,2'-bipyrimidine, 1,10-*

phenanthroline, and 2,2':6',2''-terpyridine and their reduction products. Inorganic Chemistry, 1992. **31**(4): p. 555-559.

66.   Carstens, D.H.W. and G.A. Crosby, *Luminescence from complexes of rhodium(III).* Journal of Molecular Spectroscopy, 1970. **34**(1): p. 113-135.

67.   Crosby, G.A. and W.H. Elfring, *Excited states of mixed ligand chelates of ruthenium(II) and rhodium(III).* The Journal of Physical Chemistry, 1976. **80**(20): p. 2206-2211.

68.   Hillis, J.E. and M.K. DeArmond, *Nonradiative processes in transition metal complexes: Luminescence data for Rh (III) and Ir (III) complexes.* Journal of Luminescence, 1971. **4**(4): p. 273-290.

69.   Houlding, V.H. and V.M. Miskowski, *The effect of linear chain structure on the electronic structure of pt(II) diimine complexes.* Coordination Chemistry Reviews, 1991. **111**(0): p. 145-152.

70.   Keller, H.J., *Chemistry and physics of one-dimensional metals*. 1977, New York: Plenum Press.

71.   Miller, J.S., *Extended linear chain compounds*. 1982, London ; New York: Plenum.

72.   Balzani, V., S. Campagna, and A. Barbieri, *Photochemistry and photophysics of coordination compounds II*. 2007, Berlin: Springer.

73.   Kober, E.M., et al., *Application of the energy gap law to excited-state decay of osmium(II)-polypyridine complexes: calculation of relative nonradiative decay rates from emission spectral profiles.* The Journal of Physical Chemistry, 1986. **90**(16): p. 3722-3734.

74.   Schanze, K.S., et al., *Studies of intramolecular electron and energy transfer using the fac-(diimine)ReI(CO)3 chromophore.* Coordination Chemistry Reviews, 1993. **122**(1–2): p. 63-89.

75.   Yersin, H. and K.L. Bray, *Transition metal and rare earth compounds : excited states, transitions, interactions*: Berlin ; London : Springer, c2001-.

76.   Armaroli, N., et al., *Highly Luminescent CuI Complexes for Light-Emitting Electrochemical Cells (Adv. Mater. 10/2006).* Advanced Materials, 2006. **18**(10): p. n/a-n/a.

77.   Prokhorov, A.M., et al., *2,2[prime or minute]-Bipyridinyl carboranes as B,N,N-ligands in cyclometallated complexes of platinum(ii).* Chemical Communications, 2011. **47**(27): p. 7713-7715.

78. Barbieri, A., G. Accorsi, and N. Armaroli, *Luminescent complexes beyond the platinum group: the d10 avenue.* Chemical Communications, 2008(19): p. 2185-2193.

79. Zhang, Q., et al., *Highly Efficient Green Phosphorescent Organic Light-Emitting Diodes Based on CuI Complexes.* Advanced Materials, 2004. **16**(5): p. 432-436.

80. Yam, V.W.-W., K. Kam-Wing Lo, and K. Man-Chung Wong, *Luminescent polynuclear metal acetylides.* Journal of Organometallic Chemistry, 1999. **578**(1–2): p. 3-30.

81. Yam, V.W.-W., *Luminescent metal alkynyls – from simple molecules to molecular rods and materials.* Journal of Organometallic Chemistry, 2004. **689**(8): p. 1393-1401.

82. Long, N.J. and C.K. Williams, *Metal Alkynyl σ Complexes: Synthesis and Materials.* Angewandte Chemie International Edition, 2003. **42**(23): p. 2586-2617.

83. Evans, R.C., P. Douglas, and C.J. Winscom, *Coordination complexes exhibiting room-temperature phosphorescence: Evaluation of their suitability as triplet emitters in organic light emitting diodes.* Coordination Chemistry Reviews, 2006. **250**(15–16): p. 2093-2126.

84. Diez, J., et al., *Synthesis and characterization of triangulo copper(I) complexes containing mono- and bicapping systems of asymmetric .mu.3-.eta.1-acetylide ligands: molecular structures of [Cu3(.mu.3-.eta.1-C.tplbond.CPh)(.mu.-dppm)3][BF4]2, [Cu3(.mu.3-.eta.1-C.tplbond.CPh)2(.mu.-dppm)3][BF4], and [Cu3(.mu.3-.eta.1-C.tplbond.CPh)(.mu.3-Cl)(.mu.-dppm)3][BF4] [dppm = bis(diphenylphosphino)methane].* Organometallics, 1993. **12**(6): p. 2213-2220.

85. Hou, R., et al., *Synthesis, structural characterization and luminescent properties of a series of Cu(i) complexes based on polyphosphine ligands.* Dalton Transactions, 2011. **40**(29): p. 7551-7558.

86. Min, J., et al., *Neutral copper(i) phosphorescent complexes from their ionic counterparts with 2-(2[prime or minute]-quinolyl)benzimidazole and phosphine mixed ligands.* Dalton Transactions, 2011. **40**(3): p. 686-693.

87. Wada, A., et al., *Efficient luminescence from a copper(i) complex doped in organic light-emitting diodes by suppressing C-H vibrational quenching.* Chemical Communications, 2012. **48**(43): p. 5340-5342.

88. Yam, V.W.-W., *Molecular Design of Transition Metal Alkynyl Complexes as Building Blocks for Luminescent Metal-Based Materials: Structural and Photophysical Aspects.* Accounts of Chemical Research, 2002. **35**(7): p. 555-563.

89. Armaroli, N., et al., *Highly Luminescent CuI Complexes for Light-Emitting Electrochemical Cells.* Advanced Materials, 2006. **18**(10): p. 1313-1316.

90. Coppo, P., E.A. Plummer, and L. De Cola, *Tuning iridium(iii) phenylpyridine complexes in the "almost blue" region.* Chemical Communications, 2004(15): p. 1774-1775.

91. Yam, V.W.-W., W.K.-M. Fung, and M.-T. Wong, *Synthesis, Photophysics, Electrochemistry, and Excited-State Redox Properties of Trinuclear Copper(I) Acetylides with Bis(diphenylphosphino)alkylamines and -arylamines as Bridging Ligands.* Organometallics, 1997. **16**(8): p. 1772-1778.

92. Ma, Y., et al., *High Luminescence Gold(I) and Copper(I) Complexes with a Triplet Excited State for Use in Light-Emitting Diodes.* Advanced Materials, 1999. **11**(10): p. 852-857.

93. Cheung, K.-L., S.-K. Yip, and V.W.-W. Yam, *Synthesis, characterization, electrochemistry and luminescence studies of heterometallic gold(I)–rhenium(I) alkynyl complexes.* Journal of Organometallic Chemistry, 2004. **689**(24): p. 4451-4462.

94. Ziolo, R.F., S. Lipton, and Z. Dori, *The photoluminescence of phosphine complexes of d10 metals.* Journal of the Chemical Society D: Chemical Communications, 1970(17): p. 1124-1125.

95. Yam, V.W.-W., T.-F. Lai, and C.-M. Che, *Novel luminescent polynuclear gold(I) phosphine complexes. Synthesis, spectroscopy, and X-ray crystal structure of [Au3(dmmp)2]3+[dmmp = bis(dimethylphosphinomethyl)methylphosphine].* Journal of the Chemical Society, Dalton Transactions, 1990(12): p. 3747-3752.

96. Yam, V.W.-W. and W.-K. Lee, *Synthesis, spectroscopy and excited-state redox properties of novel luminescent trinuclear three-co-ordinate gold(I)*

phosphine complexes. Journal of the Chemical Society, Dalton Transactions, 1993(14): p. 2097-2100.

97.   Li, D., et al., *Luminescent gold(I) acetylide complexes. Photophysical and photoredox properties and crystal structure of [{Au(C[triple bond, length half m-dash]CPh)}2([small micro]-Ph2PCH2CH2PPh2)].* Journal of the Chemical Society, Dalton Transactions, 1993(19): p. 2929-2932.

98.   Che, C.-M., et al., *Luminescent metal clusters. Spectroscopic properties and X-ray structure of a trinuclear gold(I) complex containing bis(diphenylphosphino)methane and phenylacetylide.* Polyhedron, 1994. **13**(6–7): p. 887-890.

Chapter 2: Procedures for synthesis of trinuclear and mononuclear copper (I) complexes

2.1. Experimental procedures

All the chemical were purchased from Sigma Aldrich, Fisher Scientific and Acros Organic, with the highest purity commercially available and used without further purification.

NMR were recorded on a JEOL 400 MHz spectrometer using the resonance peak of the solvent as an internal reference.

2.2. Synthesis of trinuclear copper (I) complexes

A range of trinuclear copper (I) complexes were prepared following the procedure described in the literature [1], as shown in Figure 23. The synthesis of these complexes involves two steps:

Step 1:

 To a dichloromethane solution (20 ml) was added tetrakis (acetonitrile) copper (I) hexafluoroborate (0.314 g; 1 mmol), $[Cu(NCCH_3)_4(BF_4)$ and bis(diphenylphosphine) methane (μ-dppm) (1 mmol) . The reaction was stirred at room temperature for 6 hours. The obtained precursor was labelled as 1.

Step 2:

To a dichloromethane solution (20 ml) of the complex 1(0.87 mmol) , the corresponding alkynyl ligand R (1.17 mmol) was added (Figure 24). The reaction was stirred at room temperature for 24 hours under inert atmosphere. The crude products were purified by precipitating twice in mixtures of hexane and diethyl ether. The products were vacuum filtered and allowed to dry in air. They were labelled 2-8. The yields of the reactions are shown in Table 1.

Table 1. *Yield of the labelled complexes 2 to 8.*

Complex	Yield / %
1	89.0
2	98.8
3	72.1
4	30.2
5	34.1
6	92.9
7	63.1
8	40.0

The obtained products were characterized by:

- ^1H NMR analysis in $CDCl_3$.

  Complex 2: 7.13 (dt, 2H, J1=8.7 Hz, J2 = 2.3 Hz); 6.99-7.09 (m, 36H); 6.92 (dt, 2H, J1=8.7 Hz, J2=2.3 Hz); 6.79 (t, 24H, J=7.5 Hz); 3.12 ppm (s, 6H).

  Complex 3: 7.04-7.11 (m, 36H); 6.95 (tt, 2H, J1=8.9 Hz, J2=2.3 Hz); 6.86 (t, 24H, J=7.5 hz); 6.77 (td, 4H, J1=5.9 Hz, J2=2.3 Hz); 3.08 ppm (s, 6H).

  Complex 4: 8.01 (s, 2H); 7.45 (s, 4H); 7.01-7.19 (m, 36H); 6.90 (t, 24H, J=7.5 Hz); 3.11 ppm (s, 6H).

  Complex 5: 7.69 (d, 4H, J=8.0 Hz); 7.37 (d, 4H, J=8.0 Hz); 7.05-7.11 (m, 36H); 6.83 (t, 24H, J=7.5 Hz), 3.10 ppm (s, 6H).

  Complex 6: 9.02 (d, 2H, J=8.3 Hz); 8.93 (d, 2H, J=8.5 Hz); 8.00 (t, 2H, J=7.5 Hz); 7.92 (s, 2H); 7.88 (t, 2H, J=7.5 Hz); 7.66 (d, 2H, J=8.0 Hz); 7.61 (t, 2H, J=7.5 Hz); 6.98-7.08 (m, 36H); 6.69 (t, 24H, J=7.5 Hz); 3.17 ppm (s, 6H).

  Complex 7: 8.05 (d, 2H, J=8.3 Hz); 7.97(d, 2H, J=8.3Hz); 7.86 (s, 2H); 7.68 (d, 2H, J=8.3 Hz); 7.58 (d, 2H, J=8.4 Hz); 7.36 (s, 2H); 3.90 (s, 6H); 3.09 ppm (s, 6H).

- ^{19}F NMR analysis in $CDCl_3$.

  Complex 2: -105.36; -107.04; -154.31ppm.

Complex 3: -108.78; -154.69 ppm.

Complex 4: -62.15; -151.25 ppm.

Complex 5: -62.23; -154.31 ppm.

- ^{13}C *in CDCl$_3$.*

Complex 2: 162.86 (C-F); 161.91 (C-F);134.62; 132.71; 132.34; 129.88; 128.30; 111.90;104.60; 27.34 ppm.

Complex 3: 163.20 (C-F); 132.62; 132.11; 130.19; 128.51; 113.90; 103.85; 27.54 ppm.

Complex 4: 133.27; 132.27; 131.01; 130.06; 128.93; 128.68; 126.95; 125.24; 124.24; 123.94; 122.72; 121.51; 118.79; 26.28 ppm.

Complex 5: 132.67; 132.21; 131.31; 130.39; 130.11; 129.98; 129.10 (C-F); 128.46; 125.77; 27.60 ppm.

Complex 6: 132.77; 132.12; 131.68; 131.33; 130.88; 130.31; 129.77; 128.96; 128.43; 128.10; 127.94; 127.84; 127.73; 127.53; 123.40;121.99; 26.44 ppm.
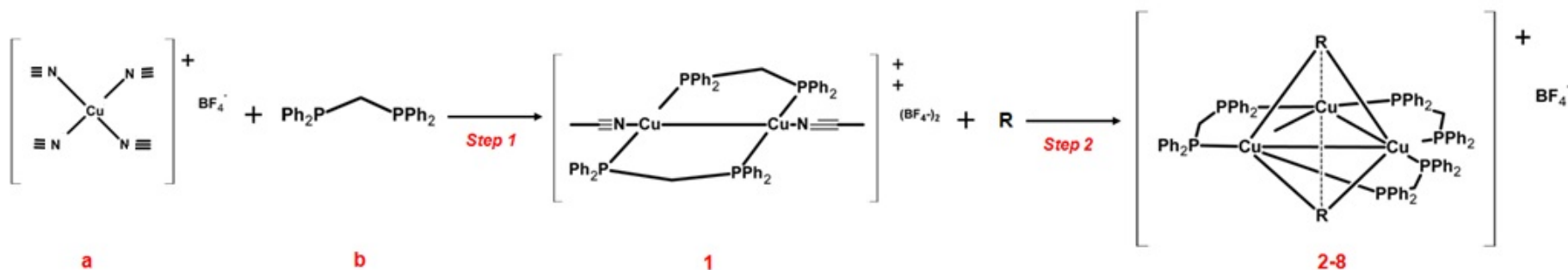
Figure 23. *Method of synthesis for trinuclear alkynyl copper complexes 2 to 8, via two steps, where: (a) tetrakis(acetronitrile) copper (I) tetrafluoroborate; (b) bis(diphenylphosphine) methane; (1) binuclear copper complex and (R) is the alkynyl ligand.*
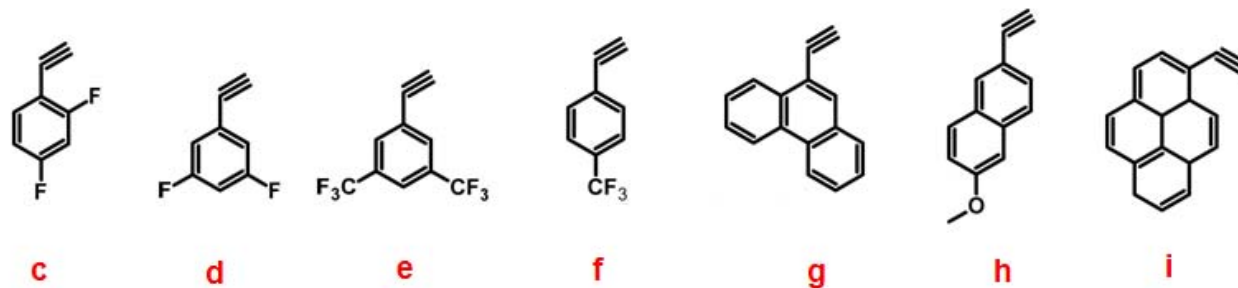

Figure 24. *The used alkynyl ligands in the reactions were: (c) 1-ethynyl-2,4-difluorobenzene; (d)1-ethynyl-3,5-difluorobenzene; (e) 1-ethynyl-3,5-bis(trifluoromethyl)benzene; (f) 1-ethynyl-α,α,α-4-(trifluoromethyl)benzene; (g) 9-ethynylphenanthrene; (h) 2-ethynyl-6-methoxynaphthalene; i) 1-ethynylpyrene.*

2.2.1. Other ligands

Other alkynyl ligands and phosphine ligand, Figure 25, were employed for the synthesis of trinuclear copper complexes [2-6], however the lack of emission indicated poor reactivity.
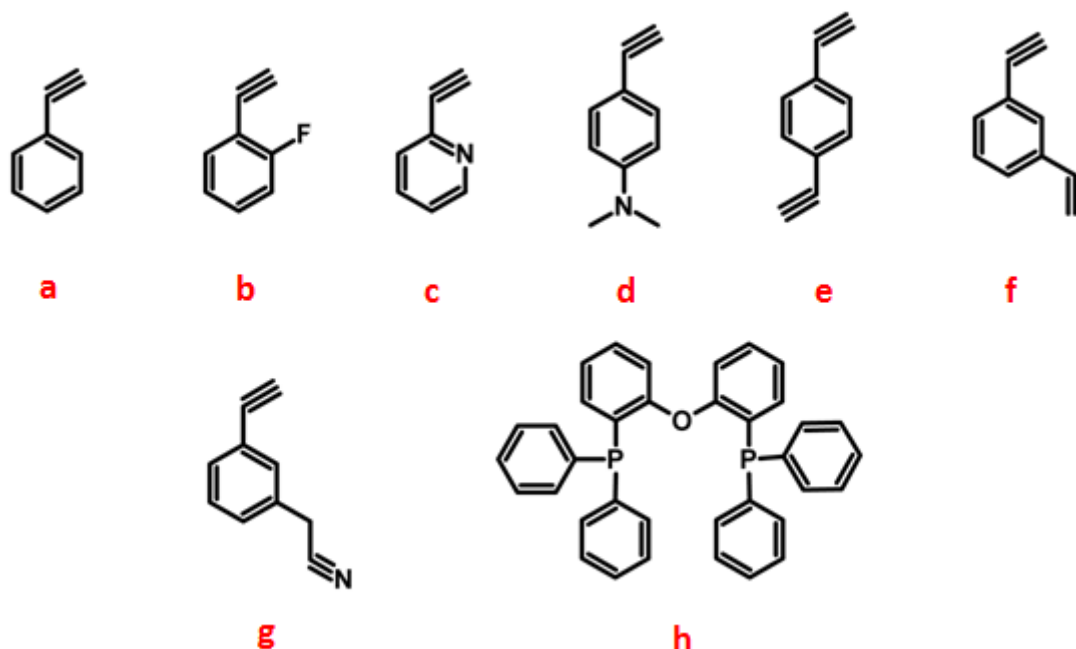

Figure 25. *Other alkynyl ligands and phosphine ligand: (a) ethylbenzene; (b) 1-ethynyl 2-fluorobenzene; (c) 1-ethynylpyridine; (d) 4-ethynyl-N,N-dimethylaniline; (e) 1,4-diethynylbencene; (f) 1,3-diethynylbenzene; (g) (4-ethynyl)phenylacetronitrile and (h) bis(2-diphenylphosphinophenyl)ether.*

2.3. Synthesis of mononuclear copper (I) complexes

A range of mononuclear copper (I) complexes were synthesized via one step following the method published by Min [7], Figure 26. To a dichloromethane solution (10 ml) of the bipyridyl ligand (1 mmol) and the diphosphine ligand (1 mmol; thriphenylphosphine 2 mmol) was added tetrakis (acetonitrile) copper(I) tetrafluoroborate (0.314g; 1 mmol). The reaction was stirred at room temperature for 1 hour in air. The crude products were purified by precipitating twice in mixtures of hexane and diethyl ether. The products were vaccum filtered and allowed to dry in air. They were labelled 9-16. In the bipyridine ligand, for the complexes 9, 12 and 14, R_1 and R_2 is H; for complexes 10, 13 and 15, R_1 is H and R_2 is CH_3; for complexes 11 and 16 R_1 is CH_3 and R_2 is H .The yields of the reactions are shown in Table 2.

Table 2. *Yield of the labelled complexes 9 to 16.*

Complex	Yield / %
9	95.0
10	84.5
11	74.0
12	33.6
13	61.2
14	66.3
15	88.3
16	53.0

The obtained products were characterised by:

- ^{1}*H NMR analysis in CDCl$_3$.*

Complex 9: 8.42 (d, 2H, J = 3.9 Hz, pyr.); 8.33 (d, 2H, J = 8.0 Hz, pyr.); 8.00 (t, 2H, J = 7.8 Hz pyr.); 7.20-7.31 (m, 8H, arom.); 7.16 (t, 8H, J = 7.3 Hz, arom.); 7.02 (d, 2H, J = 7.7 Hz, pyr.); 6.90-6.99 (m, 10H, arom.); 6.69-6.75 ppm (m, 2H, arom.).

Complex 10: 8.26 (d, 2H, J = 7.9 Hz, pyr.); 8.15 (d, 2H, J = 8.0 Hz, pyr.); 7.20-7.30(m, 8H, arom.); 7.16 (t, 8H, J = 7.3 Hz, arom.); 7.00 (d, 2H, J = 7.7 Hz, pyr.); 6.90-6.99 (m, 10H, arom.); 6.69-6.75 ppm (m, 2H, arom.).

Complex 11: 8.06 (d, 2H J = 8.0 Hz. Pyr.); 7.90 (d, 2H, J = 7.9 Hz., pyr.); 7.20-7.30 (m, 8H, arom.); 7.16 (t, 8H, J = 7.3 Hz, arom.); 6.92 (d, 2H, J = 7.7 Hz, pyr.); 6.90-6.99 (m, 10H, arom.); 6.85-6.91 (m, 2H, arom.). 2.18 ppm (s, 6H, CH3).

Complex 12: 8.50 (d, 2H, J = 3.9 Hz, pyr.); 8.28 (d, 2H, J = 8.0 Hz, pyr.); 8.08 (t, 2H, J = 7.8 Hz, pyr.); 7.34 (t, 6H, J = 7.7 Hz, arom.); 7.18 (t, 12H, arom); 6.94-7.10 ppm (m, 12H, arom.).

Complex 13: 8.37 (d, 2H, J = 8.0 Hz., pyr.); 8.09 (d, 2H, J = 7.9 Hz., pyr.); 7.34 (t, 6H, J = 7.7 Hz. Arom.); 7.18 (t, 12H, J = 7.5 Hz. Arom.); 7.11 (m, 2H, pyr.); 7.03 (m, 12H, arom.); 2.54 ppm (s, 6H, CH3).

Complex 14: 8.54 (d, 2H, J = 8.0 Hz, pyr.); 8.09 (d, 2H, J = 7.8, pyr.); 8.02 (d, 2H, J = 7.8 Hz, pyr); 7.62 (t, 2H, J = 7.5 Hz, arom.); 7.26 (t, 6H, J = 7.7 Hz, arom.); 7.12 (t, 10H, arom.); 6.79-6.95 (m, 8H, arom.); 6.50 (d, 2H, J = 7.9 Hz, pyr.); 1.76 ppm (s, 6H, CH3).

Complex 15: 8.42 (d, 2H, J = 7.9 Hz., pyr.); 7.79 (d, 2H, J = 7.8 Hz., pyr.); 7.62 (d, 2H, J = 7.9 Hz, pyr.); 7.26 (t, 6H, J = 7.7 Hz, arom.); 7.12 (t, 10H, arom.); 6.82-6.94 (m, 8H, arom.); 6.45 (m, 2H, arom.); 2.55 (s, 6H, CH3); 1.79 ppm (s, 6H, CH3).

Complex 16: 8.02 (d, 2H, J = 7.9 Hz., pyr.); 7.87 (d, 2H, J = 7.8 Hz., pyr.); 7.61 (d, 2H, J = 7.9 Hz, pyr.); 7.30 (t, 6H, J = 7.7 Hz, arom.); 7.16 (t, 10H, arom.); 7.00-7.09 (m, 8H, arom.); 6.82 (m, 2H, arom.); 1.98 (s, 6H, CH3); 1.66 ppm (s, 6H, CH3).

- ^{13}C *NMR analysis in CDCl$_3$.*

Complex 9: 158.30; 151.71; 149.22; 138.97; 134.39; 133.06; 132.08; 130.08; 130.22; 128.89; 125.98; 125.23; 122.94; 120.51 ppm.

Complex 10: 58.32; 151.75; 150.85; 148.71; 134.39; 133.17; 133.05; 130.14; 128.86; 123.54; 21.44 ppm.

Complex 11: 158.13; 152.42; 132.98; 132.91; 130.07; 128.8; 126.09; 120.46; 26.54 ppm.

Complex 12: 151.90; 149.23; 139.47; 133.05; 132.02; 130.37; 129.01; 126.18; 123.55 ppm.

Complex 13: 151.97; 151.47; 148.68; 133.15; 132.33; 130.24; 128.94; 126.84; 124.21; 21.45 ppm.

Complex 14: 154.91; 151.74; 148.65; 139.60; 133.80; 132.78; 131.20; 130.08; 128.93; 127.18; 123.53; 119.90; 36.26; 28.12 ppm.

Complex 15: 155.04; 151.79; 151.32; 148.08; 132.90; 129.99; 128.86; 126.98; 124.90; 124.12; 120.04; 36.25; 28.06; 21.44 ppm.

Complex 16: 157.73; 155.11; 152.11; 139.11; 133.17; 130.18; 128.88; 125.72; 120.05; 36.17; 28.39; 26.66 ppm.

- *Mass spectroscopy.*

Complex 9: 757.1 M+. 601.0 Cu(P^P)+. Elem. Anal. %: C: 65.56 (calc. 65.38) H: 3.92 (calc. 4.29).

Complex 10: 784.9 M+; 600.9 Cu(P^P)+. Elem. Anal. %: C: 65.61 (calc. 66.03); H: 4.11 (calc. 4.62); N: 3.21 (calc. 3.21).

Complex 11: 784.9 M+; 600.9 Cu(P^P)+. Elem. Anal. %: C: 65.26 (calc. 66.03); H: 4.12 (calc. 4.62); N: 2.93 (calc. 3.21).

Complex 12: 481.0 N^NCuPPh3+; 219.0 N^NCu+. Elem. Anal. %: C: 66.33 (calc. 66.48) H: 4.20 (calc. 4.61).

Complex 13: 509.12 N^NCuPPh3+. Elem. Anal. %: C 66.96 (calc. 67.10); H: 4.46 (calc. 4.93); N: 3.33 (calc. 3.26).

Complex 14: 796.9 M+. 641.0 Cu(P^P)+. Elem. Anal. %: C: 66.79 (calc. 66.49; H: 4.47 (calc. 4.55); N: 3.13 (calc. 3.16).

Complex 15: 824.9 M+; 640.9 Cu(P^P)+. Elem. Anal. %: C: 67.68 (calc. 67.08); H: 4.40 (calc. 4.86); N 2.65 (calc. 3.07).

Complex 16: 824.9 M+; 640.9 Cu(P^P)+. Elem. Anal. %: C: 66.42 (calc. 67.08); H: 4.41 (calc. 4.86); N: 3.00 (calc. 3.07).
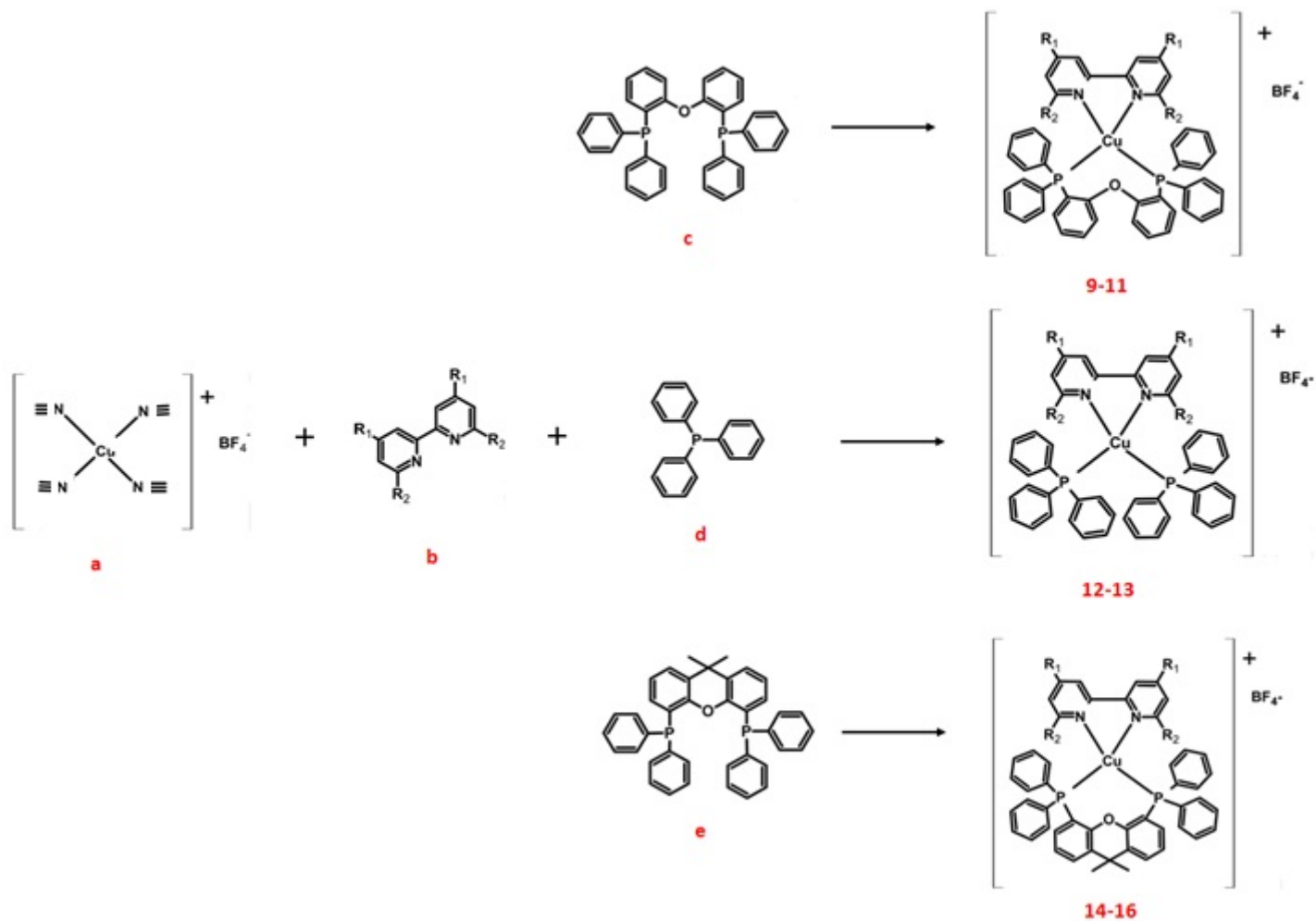
Figure 26. *Method of synthesis for mononuclear copper complexes 9 to 16, where: (a) tetrakis (acetronitrile) copper (I) tetrafluoroborate; (b) pyridine ligand, complexes 9,12 and 14 $R_1=R_2=$ H, complexes 10, 13 and 15 $R_1=$H and $R_2=$ CH_3, complexes 11 and 16 $R_1=$ CH_3 and $R_2=$ H; (c) bis(2-diphenylphosphinophenyl) ether; (d) triphenylphosphine; (e) 9,9-dimethyl-4,5-bis(diphenylphosphino) xanthenes.*

2.3.1. Other ligands

Other pyridine and phosphine ligands, Figure 27, were employed for the synthesis of mononuclear copper complexes [7-11], however the reaction products were non emissive. Given the limited access to NMR and MASS characterisation facilities, no attempt to characterise the products was made.
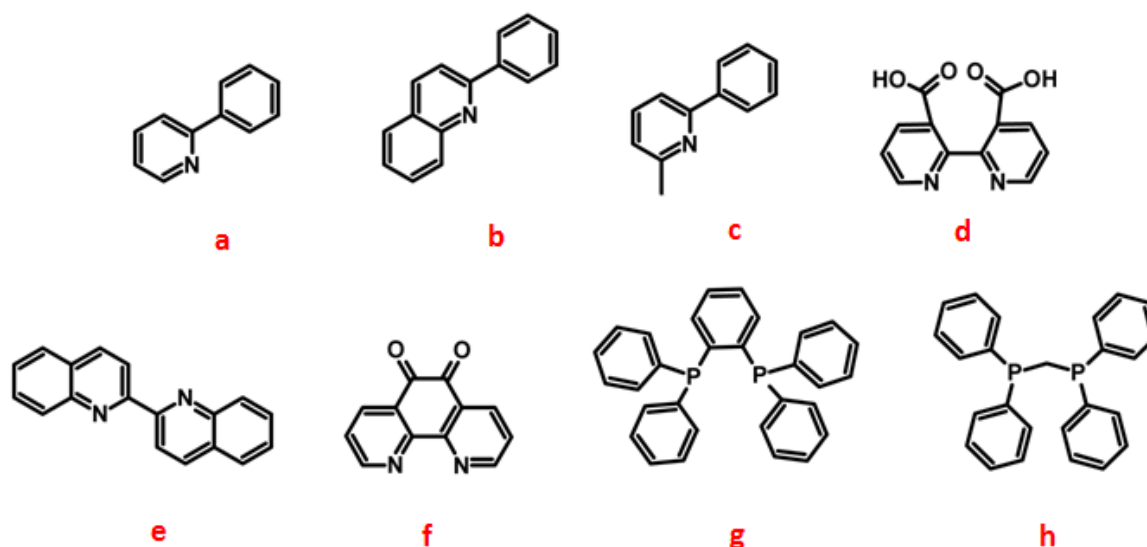

Figure 27. *Other pyridine and phosphine ligands: (a) 2-phenyl pyridine; (b) 2-phenyl quinoline; (c) 2-methyl-6-phenyl pyridine; (d) 2,2-bipyridine-3,3-dicarboxylic acid; (e) 2,2'-bipyridyl; (f) 1,10-phenanthroline-5,6-dione; (g) 1,2-bis(diphenylphosphino) benzene and (h) diphenyl phosphine methane.*

2.4. References

1.	Yam, V.W.-W., W.K.-M. Fung, and M.-T. Wong, *Synthesis, Photophysics, Electrochemistry, and Excited-State Redox Properties of Trinuclear Copper(I) Acetylides with Bis(diphenylphosphino)alkylamines and -arylamines as Bridging Ligands.* Organometallics, 1997. **16**(8): p. 1772-1778.

2.	Diez, J., et al., *Synthesis and characterization of triangulo copper(I) complexes containing mono- and bicapping systems of asymmetric .mu.3-.eta.1-acetylide ligands: molecular structures of [Cu3(.mu.3-.eta.1-C.tplbond.CPh)(.mu.-dppm)3][BF4]2, [Cu3(.mu.3-.eta.1-C.tplbond.CPh)2(.mu.-dppm)3][BF4], and [Cu3(.mu.3-.eta.1-C.tplbond.CPh)(.mu.3-Cl)(.mu.-dppm)3][BF4] [dppm = bis(diphenylphosphino)methane].* Organometallics, 1993. **12**(6): p. 2213-2220.

3.	Babudri, F., et al., *Photochemical tuning of light emission in a conjugated polymer containing norbornadiene units in the main chain.* Photochemical & Photobiological Sciences, 2007. **6**(4): p. 361-364.

4.	Yam, V.W.-W., *Luminescent metal alkynyls – from simple molecules to molecular rods and materials.* Journal of Organometallic Chemistry, 2004. **689**(8): p. 1393-1401.

5.	Long, N.J. and C.K. Williams, *Metal Alkynyl σ Complexes: Synthesis and Materials.* Angewandte Chemie International Edition, 2003. **42**(23): p. 2586-2617.

6.	Cade, I., et al., *Synthesis and spectroscopy of anthracene-containing linear and 'T'-shaped π-conjugated ligands.* Journal of Organometallic Chemistry, 2006. **691**(7): p. 1389-1401.

7.	Min, J., et al., *Neutral copper(i) phosphorescent complexes from their ionic counterparts with 2-(2[prime or minute]-quinolyl)benzimidazole and phosphine mixed ligands.* Dalton Transactions, 2011. **40**(3): p. 686-693.

8.	Zhang, Q., et al., *Highly Efficient Green Phosphorescent Organic Light-Emitting Diodes Based on CuI Complexes.* Advanced Materials, 2004. **16**(5): p. 432-436.

9.   Zhang, Q., et al., *Highly Efficient Electroluminescence from Green-Light-Emitting Electrochemical Cells Based on CuI Complexes.* Advanced Functional Materials, 2006. **16**(9): p. 1203-1208.

10.   Koga, Y., et al., *Synthesis, Structures, and Unique Luminescent Properties of Tridentate C∧C∧N Cyclometalated Complexes of Iridium.* European Journal of Inorganic Chemistry, 2011. **2011**(18): p. 2869-2878.

11.   Kuang, S.-M., et al., *Synthesis and Structural Characterization of Cu(I) and Ni(II) Complexes that Contain the Bis[2-(diphenylphosphino)phenyl]ether Ligand. Novel Emission Properties for the Cu(I) Species.* Inorganic Chemistry, 2002. **41**(12): p. 3313-3322.

Chapter 3: Optical, thermal and electrochemical Properties of novel trinuclear and mononuclear copper (I) complexes

3.1. Introduction

This chapter discusses the optical, thermal and electrochemical properties of the synthesised copper (I) complexes, the preparation was described in Chapter 2. The properties were investigated to understand the emission of the novel complexes and compare them with previously published complexes for organic light emitting diodes (OLEDs). There are three main aspects to define the complexes as suitable material for OLEDs: the optical, the thermal and the electrochemical characterisation.

3.2. Photochemical studies

The photophysical properties of the novel complexes, which have been synthesised by the method outlined in the previous chapter, were investigated by UV-vis absorption and emission.

Absorption spectra were measured on a PerkinElmer Lambda 650S spectrometer, , the emission spectra were measured on a spectrofluorimeter Fluorolog-3, Horiba Jobin Yvon and the lifetime curves were recorded in "phosphorimeter" mode, using a pulsed white lamp as excitation source.

3.2.1. Trinuclear copper (I) complexes

3.2.1.1. UV-vis absorption properties

The absorption spectra of complexes 2 to 8 were recorded at room temperature in 10^{-5} M dichloromethane solutions, (Graph 1) and in processed films with 4% poly(methylmethacrylate) (PMMA) by spin coating (Graph 2).

There are two main regions in the spectra (Table 3). The intense bands (range of ε = 2 - 3 x 10^4 M^{-1} cm^{-1}) at high energy (200 - 325 nm) are assigned to the transitions between the molecular orbital π and π^* [1], which appear to depend on the alkynyl ligands present, as reported in previous spectroscopic works on other transition metal alkynyl systems [2]. The highest energy absorptions are due to singlet-to-singlet metal-to-ligand charge transfer (^{1}MLCT) and spin-forbidden singlet-to-triplet metal-to-ligand charge transfer (^{3}MLCT) transitions, in a range of ε = 2 - 3 x 10^4 M^{-1} cm^{-1}. This low-energy absorption implies a relatively small singlet-triplet energy gap,

in other words a small HOMO-LUMO exchange integral, consistent with a MLCT transition. The wavelength associated with the MLCT is determined by the degree of conjugation of the alkynyl ligand for these complexes.
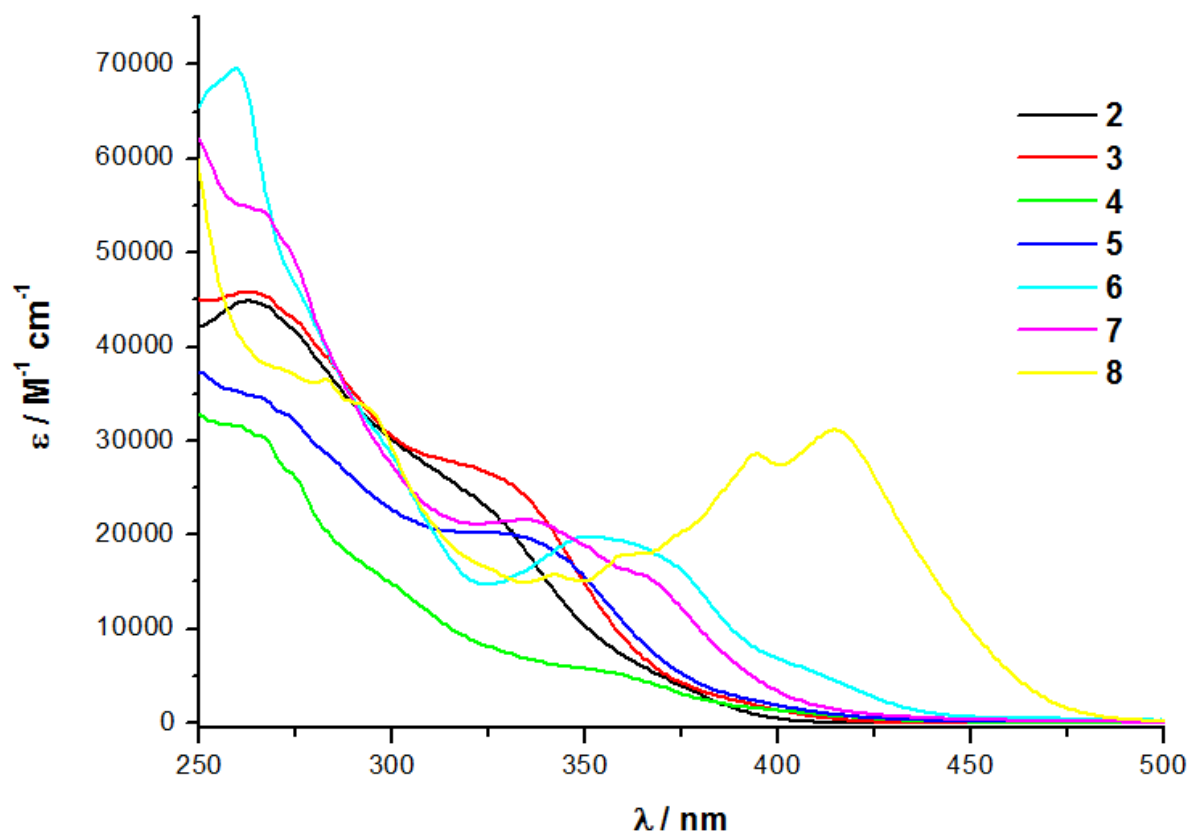
Graph 1. *Absorption spectra of the complexes 2 to 8 in a solution of DCM.*
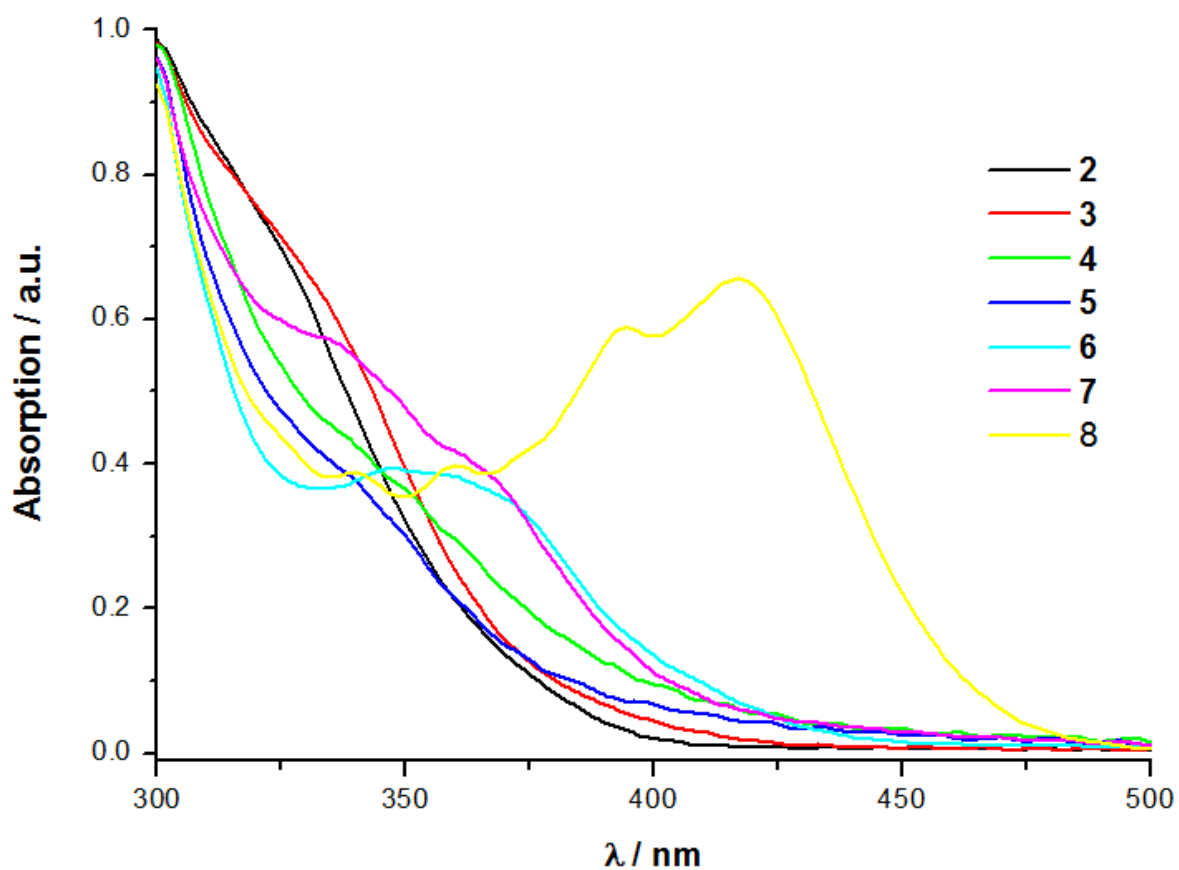
Graph 2. *Absorption spectra of the complexes 2 to 8 which have been processed as amorphous films with 4% PMMA by speed coating.*

Table 3. *Absorption maximum of the complexes 2-8 in a solution of DCM and in 4% PMMA films.*

Complex	$\lambda_{max} \pm 2$ (nm)
2	324; 262
3	329; 262
4	353; 259
5	331; 260
6	351; 259
7	336; 266
8	414; 283

3.2.1.2. Emission properties

The emission properties were analysed by three parameters: λ maximum emission, quantum yield (Φ) and lifetime (τ) [3] (Table 4). The trinuclear copper (I) alkynyl complexes have shown luminescence in solid state and solution. As in the case of other reported copper complexes, in order to obtain the emission spectra, the solutions were degassed the emission as the presence of oxygen quenches [4].

Moreover, significant Stoke shifts for complexes 5-8 between the high wavelength of the MLCT absorption band and the emission maximum. Complexes 2-5 show emission $\lambda_{maximum}$ between 490 - 527 nm. The effect of the fluorine and trifluoromethyl groups in different positions on the phenyl ligand lead to different emission properties and tune of the emission. As well, these groups of electron withdrawing substituent on the phenyl ring does not contribute to shift significantly the emission to higher frequency, unlike in the case of iridium (III) cyclometallated coordination complexes [1, 6].

The copper (I) complexes, 2-8, showed an emission from 490 to 678nm, with the emission energy dependent on the electron-donating ability of the alkynyl ligand, as displayed in Graphs 3 and 4. The origin of the emission has been proposed to involve a mixture of the triplet ligand-to-metal charge transfer (LMCT) [alkynyl→Cu$_3$] alkynyl character, metal centered $3d^9 4s^1$ character which could be modified by copper-copper interaction and mixing of a ligand centrered π-π* (alkynyl) excited state is also involved which is due to the π-conjugation effect [5].
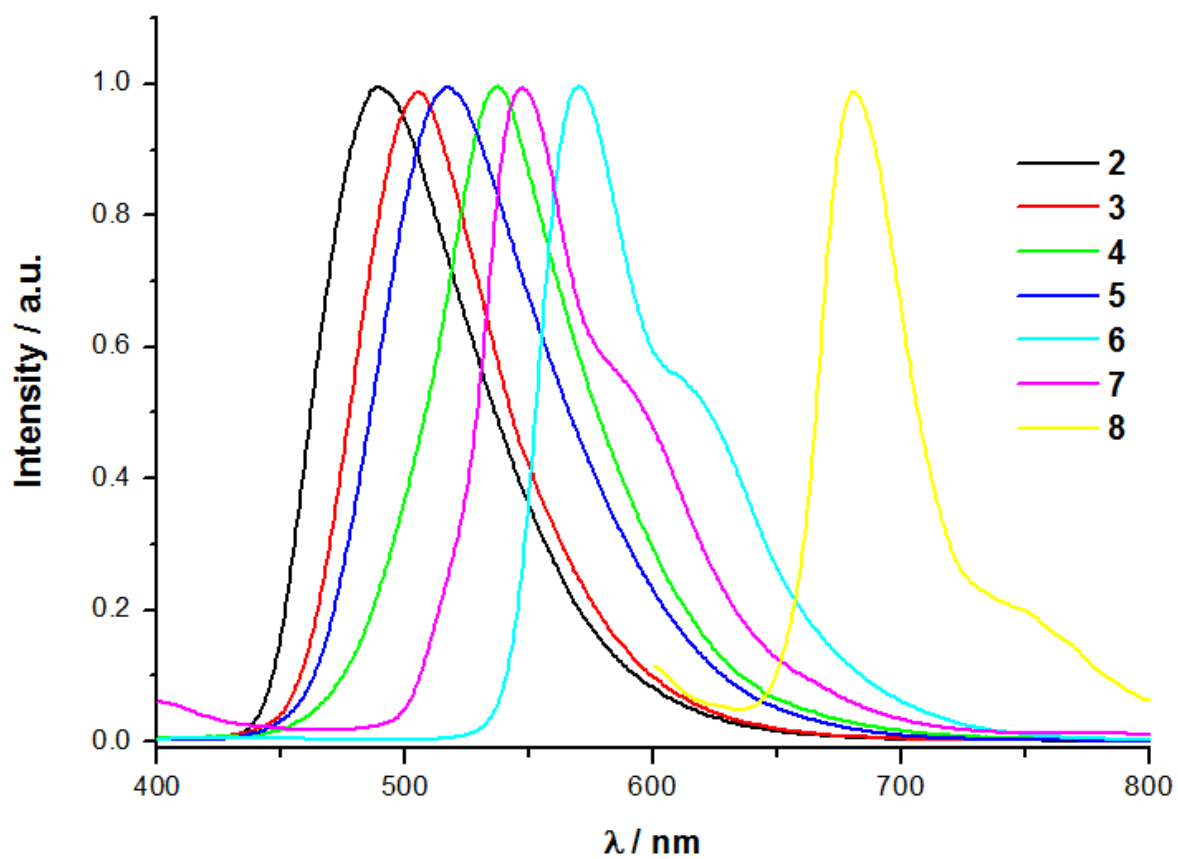
Graph 3. *Emission spectra of the complexes 2 to 8 in a solution of DCM.*
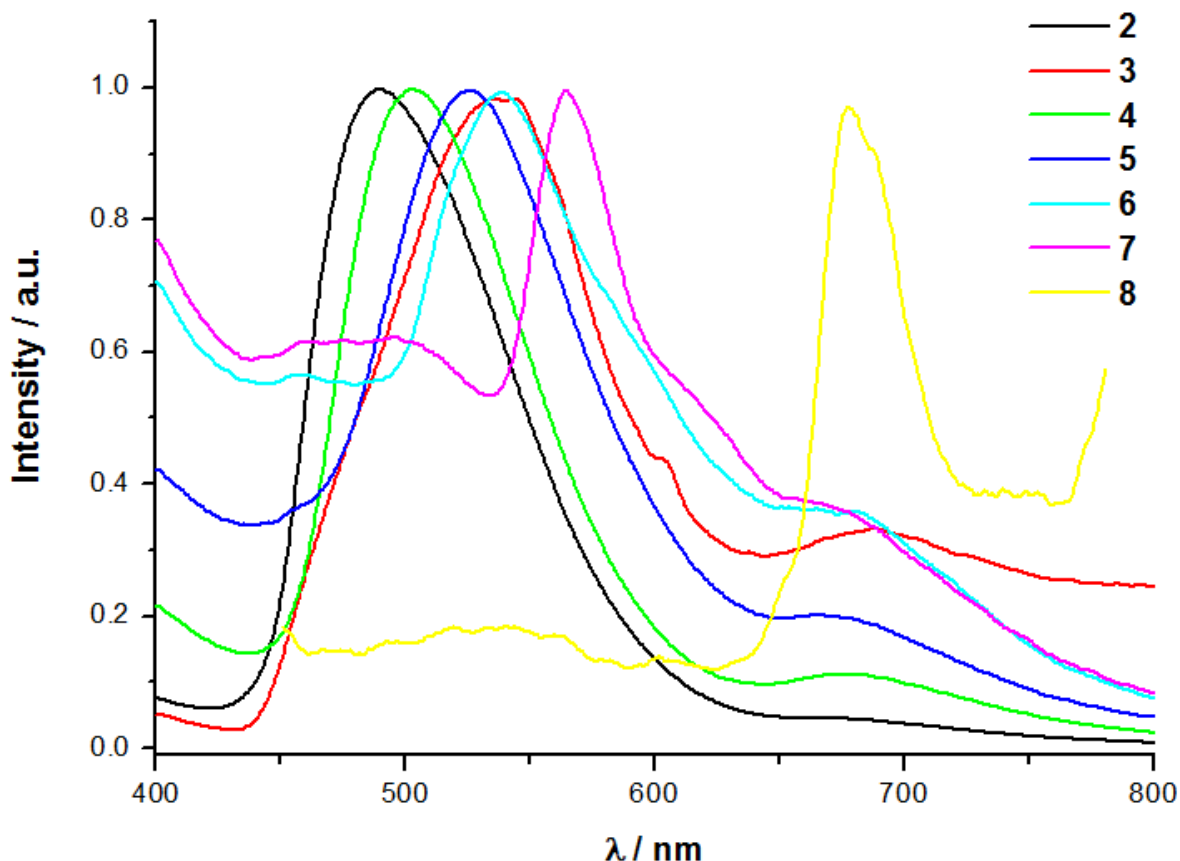
Graph 4. *Emission spectra of the complexes 2 to 8 which have been processed as amorphous films with 4% w/w PMMA by spin coating.*

Complexes 6-8, show an emission $\lambda_{maximum}$ between 547 – 678 nm. The presence of extended π-conjugated systems on the alkynyl ligand contributes to shift the emission to higher wavelengths (bathochromic shift), in agreement with other reported transition metal system [7].

Quantum yield calculations showed the fraction of molecules that emit a photon after direct excitation by a light source. They were calculated for each complex using the Equation 1, where quinine sulphate in 0.5M H_2SO_4 as standard reference and an integrating sphere were used. All the quantum yields were measured at their respective excitation wavelength for the sample and the reference, cancelling the $I(\lambda_r)/I(\lambda_x)$.

$$\Phi_x = \Phi_r \left[\frac{A_r(\lambda_r)}{A_x(\lambda_x)} \right] \left[\frac{I_r(\lambda_r)}{I_x(\lambda_x)} \right] \left[\frac{n_x^2}{n_r^2} \right] \left[\frac{D_x}{D_r} \right]$$

Equation 1. *Formula to calculate luminescence quantum yield, where A is the absorbance at the excitation wavelength (λ); I is the intensity of the excitation light at the excitation λ; n is the refractive index of the solvent; D is the integrated intensity of the luminescence; r is the reference; x is the sample and λ is the wavelength.*

Table 4. *Parameters of the emission spectroscopy of the complexes 2-9: λ maximum emission, quantum yield (Φ) and lifetime (τ).*

Complex	$\lambda_{max} \pm 2$ (nm)	$\Phi \pm 0.1$ (%)	$\tau \pm 0.5$ (µs)
2	490	1.7	35
3	507	24.0	105
4	527	57.4	88
5	519	14.4	67
6	570	19.9	976
7	547	27.3	525
8	678	N.A.	216

One of the main requirements for phosphorescent material for OLEDs is that they should exhibit very high quantum yield [8]. The complexes show a range of quantum yield from 1.7 to 57.4 %. This range could be divided into two groups: for complexes 3, 4 and 7 the values are all high (>20 %), while for complexes 2, 5 and 6 the values are lower. As it is shown in the Table 1, the complexes, which possess electron-rich subtituents on position 3 and 5 of the phenyl ring (complexes 3 and 4) or π-conjugated systems (complex 7), experience a positive effect on their emission quantum yield. However, when the position of the electron-rich subtituent changes on the phenyl ring, such as in the position 2 and 4 or in the position *para*-, complexes 2 and 5 exhibit a low quantum yield. Moreover, complexes 2-5 show higher quantum yields than their unsusbtitued equivalent benzene trinuclear complex, which suggest the beneficial effect of fluorine atoms on the π-conjugated system attached to the alkynyl ligand.

The lifetimes are in the µs range, which indicate a spin-forbidden triplet origin [9]. As well, the lifetime of the complexes can be divided in two groups: complexes 2-

5 show an excited-state lifetime which is similar to other metal complexes while complexes 6-8 show a lifetime significantly longer than complexes 2-5. These long lifetimes are a consequence of the d^{10} configuration of the copper (I) metal, which provide stabilisation of the excited states via the ligand field and consequently charge transfer and intraligand transitions [5]. Some of the lifetime curves are shown on the graphs 5 and 6 .All the lifetime curves can be seen in the Appendix 1.
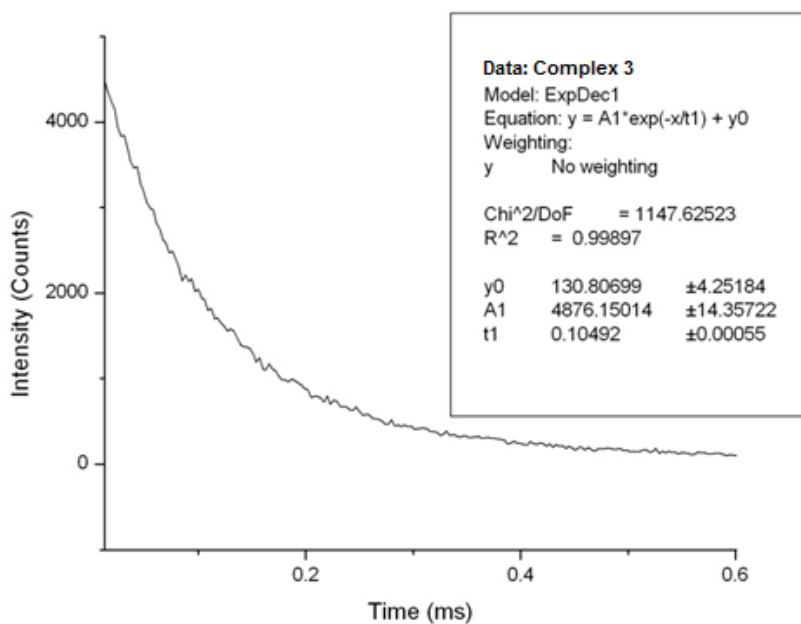
Graph 5. *Lifetime curve of trinuclear copper complex 3 which possess 1-ethynyl-3,5-difluorobenzene as alkynyl ligand.*
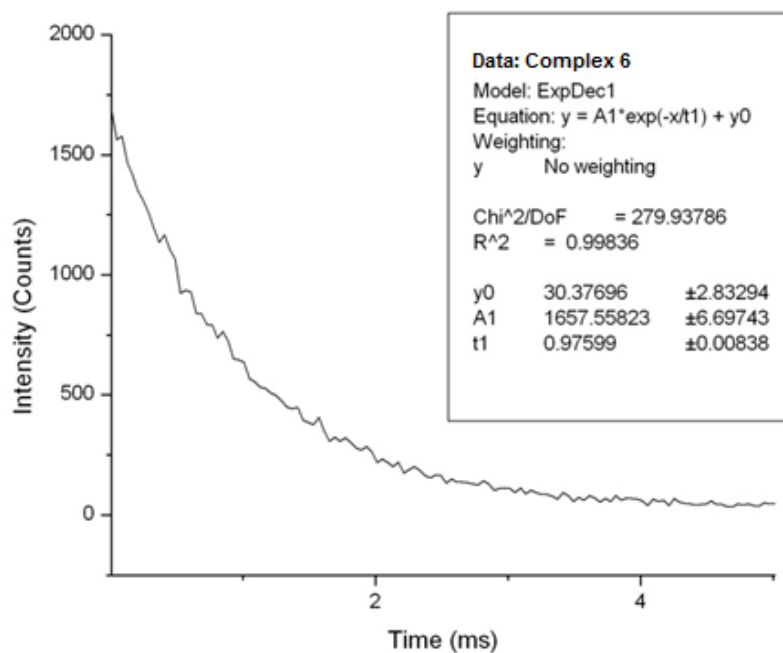
Graph 6. *Lifetime curve of trinuclear copper complex 6 which possess 9-ethynylphenanthrene as alkynyl ligand.*

Some of the complexes were exposed under a UV lamp; the figure shows the emission of these complexes (Figure 1).
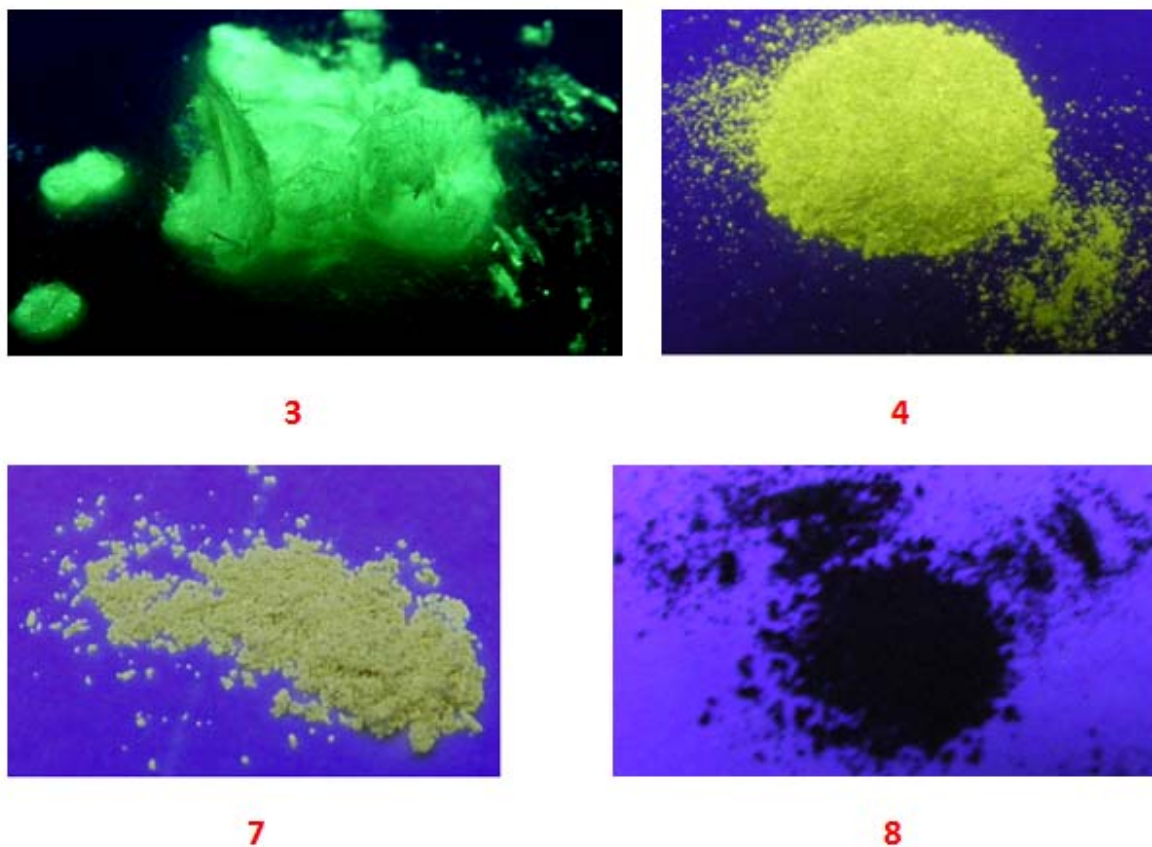
Figure 28. *Complexes, 3, 4, 7 and 8, were exposure under an UV lamp at 365nm.*

3.2.2. Mononuclear copper (I) complexes

3.2.2.1. UV-vis absorption properties

The electronic absorption spectra of the complexes 9-16 in dichloromethane (DCM) are displayed in Graph 7. The complexes show intense absorption bands at 280nm (ε = 10000 – 50000 l mol^{-1} cm^{-1}), which are assigned to the π-π* transition on the aromatic ligands (Table 5). The less intense absorption band is centred around 370nm (1-5000 l mol^{-1} cm^{-1}), is attributed to metal-to-ligand charge transfer (MLCT) absorption, which possess a magnitude of the extinction coefficient expected for a dπ-π* transition. Both bands were predicted by previously investigated analogous [Cu(NN)(PP)]$^{+}$ complexes, which contain bipyridine and phosphine ligands [10].

The absorption spectra of the complexes in PMMA film could not be measured, as it was not reproducible.
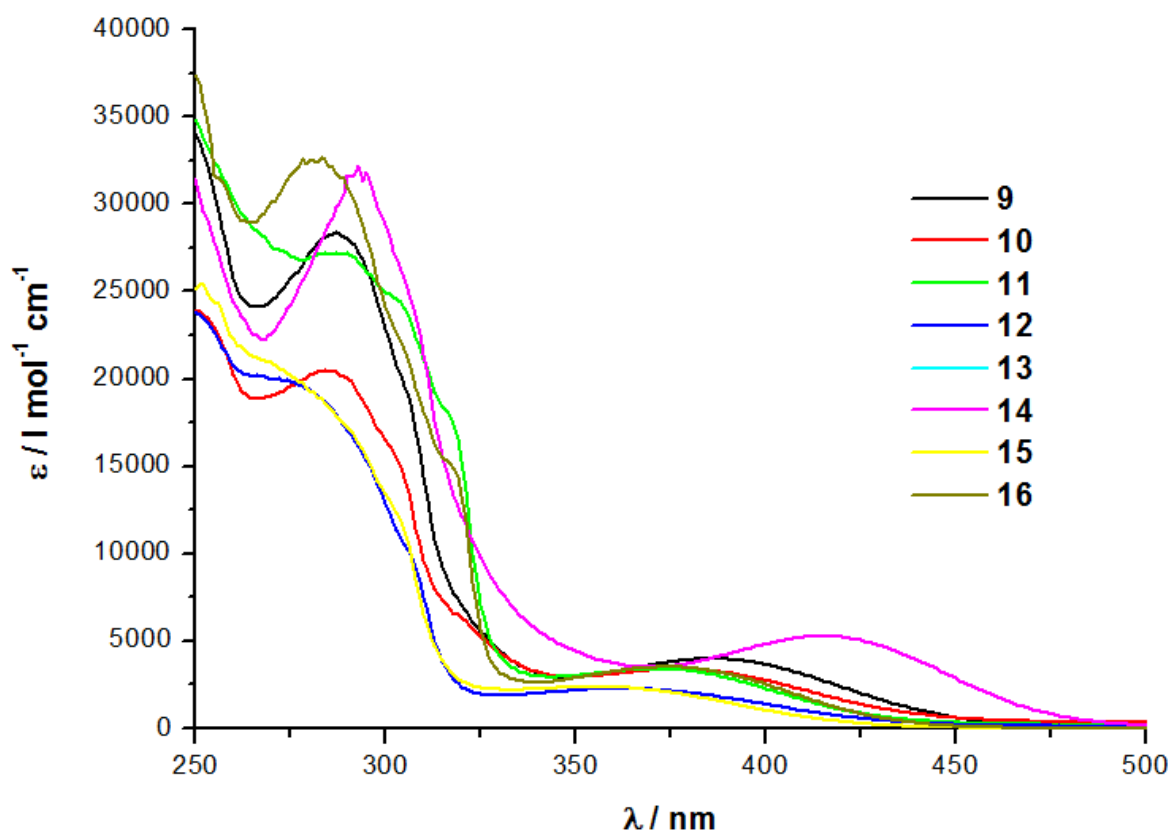
Graph 7. *Emission spectra of the complexes 9 to 16 in a solution of DCM.*

Table 5. *Absorption maximum of the complexes 9-16 in a solution of DCM.*

Complex	$\lambda_{max} \pm 2$ (nm)
9	385; 287
10	377; 284
11	372; 286
12	357; 270
13	354; 264
14	382; 281
15	375; 280
16	375; 282

3.2.2.2. Emission properties

In order to get the optical properties of this range of mononuclear complexes, they were processed in films with poly(methylmethacrylate), 5% w/w PMMA by spin coating. These complexes, as other previously reported, exhibit higher phosphorescence in solid state than that in solution because of the absence of solvent-induced quenching [8, 11, 12].

Their optical properties are shown in Table 6. All complexes show emission bands attributable to deactivation from π-π* excited levels (Graph 8). As the trinuclear copper (I) complexes, these mononuclear complexes exhibit considerable Stokes shifts, where the emission absorption gap is frequently larger than 150 nm.
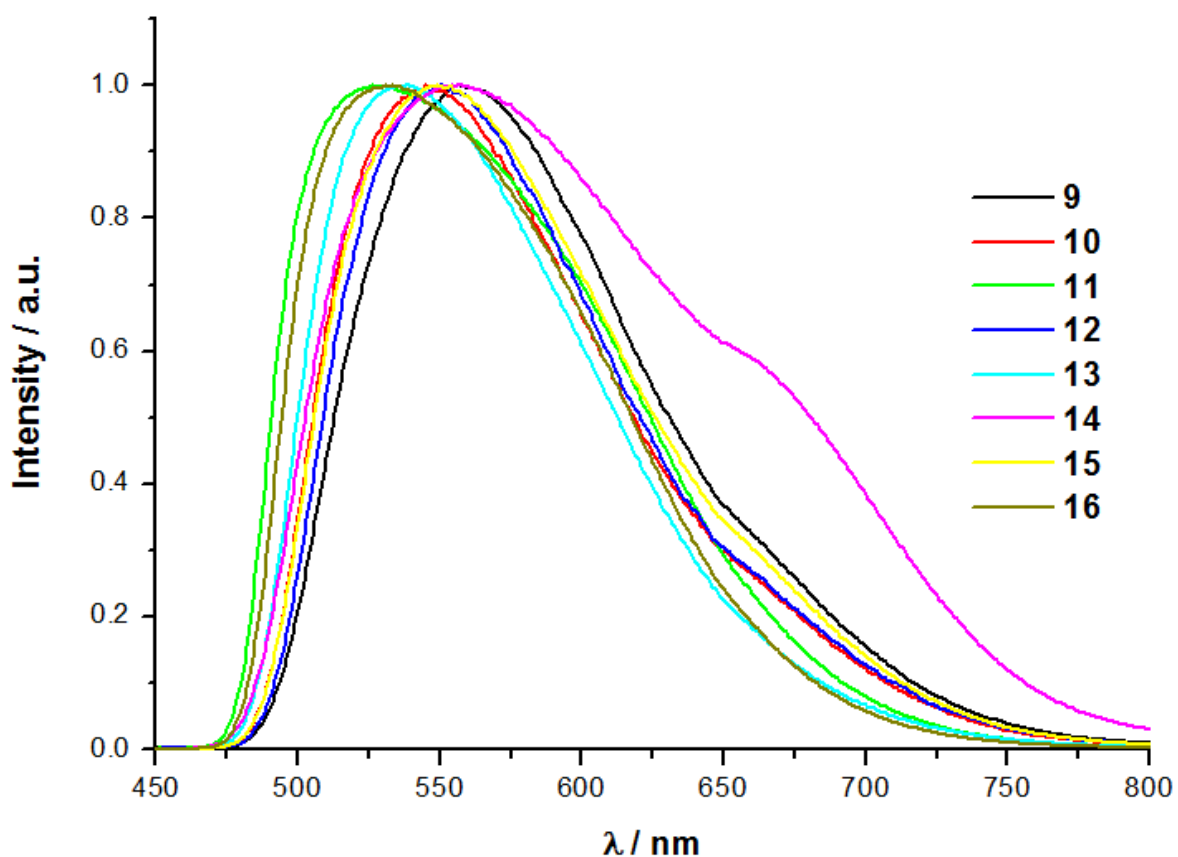
Graph 8. *Emission spectra of the complexes 9-16 which have been processed as amorphous films with 5% w/w PMMA by speed coating.*

Table 6. *Parameters of the emission spectroscopy of the processed complexes 9-16 in films with 5% w/w PMA by speed coating: λ maximum emission, quantum yield (Φ) and lifetime (τ).*

Complex	$\lambda_{max} \pm 2$(nm)	$\Phi \pm 0.1$(%)	$\tau \pm 0.5$ (µs)
9	559	3.3	9.7
10	544	0.3	11.2
11	528	14.5	15.7
12	550	0.4	10.0
13	537	0.2	10.7
14	560	0.1	11.5
15	558	1.1	10.7
16	530	33.3	15.1

All the complexes exhibit emission bands attributable to deactivation from MLCT excited levels as other reported copper complexes [4].These complexes show a relative short range of emission, from 528 to 560 nm. Complexes 9, 11 and 14, which carry a pyridine ligand without subtituents, show a red shifted emission, while complexes 11 and 16, which carry methyl groups in position 6 and 6' of the pyridine ligand, exhibit a blue shifted emission. These results indicate the effect of substituents of the bipyridyl ligands on the emission; the steric impediment of methyl groups in position 6 and 6' produce different optical characteristics than the rest of the complexes. In Figure 29, the emission of some of the complexes could be observed by exposing them under a UV lamp at 365 nm.
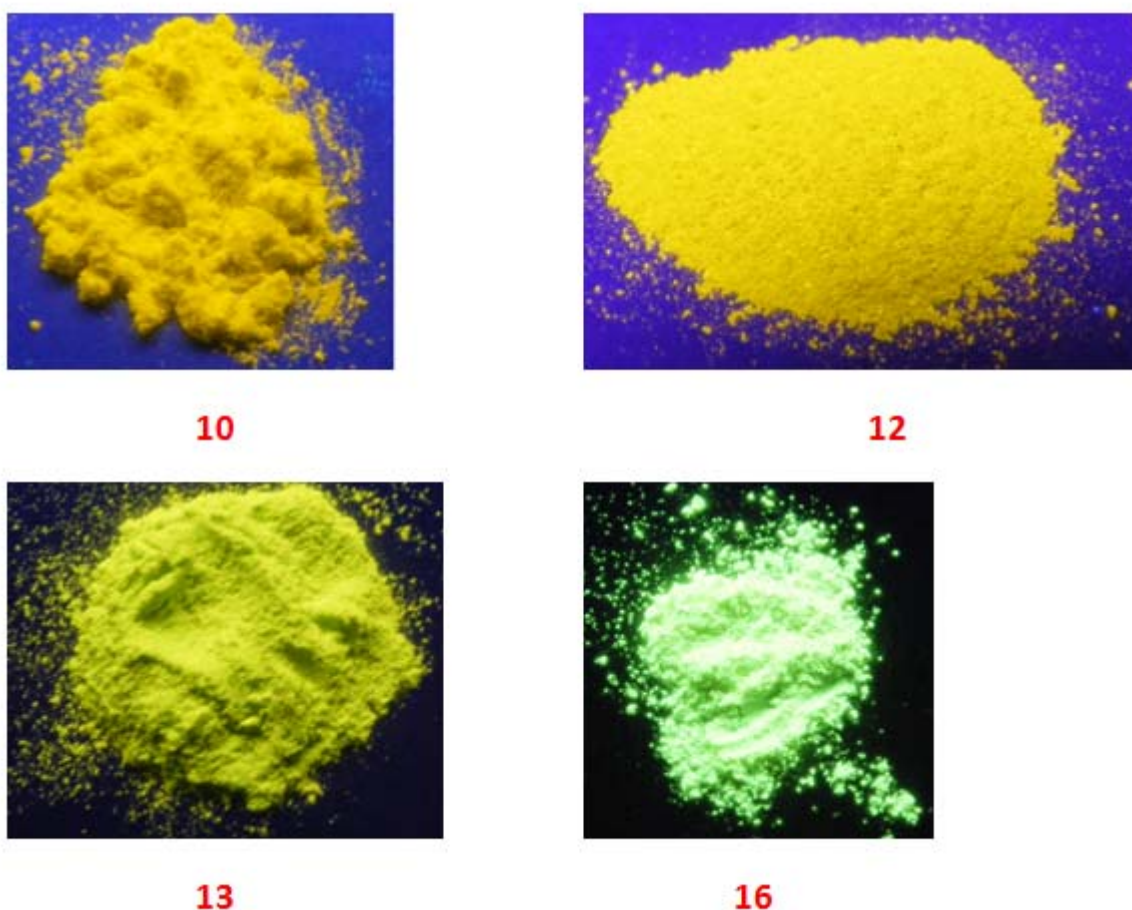
Figure 29. *Complexes, 10, 12, 13 and 14, were exposure under an UV lamp at 365nm.*

The quantum yield of photoluminescence was measured using an integrating sphere and following the method published by Porrès et al. [13]. Comparing the complexes with different pyridine ligands, incorporating methyl susbtituents in the 6 and 6' positions of the 2,2'-bipyridine ligands leads to an increased quantum yields

and excited-state lifetime. The importance of the steric impediment is shown in the results of the quantum yields and lifetime.

Lifetime measures were performed three times for each complex for consistency, some of them are shown on the graphs 9 and 10. Lifetime of all the complexes is shown in Appendix 2.
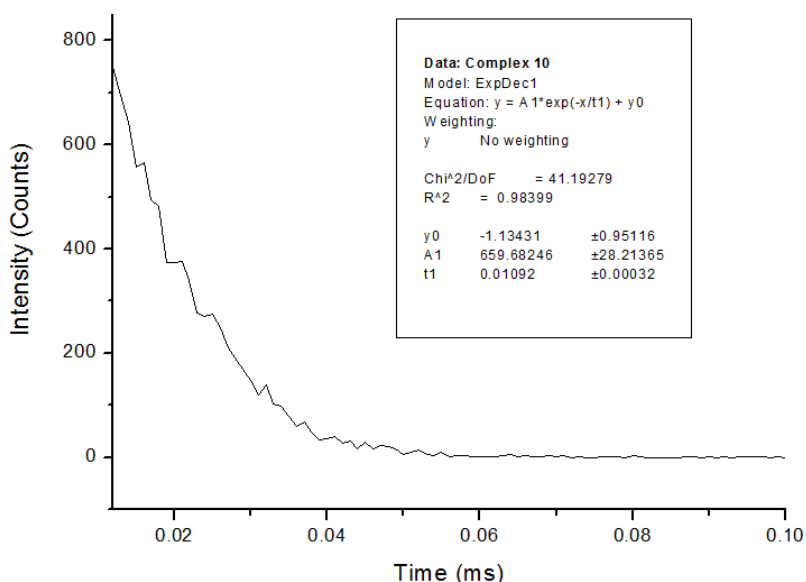
Graph 9. *Lifetime curve of mononuclear copper complex 10 which possess 4,4'-dimethyl-2,2'-bipyridyl as pyridine ligand and bis-(diphenylphosphinophenyl)ether as phosphine ligand.*
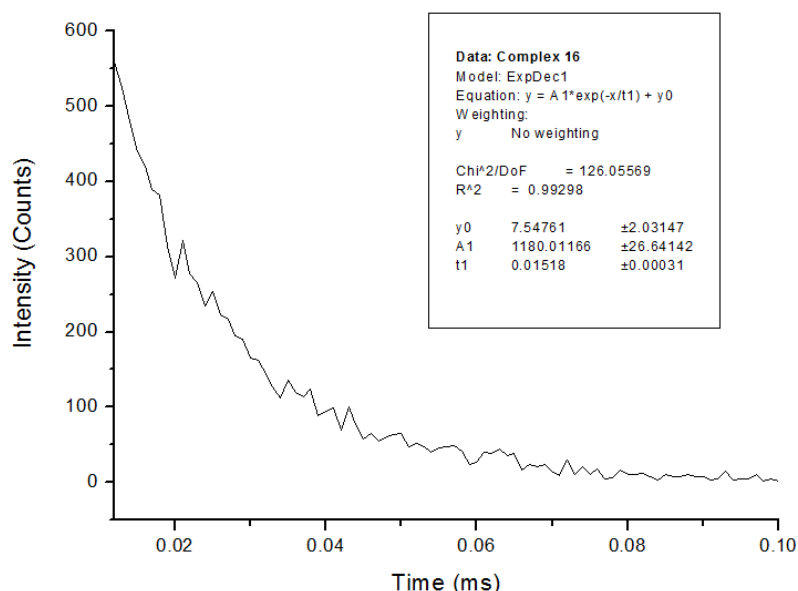
Graph 10. *Lifetime curves of mononuclear copper complex 16 which possess 6,6'-dimethyl-2,2'-bipyridyl as pyridine ligand and 9,9-dimethyl-4,5-bis(diphenylphosphino) xanthene as phosphine ligand.*

3.3. Study of the thin films by scanning electron microscopy (SEM)

Recently, studies have found an interesting phenomenon: the electroluminescence increased with an increasing thickness of the light-emiting layer [14]. A study of electroluminescence from fac-tris-(2-phenylpyridine) iridium, with 4,4'-bis(9-carbazolyl)-1,1'-biphenyl (CBP) as host, indicated that carrier transport and recombination guest-host processes change depending on EML thickness [15]. Some studies have shown the influence of the thickness and its control for WOLEDs [16]. Ultrathin emitting layers were reported [17-19], where the produced devices showed a strong dependency on the thickness of ultrathin EML. The thickness of EML effects not only the operating voltage but also the emission characteristics and efficiencies. Thinner EML layers reduce the voltage of the device, but decrease the efficiency. In contrast, other studies have reported devices with thicker EML exhibits high voltage, low luminescence and low efficiency as the charge carrier quenching. As conclusion, it has been assumed that the amount of phosphorescent material is the main factor which controls the electroluminescence of these devices [20, 21].

Films which contained the trinuclear or mononuclear copper complexes were analysed by scanning electron microscopy (SEM) in order to measure the thickness and concentration. The luminescence of the processed films of trinuclear copper (I) complexes, with 2 % w/w PMMA and made by spin coating, could not be measured, as it was not detected. As a consequence, mononuclear copper (I) complexes were processed with 5 % w/w PMMA and the thickness increased. The SEM shows the morphology of one of these films (Figure 30 to 32). The thicknesses were estimated around 1 μm (Figure 33). These results show the effect of the thickness on their luminescence and their quantum efficiency.
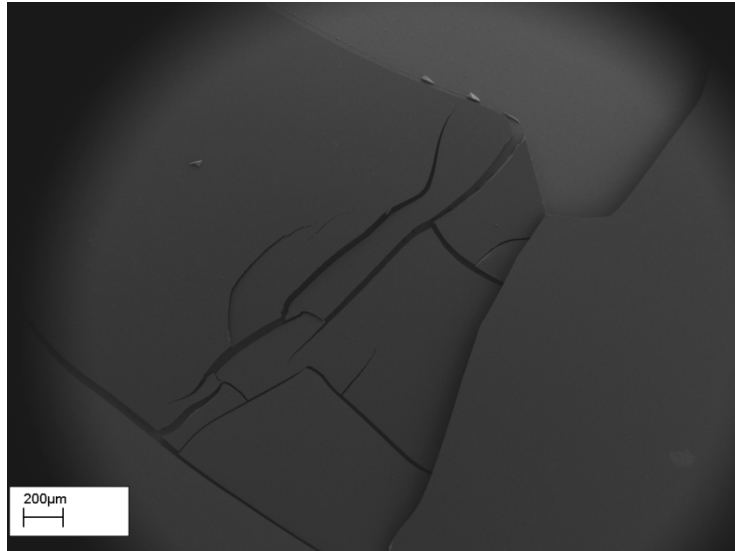
Figure 30. *SEM image of a film of complex which have been processed as amorphous films with 8% w/w PMMA by solution casting at 100 times magnification.*
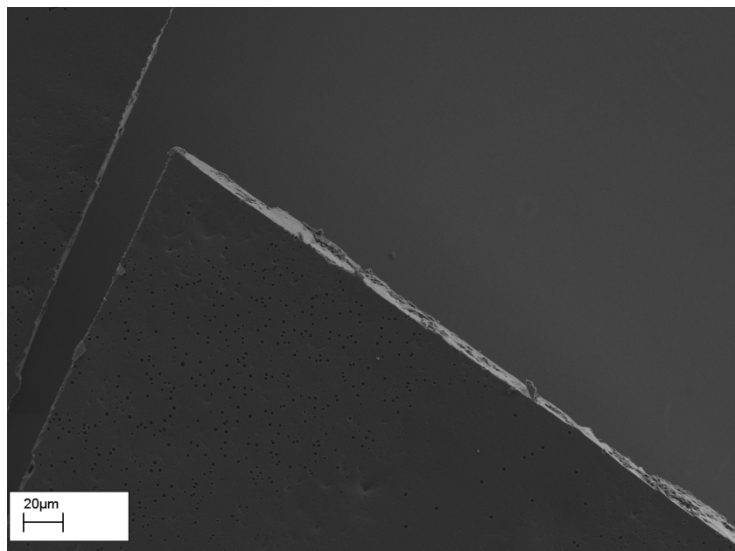
Figure 31. *SEM image of a film of complex which have been processed as amorphous films with 8% w/w PMMA by solution casting at 1000 times magnification.*
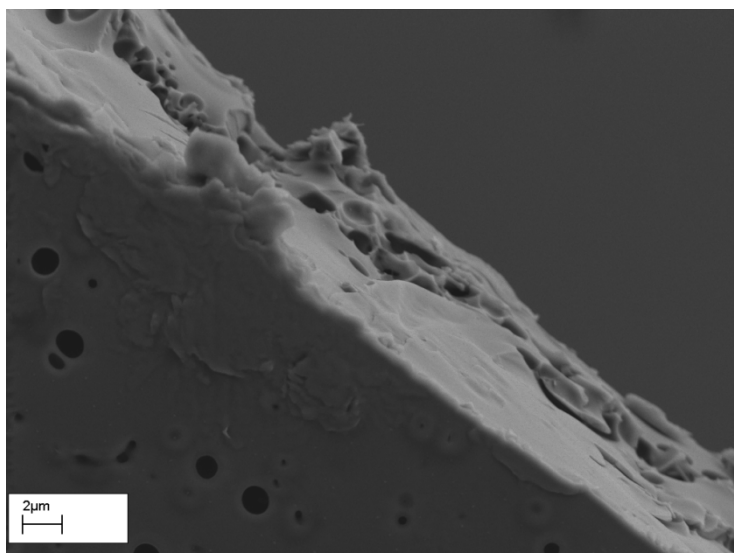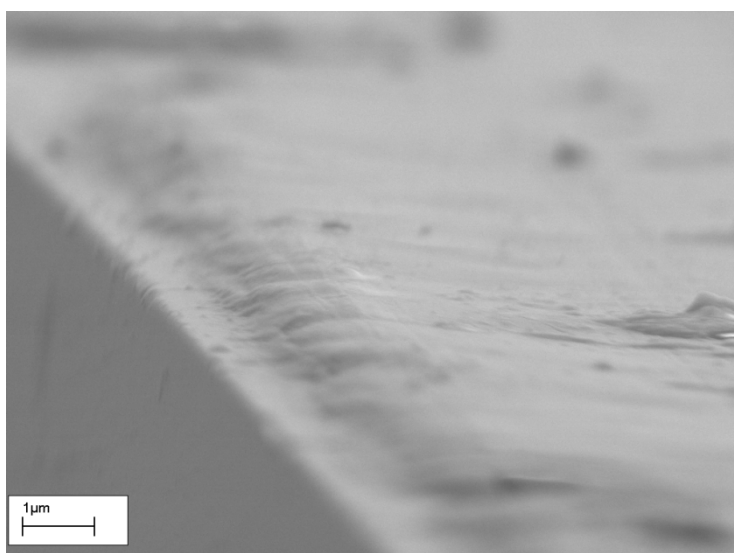
Figure 32. *SEM image of a film of complex which have been processed as amorphous films with 8% w/w PMMA by solution casting at 10000 times magnification.*

Figure 33. *SEM image of a film of the doped complex 16 with PVCz (3:7, dopper:complex), which have been processed as amorphous films by speed coating at 36500 times magnification.*

3.4. Thermal studies

The complexes, mononuclear and trinuclear, were characterised by two thermal techniques: thermogravimetric analysis and differential scanning calorimetry.

3.4.1. Thermogravimetric analysis (TGA)

Thermogravimetric analysis is an experimental technique, which is used in order to obtain the decomposition temperature. In this technique, the mass of the samples is a function of the temperature. A sample of each complex was heated at a constant rate of 10 ^{o}C/min. Additionally, the atmosphere during the experiment was saturated with nitrogen.

Graphs 11 and 12 show the thermogravimetric analisys of the trinuclear and mononuclear copper (I) complexes, respectively. As well, the respective temperatures of decomposition of each complex are shown in the following Tables 7 and 8.

The synthesised trinuclear copper (I) complexes show a very diverse range of decomposition temperatures, from 184 ^{o}C to 269 ^{o}C. Complex 4 is more stable than complex 5, which means that this electron withdrawing subtituent stabilises the complex when they are carried in position 3 and 5 on the phenyl ring. However, the same is not observed when the alkynyl ligand carries the fluorine, in Complexes 2 and 3.
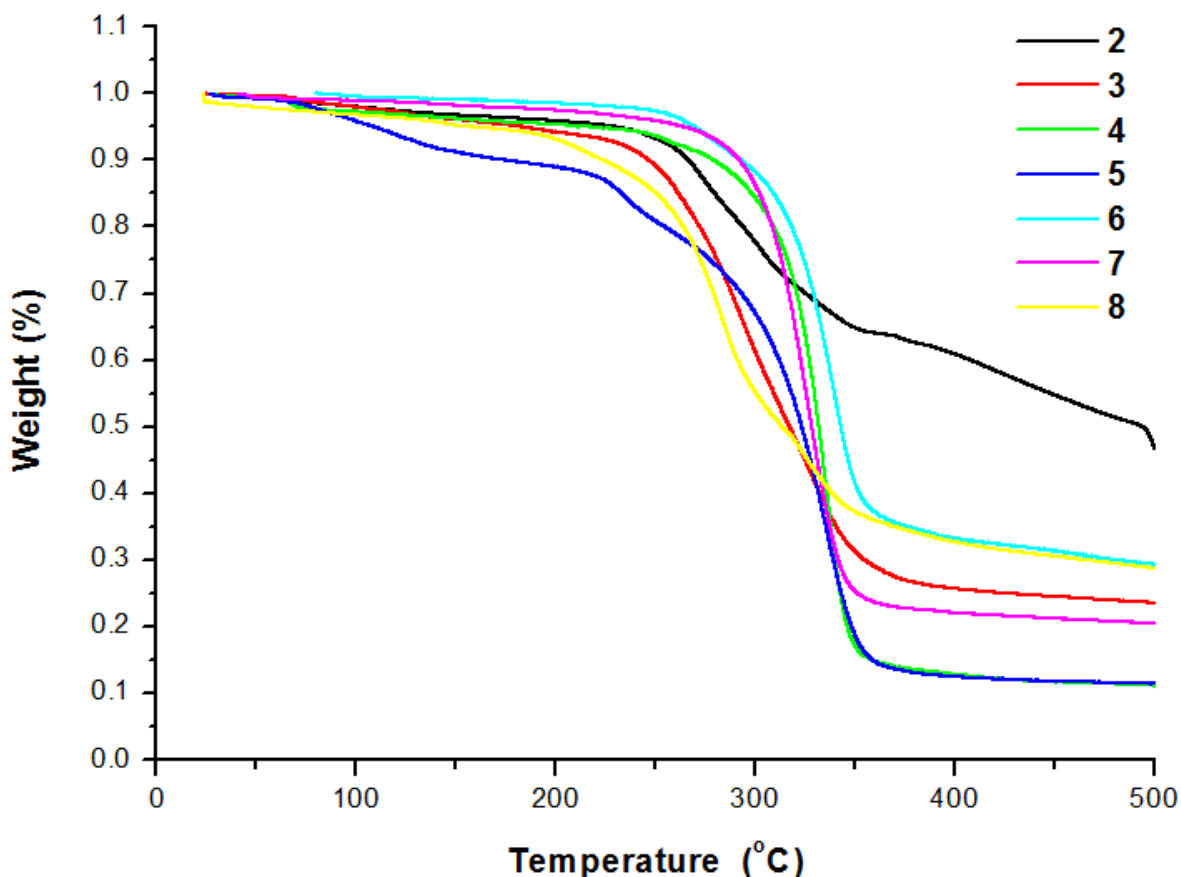
Graph 11. *TGA graphs of complexes 2 to 8.*

Table 7. *Temperature of decomposition of the complexes 2 to 8.*

Complex	T $_{decomp.}$ ± 0.5 (^{o}C)	Weight Lost ± 0.05 (%)
2	229.90	5.03
3	224.66	7.15
4	245.75	6.05
5	214.48	11.93
6	256.17	3.09
7	269.46	5.49
8	184.00	5.78

The range of the decomposition temperatures shown by the mononuclear copper (I) complexes reveals that when triphenylphosphine ligand was used, the complexes are more unstable. In other words, the thermal stability of this range of mononuclear complexes depends on the phosphine ligand.
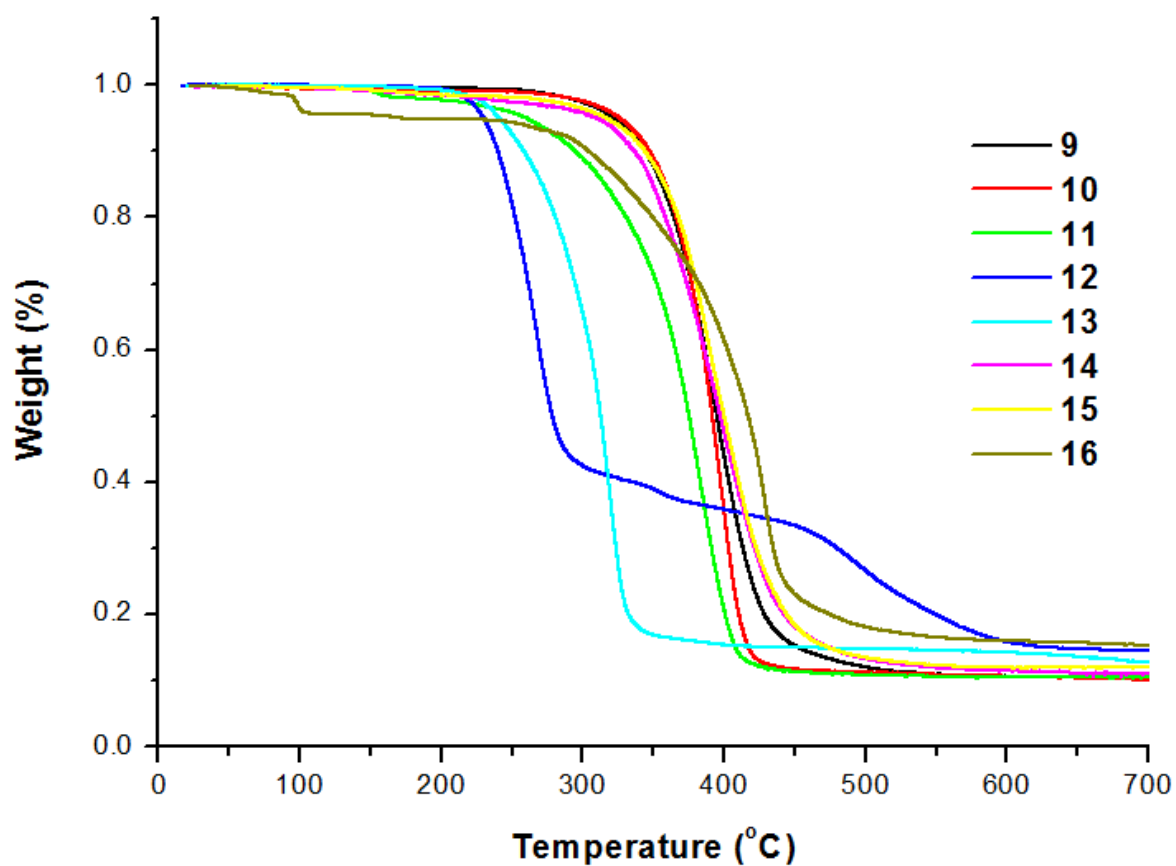
Graph 12. *TGA graphs of complexes 9 to 16.*

Table 8. *Temperature of decomposition of the complexes 9 to 16.*

Complex	T $_{decomp.}$ ± 0.5 (^{o}C)	Weight Lost ± 0.05 (%)
9	310.00	4.93
10	257.55	5.60
11	226.95	3.80
12	212.00	7.73
13	205.09	5.66
14	290.64	2.16
15	272.08	3.36
16	246.25	6.19

3.4.2. Differential scanning calorimetry (DSC)

Differential scanning calorimetry was the second thermal analysis used to characterise the obtained complexes. In this analysis, we measure the energy changes that occur when we heated, cooled or held the sample at constant temperature. The starting temperature for each complex, was room temperature and the highest temperature was bellow the decomposition temperature, which was obtained by TGA. The scan heating rate was 10 ^{o}C/min and the cooling rate was 5 ^{o}C/min.

Melting point or recrystallisation peaks were not detected in any of the trinuclear Complexes 2 to 8, which indicates an irreversible thermal behaviour. However, some thermal peaks were detected such as an endothermic peak around 70 ^{o}C in all the complexes (Table 9), less the labelled Complex 2. Complexes 3, 5, 7 and 8 show a glass transition (T_{g}), during the cooling step, as it is the reversible transition for these amorphous materials. All the graphs are shown in the Appendix 3.

Table 9. *Signal detectable by scanning differential calorimetry for the complexes 2 to 8, where T_{exo} is the temperature of an exothermic peak, T_{endo} is the temperature of a endothermic peak and T_g is the temperature of the glass transition.*

Complex	Heating Step	Cooling Step
2	T_{endo} = 109.51 ^{o}C T_{endo} = 189.54 ^{o}C	-
3	T_{endo} = 73.20 ^{o}C T_{exo} = 173.30 ^{o}C	T_g = 91.87 ^{o}C
4	T_{endo} = 53.49 ^{o}C T_{endo} = 81.00 ^{o}C T_{exo} = 166.13 ^{o}C	T_{exo} = 196.13 ^{o}C
5	-	T_g = 52.82 ^{o}C
6	T_{endo} = 68.63 ^{o}C T_{exo} = 165.43 ^{o}C T_{endo} = 224.12 ^{o}C	-
7	T_{endo} = 65.38 ^{o}C T_{endo} = 139.93 ^{o}C T_{endo} = 197.44 ^{o}C	T_g = 112.37 ^{o}C
8	T_{endo} = 63.61 ^{o}C T_{endo} = 141.37 ^{o}C	T_g = 130.53 ^{o}C

The DSC analysis of Complexes 9 to 16 show different thermal peaks. Table 10 and the graphs in the Appendix 4 show a detectable melting point for Complexes 9 and 16, which is significanty higher for Complex 16, probably induced by a distorted geometry. A recrystallisation could not be detected for any of the complexes, which indicates their irreversible thermal behaviour.

Table 10. *Signal detectable by scanning differential calorimetry for complexes 9 to 16, where T_{exo} is the temperature of an exothermic peak, T_{endo} is the temperature of an endothermic peak, T_{melt} is the temperature of the melting point and T_g is the temperature of the glass transition.*

Complex	Heating Step	Cooling Step
9	T_{exo} = 189.91 ^{o}C T_{endo} = 217.98 ^{o}C T_{melt} = 246.50 ^{o}C	T_g = 108.86 ^{o}C
10	T_{endo} = 132.35 ^{o}C T_{exo} = 186.02 ^{o}C	-
11	-	T_g = 109.51 ^{o}C T_g = 144.95 ^{o}C
12	-	-
13	T_{exo} = 158.00 ^{o}C	-
14	-	-
15	-	-
16	T_{melt} = 106.42 ^{o}C	-

3.5. Processed fibres

The complexes were extruded as dopants in a polypropylene matrix,. This polymer was doped with 1 % w/w of the complexes and processed in a Haake MiniLab co-rotating twin screws extruder at 200 ^{o}C. The extruded material was manually pulled into a fibre of 1mm thickness. Bright emission was shown by the fibres under UV excitation at 360 nm (Figure 34), it demonstrates their stability at high temperature.
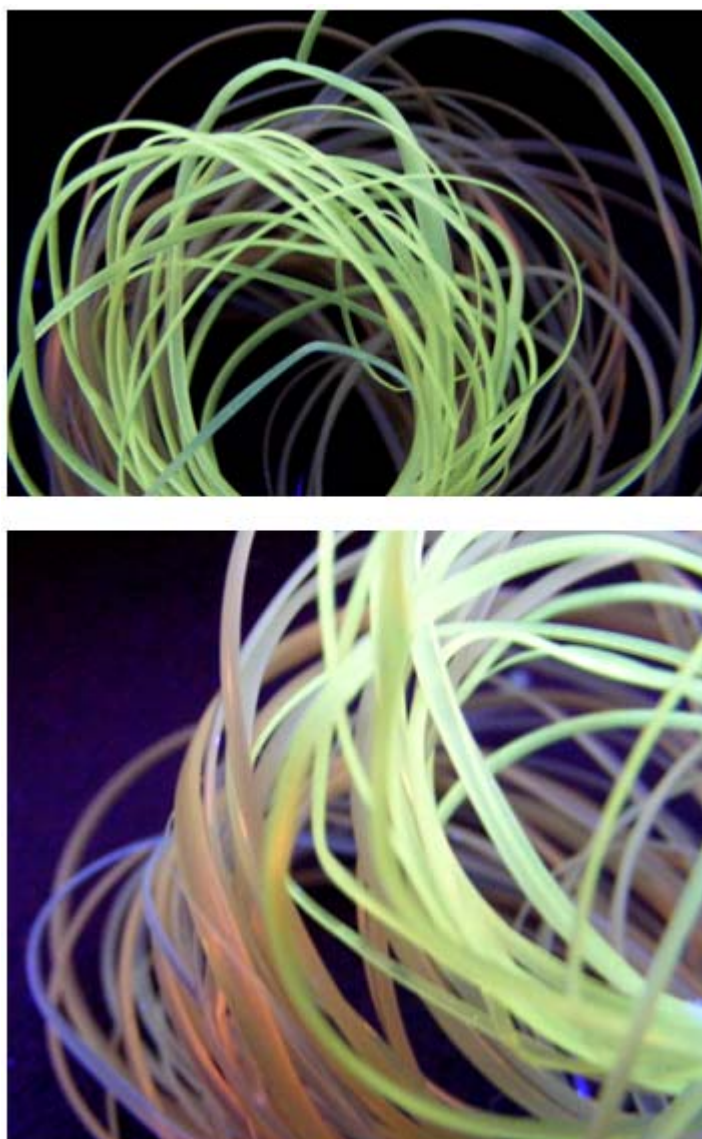
Figure 34. *Extruded phosphorescent polypropylene doped with complexes 16 (green) and 10 (orange).*

3.6. Electrochemical studies

The electrochemical properties of synthesised copper complexes were measured by cyclic voltammetry (CV). This method has provided valuable information regarding the stability of the oxidation states and the rate of electron transfer between the electrode and the electrolyte (tetrabutilamonium hexafluorophosphate, TBAH). The voltage was linearly varied from an initial (2000 mV) to a final potential (-2000 mV) and immediately swept back at the same sweep rate to the initial. The potential was applied to the working electrode (graphite electrode) with respect to a reference electrode (AgCl/Ag), while an auxiliary electrode (platinum electrode) was used to complete the electrical circuit.

Ferrocene (bis-cyclopentadienyl iron (III)) was used as standard reversible process as the rate of electron transfer is very fast and reproducible [22].

All the experiments were performed in inert gas and using anhydrous acetronile (ACN) as solvent.

3.6.1. Trinuclear copper (I) complexes

The cyclic voltammetry of some of the complexes show significant signals in acetronitrile (0.1 M TBAH) as shown in Appendix 6. Complexes 2, 3, 6 and 7 show the presence of an irreversible oxidation, assigned to one-electron oxidation at the copper (I) center [3]. However, other reported trinuclear copper (I) acetylide complexes with bis(diphenylphosphino) methane have showed a semireversible redox couple [23, 24]. These irreversible oxidation is the consequence of inestable complexes in solution.

A summary of the redox potentials, measured relative to the internal reference is given in Table 11. All the measurements were done at 1000 mV/min.

Table 11. *Redox potential of complex 2 to 8 in anhydrous, degassed acetonitrile vs Cp$_2$Fe/Cp$_2$Fe$^+$ used as internal reference.*

Complex	E$_{1/2\ ox}$ ± 0.1 (V)	E$_{1/2\ red}$ ± 0.1 (V)
2	0.94	-
3	0.95	-
4	-	-
5	-	-
6	1.01	-
7	0.95	-1.76
8	-	-

3.6.2. Mononuclear copper (I) complexes

Complexes 9-16 show oxidations in the range of +0.66 V to +0.83 V versus Fe(C$_5$H$_5$)$_2$/ Fe(C$_5$H$_5$)$_2$$^+$, Appendix 7. These oxidation processes are irreversible, as consequence of the rapid decomposition of Cu (II) species by comparison with other copper complexes with triphenylphosphine ligands [25]. The reduction of the complexes is not fully reversible, and assigned to a reduction of the phosphine ligands, in the range of -1.56 V to -1.93 V versus Fe(C$_5$H$_5$)$_2$/ Fe(C$_5$H$_5$)$_2$$^+$. Similar values, in the same range, have been reported for transition metal complexes containing bipyridine ligands [6, 26-29].

All the measurements for theses complexes were done at 3000 mV/min (Table 12).

Table 12. *Redox potential of complex 9 to 16 in anhydrous, degassed acetonitrile vs Cp_2Fe/Cp_2Fe^+ used as internal reference.*

Complex	$E_{1/2\ ox} \pm 0.1$ (V)	$E_{1/2\ red} \pm 0.1$ (V)
9	0.72	-1.73
10	0.67	-1.54
11	0.83	-1.93
12	0.66	-1.66
13	0.74	-1.71
14	0.81	-1.64
15	0.82	-1.58
16	0.81	-1.56

3.7. Study of a mononuclear copper (I) complex with different dopants

As discussed in the first chapter, in order to achieve high efficiency for electrophosphorescence based OLEDs and avoid self quenching, the emitter must be doped into an appropriate host material [30, 31]. For an efficient energy transfer from the excited triplet T_1 state of the host to the excited triplet T_1 state of the guest or direct formation of the excited phosphorescent guest molecules, providing a reasonable good efficiency [32]. Host materials should be selected to possess a higher triplet energy level than that of the guest molecules [33].

Many different organic compounds have been used as host materials. In this study we have chosen Complex 16 as it provides the emission quantum yield. The electrochemical proprieties, from cyclic voltammetry, of the complex have provided details of its energy gap which can be seen in Figure 35. Three kind of host materials have been choosen according to the HOMO-LUMO gap of the complex 16, poly (N-vinyl carbazole) (PVCz), 4,4'-N,N'-dicarbazolebiphenyl (CBP) and 3-phenyl-4-(1'-naphthyl)-5-phenyl-1,2,4-triazole (TAZ).
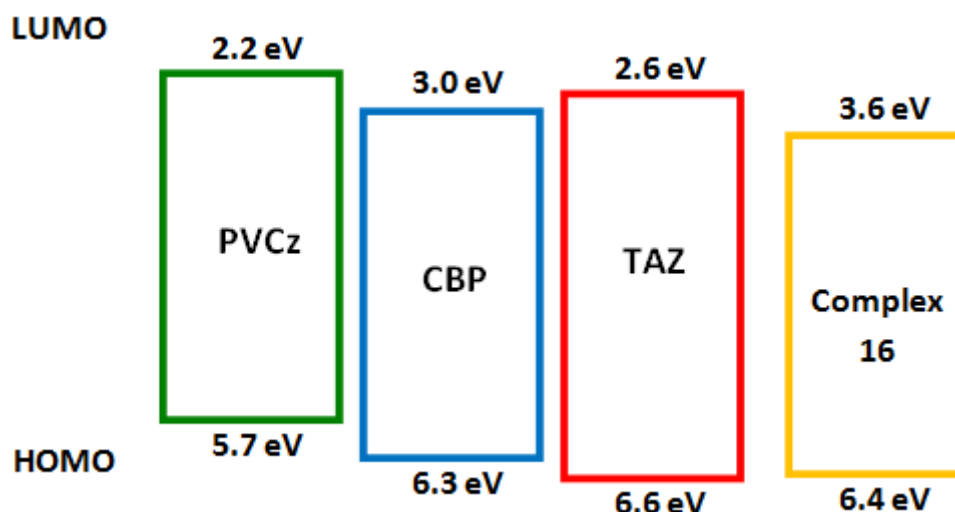
Figure 35. *An energy level diagram of the complex 16, which LUMO level is at 3.6eV and HOMO level is at 6.4eV; the host materials, PVCz which LUMO level is at 2.2eV and HOMO level is at 5.7eV [34], CBP which LUMO level is at 3.0eV and HOMO level is at 6.3eV and TAZ which LUMO level is at 2.6eV and HOMO level is at 6.6eV.*

In order to choose the perfect host material for Complex 16 and understand the host-guest system, the emission of the complex was studied at 530 nm, with different proportion of the three selected host materials (Graph 13, 14 and 15). When the host was PVCz or CBP at 90 % of weight proportion, the emission of Complex 16 was partially detected, while when TAZ was used, the emission of the complex was detected with just 0.1 % weight proportion in the system.
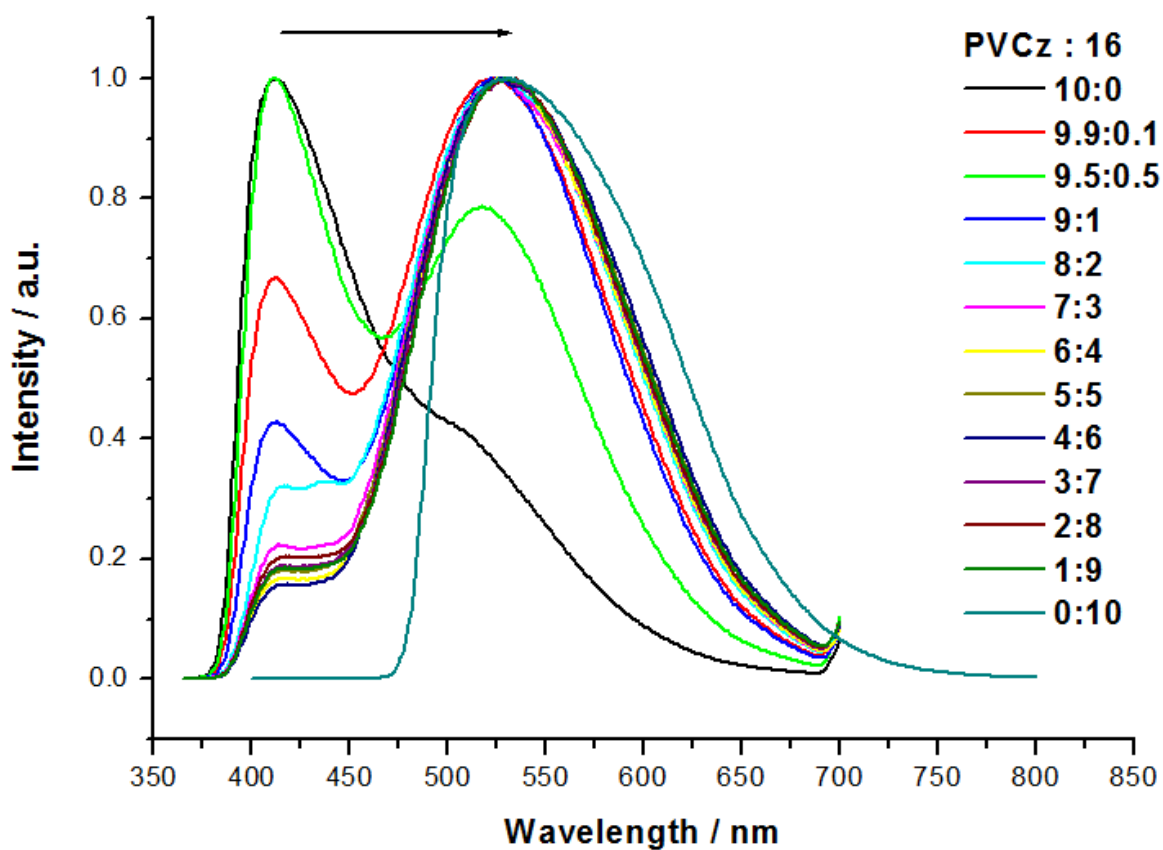
Graph 13. *Emission spectra of the complex 16 at different weight proportion of PVCz.*
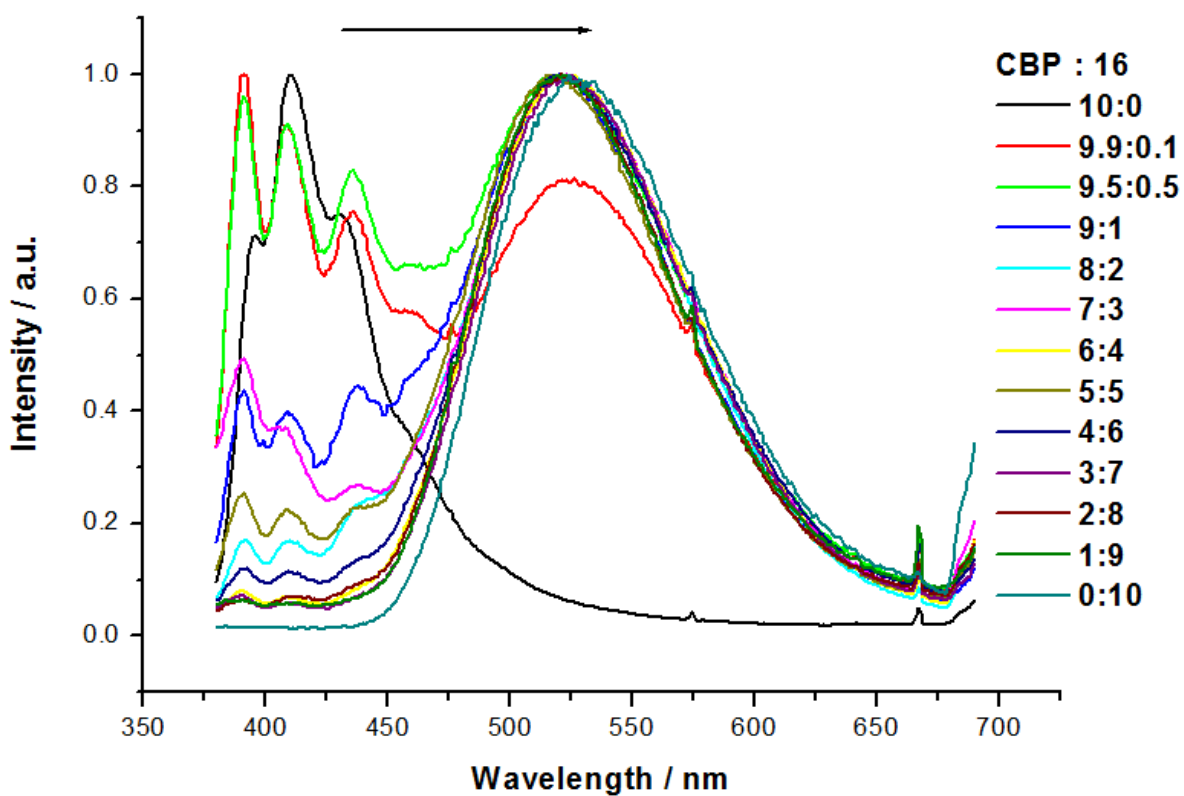
Graph 14. *Emission spectra of the complex 16 at different weight proportion of CBP.*
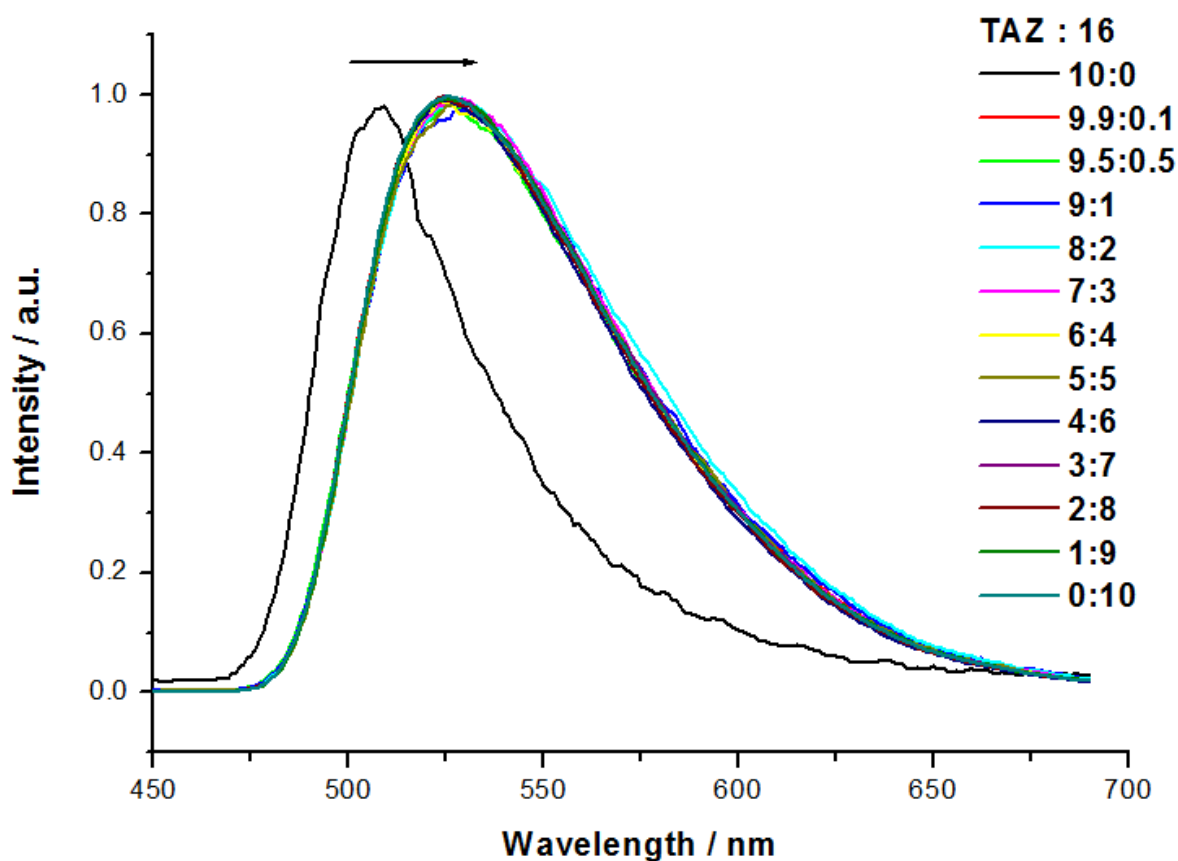
Graph 15. *Emission spectra of the complex 16 at different weight proportion of TAZ.*

The emission of Complex 16, in different proportions was compared for each host material (Graph 16). The ideal host for the complex should be CBP with a concentration of approximately 1 %, as other published research suggests, Table 13 [32].

Table 13. *Proportion of complex 16 with each host material when they show maximum intensity of emission at 530nm.*

Proportion of Complex 16 (%)	Host
1.00	CBP
0.09	TAZ
6.00	PVCz
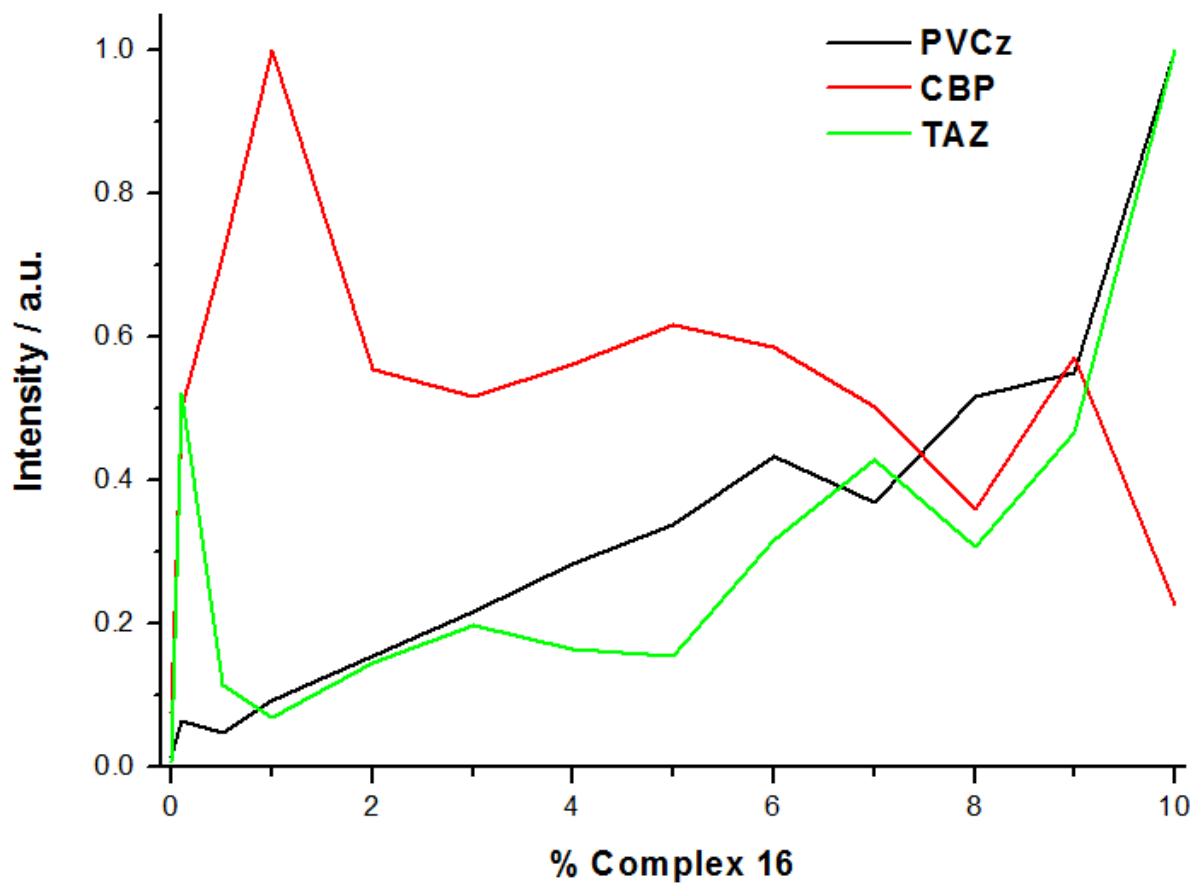
Graph 16. *Emission of the complex 16 at 530nm, in different proportion, with the host materials PVCz, CBP and TAZ.*

3.8. References

1. Orselli, E., et al., *Blue-Emitting Iridium Complexes with Substituted 1,2,4-Triazole Ligands: Synthesis, Photophysics, and Devices.* Inorganic Chemistry, 2007. **46**(26): p. 11082-11093.

2. Cheung, K.-L., S.-K. Yip, and V.W.-W. Yam, *Synthesis, characterization, electrochemistry and luminescence studies of heterometallic gold(I)–rhenium(I) alkynyl complexes.* Journal of Organometallic Chemistry, 2004. **689**(24): p. 4451-4462.

3. Yam, V.W.-W., W.K.-M. Fung, and M.-T. Wong, *Synthesis, Photophysics, Electrochemistry, and Excited-State Redox Properties of Trinuclear Copper(I) Acetylides with Bis(diphenylphosphino)alkylamines and -arylamines as Bridging Ligands.* Organometallics, 1997. **16**(8): p. 1772-1778.

4. Armaroli, N., et al., *Highly Luminescent CuI Complexes for Light-Emitting Electrochemical Cells (Adv. Mater. 10/2006).* Advanced Materials, 2006. **18**(10): p. n/a-n/a.

5. Evans, R.C., P. Douglas, and C.J. Winscom, *Coordination complexes exhibiting room-temperature phosphorescence: Evaluation of their suitability as triplet emitters in organic light emitting diodes.* Coordination Chemistry Reviews, 2006. **250**(15–16): p. 2093-2126.

6. Coppo, P., E.A. Plummer, and L. De Cola, *Tuning iridium(iii) phenylpyridine complexes in the "almost blue" region.* Chemical Communications, 2004. **0**(15): p. 1774-1775.

7. Tsuboyama, A., et al., *Homoleptic Cyclometalated Iridium Complexes with Highly Efficient Red Phosphorescence and Application to Organic Light-Emitting Diode.* Journal of the American Chemical Society, 2003. **125**(42): p. 12971-12979.

8. Zhang, Q., et al., *Highly Efficient Green Phosphorescent Organic Light-Emitting Diodes Based on CuI Complexes.* Advanced Materials, 2004. **16**(5): p. 432-436.

9. Yam, V.W.-W., *Molecular Design of Transition Metal Alkynyl Complexes as Building Blocks for Luminescent Metal-Based Materials: Structural and Photophysical Aspects.* Accounts of Chemical Research, 2002. **35**(7): p. 555-563.

10.   Hou, R., et al., *Synthesis, structural characterization and luminescent properties of a series of Cu(i) complexes based on polyphosphine ligands.* Dalton Transactions, 2011. **40**(29): p. 7551-7558.

11.   Scaltrito, D.V., et al., *MLCT excited states of cuprous bis-phenanthroline coordination compounds.* Coordination Chemistry Reviews, 2000. **208**(1): p. 243-266.

12.   McMillin, D.R. and K.M. McNett, *Photoprocesses of Copper Complexes That Bind to DNA.* Chemical Reviews, 1998. **98**(3): p. 1201-1220.

13.   Porrès, L., et al., *Absolute Measurements of Photoluminescence Quantum Yields of Solutions Using an Integrating Sphere.* Journal of Fluorescence, 2006. **16**(2): p. 267-273.

14.   Zhang, X., et al., *Obtaining high-efficiency red electrophosphorescent OLEDs by changing the thickness of light-emitting layer.* Displays, 2007. **28**(3): p. 150-153.

15.   Song, D., et al., *Dependence of carrier recombination mechanism on the thickness of the emission layer in green phosphorescent organic light emitting devices.* Organic Electronics, 2011. **12**(4): p. 582-588.

16.   Seo, J.H., et al., *White organic light-emitting diodes showing nearly 100% internal quantum efficiency.* Organic Electronics, 2010. **11**(11): p. 1759-1766.

17.   Tang, C.W. and S.A. VanSlyke, *Organic electroluminescent diodes.* Applied Physics Letters, 1987. **51**(12): p. 913-915.

18.   Liu, S., et al., *Highly efficient white organic light-emitting devices consisting of undoped ultrathin yellow phosphorescent layer.* Journal of Luminescence, 2013. **134**(0): p. 665-669.

19.   D'Andrade, B.W. and S.R. Forrest, *Effects of exciton and charge confinement on the performance of white organic p - i - n electrophosphorescent emissive excimer devices.* Journal of Applied Physics, 2003. **94**(5): p. 3101-3109.

20.   Tang, C.W., S.A. VanSlyke, and C.H. Chen, *Electroluminescence of doped organic thin films.* Journal of Applied Physics, 1989. **65**(9): p. 3610-3616.

21.   Yu, J., et al., *Film thickness influence of dual iridium complex ultrathin layers on the performance of nondoped white organic light-emitting diodes.* Displays, 2011. **32**(2): p. 87-91.

22.	Tsierkezos, N., *Cyclic Voltammetric Studies of Ferrocene in Nonaqueous Solvents in the Temperature Range from 248.15 to 298.15 K.* Journal of Solution Chemistry, 2007. **36**(3): p. 289-302.

23.	Yam, V.W.W., W.K. Lee, and T.F. Lai, *Synthesis, spectroscopy, and electrochemistry of trinuclear copper(I) acetylides. X-ray crystal structure of [Cu3(.mu.-Ph2PCH2PPh2)3(.mu.3-.eta.1-C.tplbond.CBu-tert)(.mu.3-Cl)]PF6.* Organometallics, 1993. **12**(6): p. 2383-2387.

24.	Yam, V.W.-W., et al., *Synthesis, structure, photophysics, time-resolved emission spectroscopy and electrochemistry of luminescent copper(I) acetylide complexes.* Journal of the Chemical Society, Dalton Transactions, 1996. **0**(15): p. 3283-3287.

25.	Kuang, S.-M., et al., *Synthesis and Structural Characterization of Cu(I) and Ni(II) Complexes that Contain the Bis[2-(diphenylphosphino)phenyl]ether Ligand. Novel Emission Properties for the Cu(I) Species.* Inorganic Chemistry, 2002. **41**(12): p. 3313-3322.

26.	Mydlak, M., et al., *Positively Charged Iridium(III) Triazole Derivatives as Blue Emitters for Light-Emitting Electrochemical Cells.* Advanced Functional Materials, 2010. **20**(11): p. 1812-1820.

27.	Lowry, M.S. and S. Bernhard, *Synthetically Tailored Excited States: Phosphorescent, Cyclometalated Iridium(III) Complexes and Their Applications.* Chemistry – A European Journal, 2006. **12**(31): p. 7970-7977.

28.	Bolink, H.J., et al., *Origin of the large spectral shift in electroluminescence in a blue light emitting cationic iridium(iii) complex.* Journal of Materials Chemistry, 2007. **17**(48): p. 5032-5041.

29.	De Angelis, F., et al., *Controlling Phosphorescence Color and Quantum Yields in Cationic Iridium Complexes: A Combined Experimental and Theoretical Study.* Inorganic Chemistry, 2007. **46**(15): p. 5989-6001.

30.	Schrögel, P., et al., *Meta-linked CBP-derivatives as host materials for a blue iridium carbene complex.* Organic Electronics, 2011. **12**(12): p. 2047-2055.

31.	Adachi, C., et al., *Nearly 100% internal phosphorescence efficiency in an organic light-emitting device.* Journal of Applied Physics, 2001. **90**(10): p. 5048-5051.

32.   Jeon, W.S., et al., *Ideal host and guest system in phosphorescent OLEDs.* Organic Electronics, 2009. **10**(2): p. 240-246.

33.   Guan, M., et al., *The host materials containing carbazole and oxadiazole fragment for red triplet emitter in organic light-emitting diodes.* Organic Electronics, 2006. **7**(5): p. 330-336.

34.   Ohmori, Y., H. Kajii, and Y. Hino, *Organic Light-Emitting Diodes Fabricated by a Solution Process and Their Stress Tolerance.* Display Technology, Journal of, 2007. **3**(2): p. 238-244.

Chapter 4: Conclusions and future investigations

The contribution of this research has been found an alternative materials to the expensive iridium and platinum complexes for organic light emitting diodes. In this study, novel copper (I) complexes have been synthesized, trinuclear copper (I) complexes carrying alkynyl ligands and mononuclear copper (I) complexes carrying phosphine and bipyridine ligands.

A range of emission colours, from sky blue to deep red, was shown by using alkynyl ligands with different electronic properties in the trinuclear copper (I) complexes. These novel complexes possess a quantum yield of photoluminescence comparable with other phosphorescent metal complexes used in OLEDs, such as iridium (III) cyclometalated complexes. They show another interesting optical property: their lifetime could be tuned from microseconds to milliseconds. For some of these complexes, which have conjugated alkynyl ligands, their extended lifetime is an indication of stabilised excited state. Their temperature decomposition range is from 184 ^{o}C to 269 ^{o}C, which depend on their electro withdrawing subtituents on the alkynyl ligand. However, the study of the complexes, by differential scanning calorimetry and by cyclic voltammetry, provides evidence for irreversible thermal and electrochemical behaviour, respectively. All these results suggest interesting optical properties for very novel copper (I) complexes with alkynyl ligands, but their thermal and electrochemical instability was demonstrated, which hamper their foreseeable application in organic light emitting diodes.

In order to develop more stable copper (I) complexes for organic light emitting diodes, a range of mononuclear copper (I) complexes was synthesised. These new complexes, carry a variety of bipyridyl and diphosphine ligands, which tune the optical and physical properties of the complexes. Unlike the trinuclear copper (I) complexes, the mononuclear complexes provide a narrow range of emission colours. Their high efficient emission active is only evident when bipyridyl ligand carring methyl substituients face the copper ion. These methyl groups play a role to avoid external quenching, as the geometrical arrangement provides a more rigid configuration. Conversely, the complexes without or with methyl groups out-side of the copper nucleus, show a non radiative decay path. In all cases, the thermal properties depend on the phosphine ligands. They show a temperature of decomposition from 200 ^{o}C to 300 ^{o}C, where the complexes with

thriphenylphosphine ligands show the lowest temperature. The other complexes could be processed in a polymer matrix, which demonstrate their ability to be used in plastic manufacturing. However, these complexes are not electrochemically stable, as the cyclic voltammetry shows.

In summary, this second group of synthesised copper (I) complexes gives a contribution to understand and consider copper complexes as a new generation of alternative material for organic light emitting diodes.

Both groups of synthesised copper complexes, trinuclear and mononuclear, shows that the structure of the ligands are the most important factor to define the optical, chemical and physical properties.

For future investigations, it would be recommendable to synthesize and realise a systematic study of equivalent complexes with silver and gold as it could be possible the synthesis of other d^{10} transition metal, such as gold, with phenyl pyridine ligands and another kind of ligands.

These novel complexes could be used in future applications, such as in biological systems. They have demonstrated a high sensitivity to oxygen, which could be very useful in biology.

Appendix 1: Lifetime curves of trinuclear copper (I) complexes
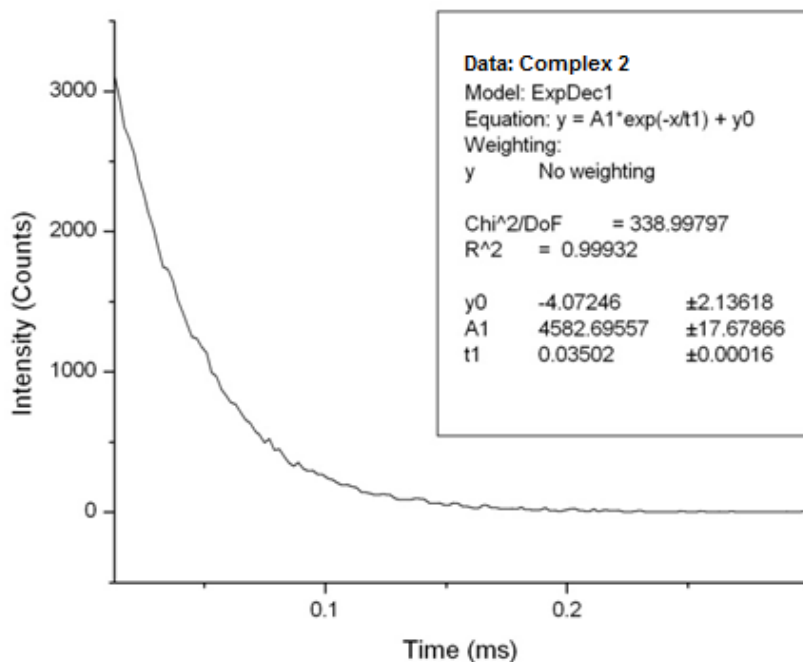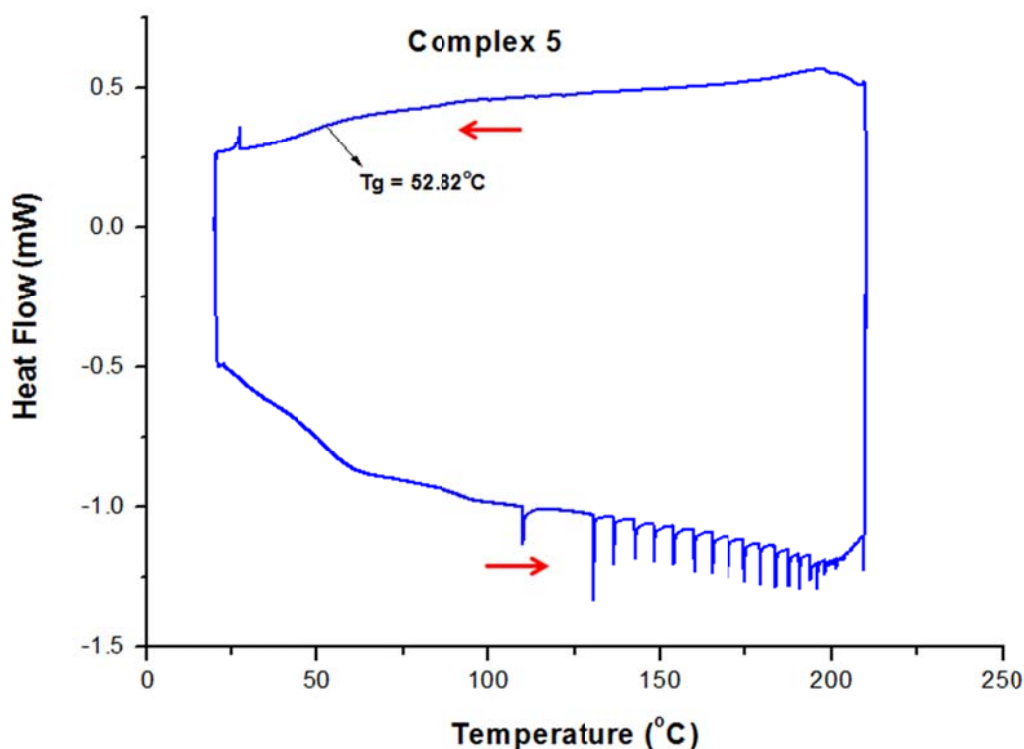
Graph 1. *Lifetime curve of trinuclear copper complex 2 which possess 1-ethynyl-2,4-difluorobenzene as alkynyl ligand.*
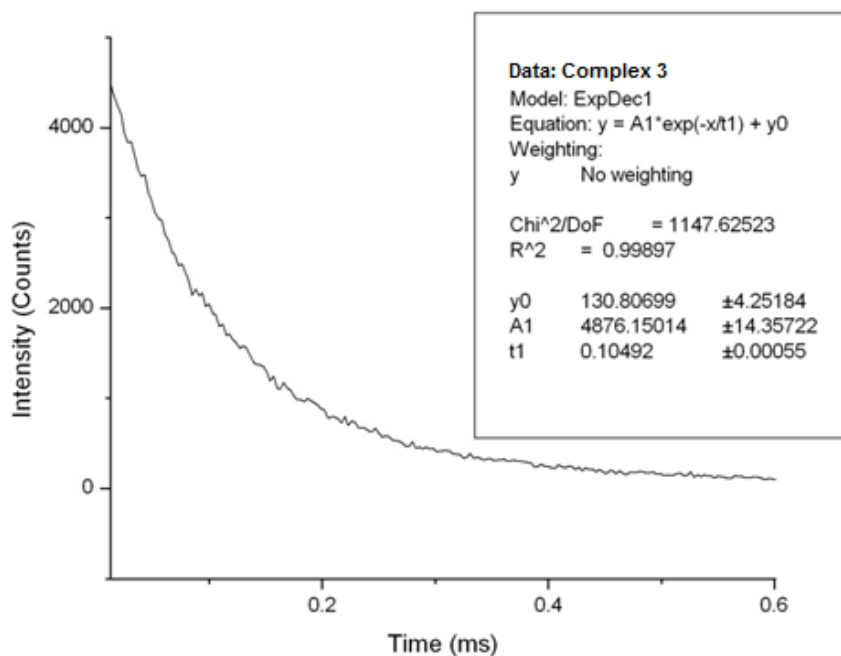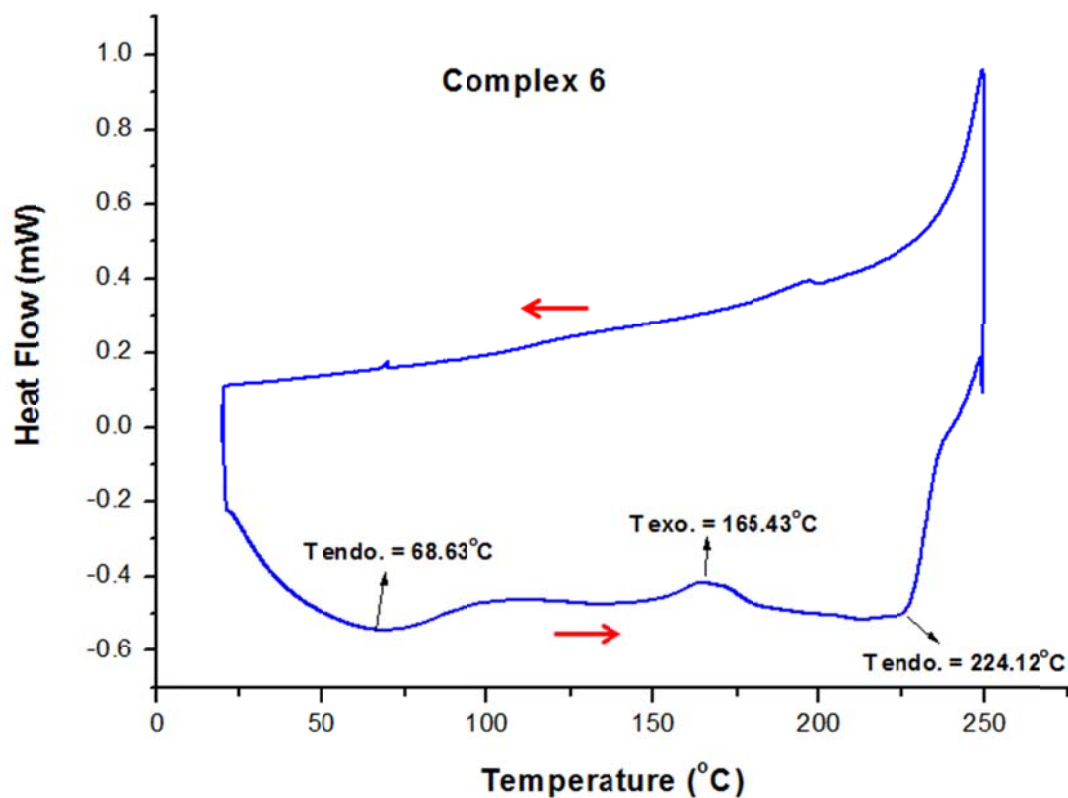

Graph 2. *Lifetime curve of trinuclear copper complex 3 which possess 1-ethynyl-3,5-difluorobenzene as alkynyl ligand.*
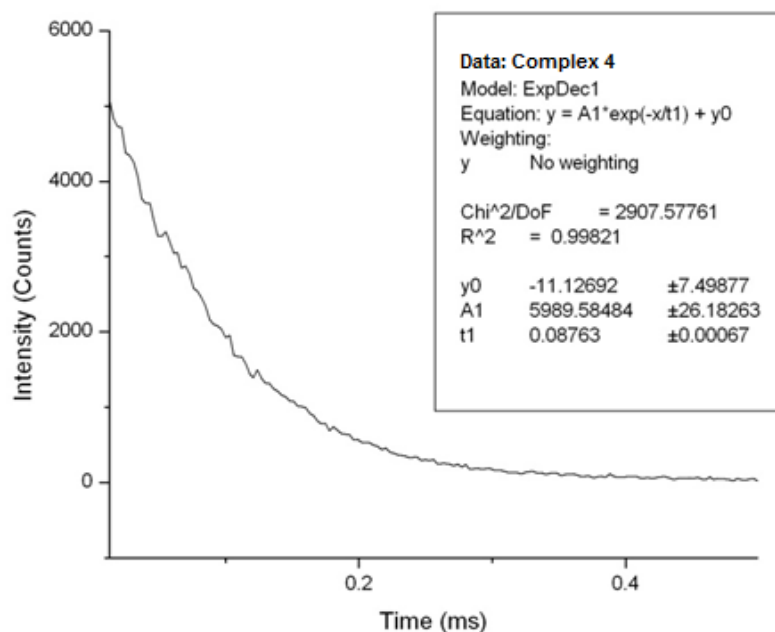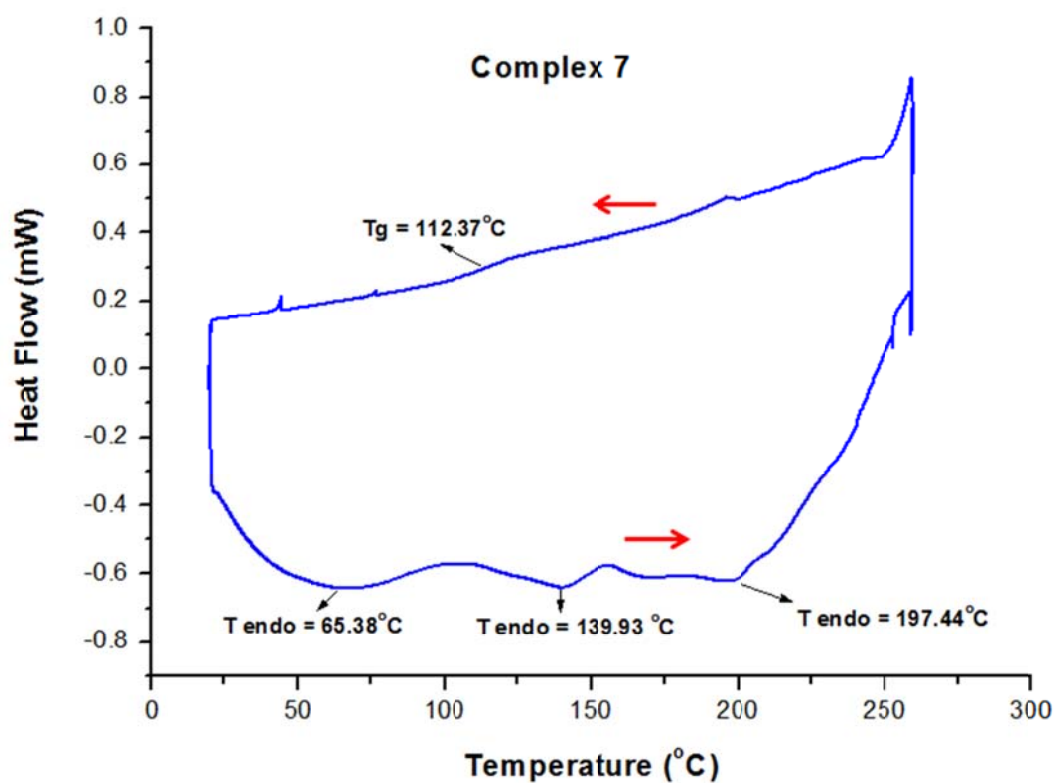
Graph 3. *Lifetime curve of trinuclear copper complex 4 which possess 1-ethynyl-3,5-bis(trifluoromethyl)benzene as alkynyl ligand.*
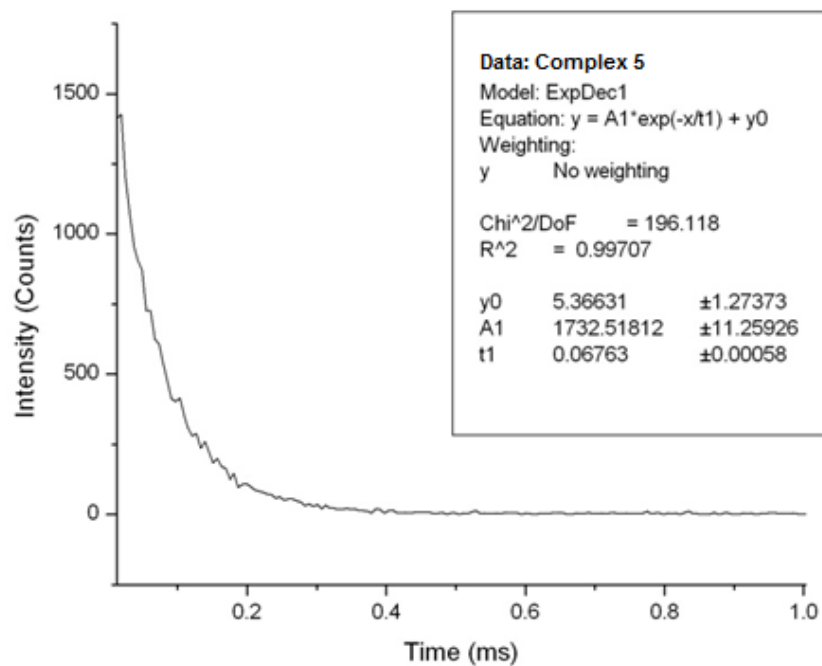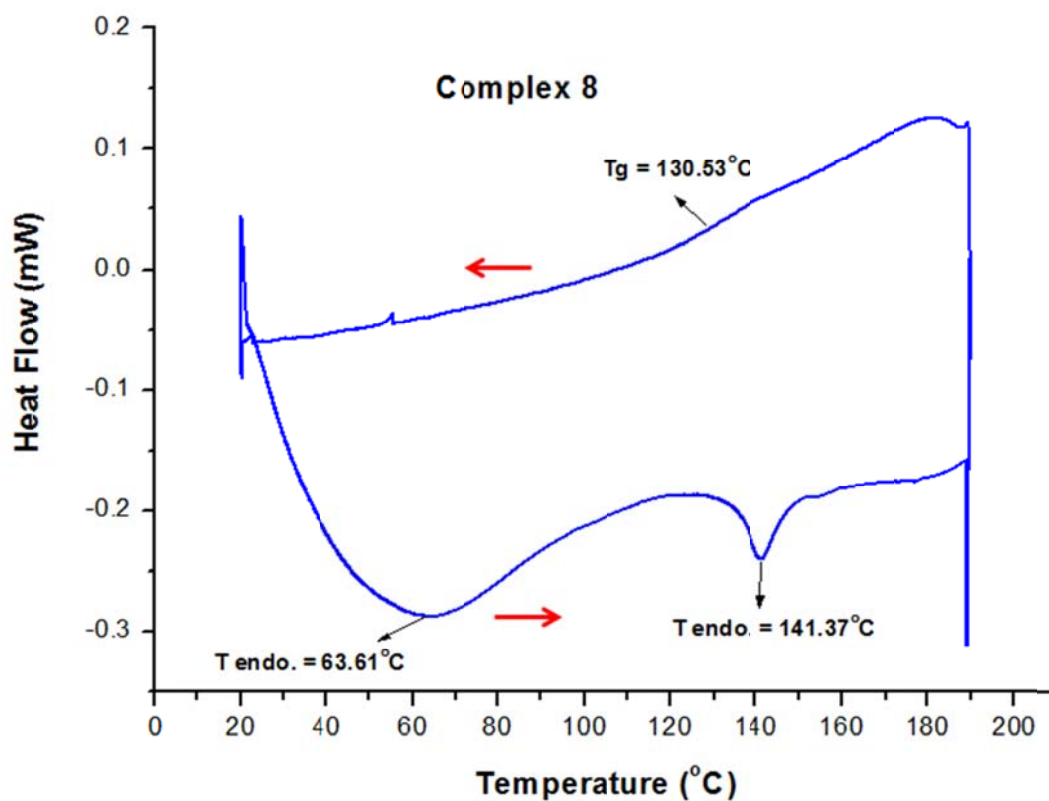

Graph 4. *Lifetime curve of trinuclear copper complex 5 which possess 1-ethynyl-α,α,α-4-(trifluoromethyl)benzene as alkynyl ligand.*
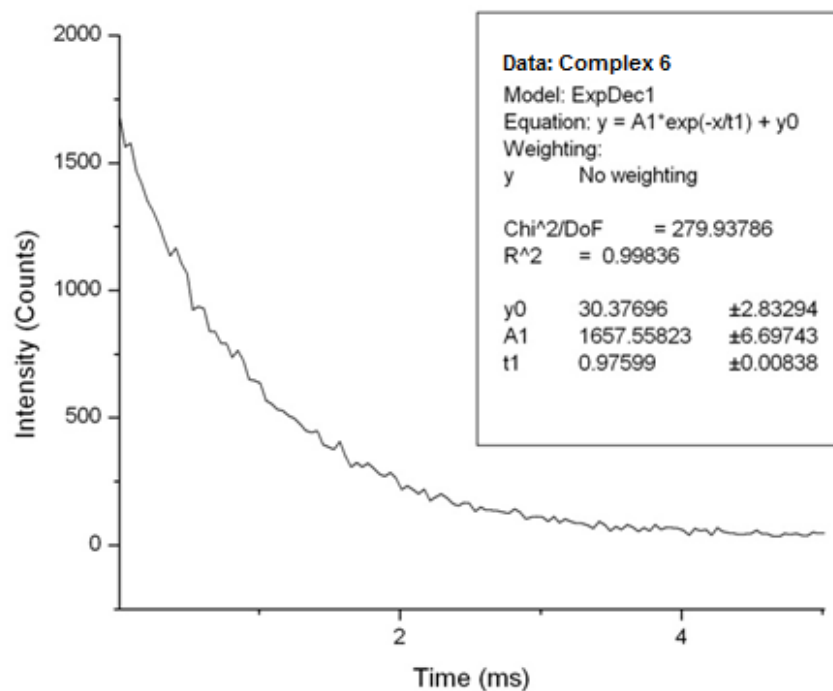
**Graph 5.** *Lifetime curve of trinuclear copper complex 6 which possess 9-ethynylphenanthrene as alkynyl ligand.*
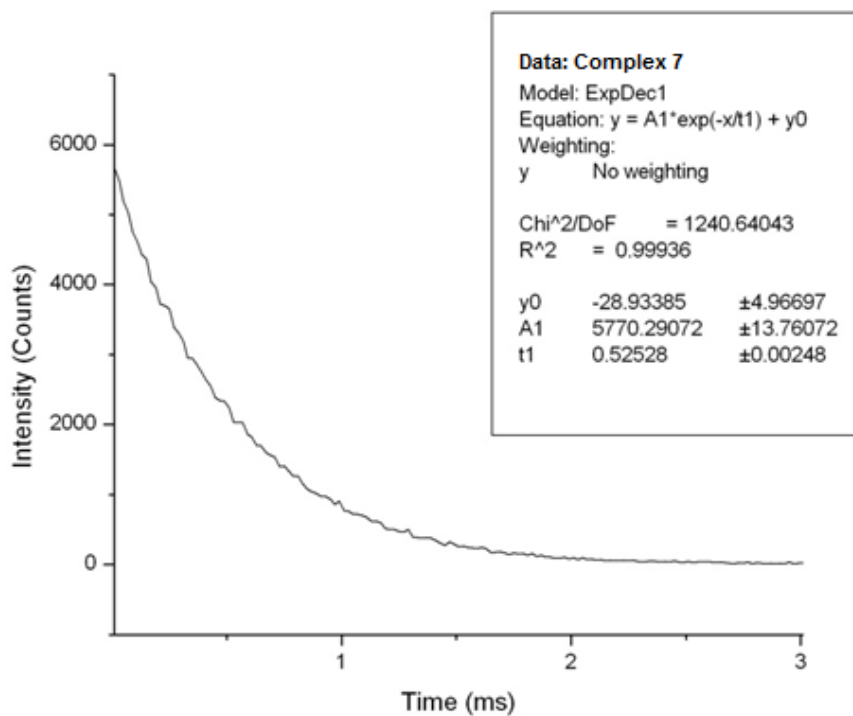
Graph 6. *Lifetime curve of trinuclear copper complex 7 which possess 2-ethynyl-6-metoxynaphthalene as alkynyl ligand.*
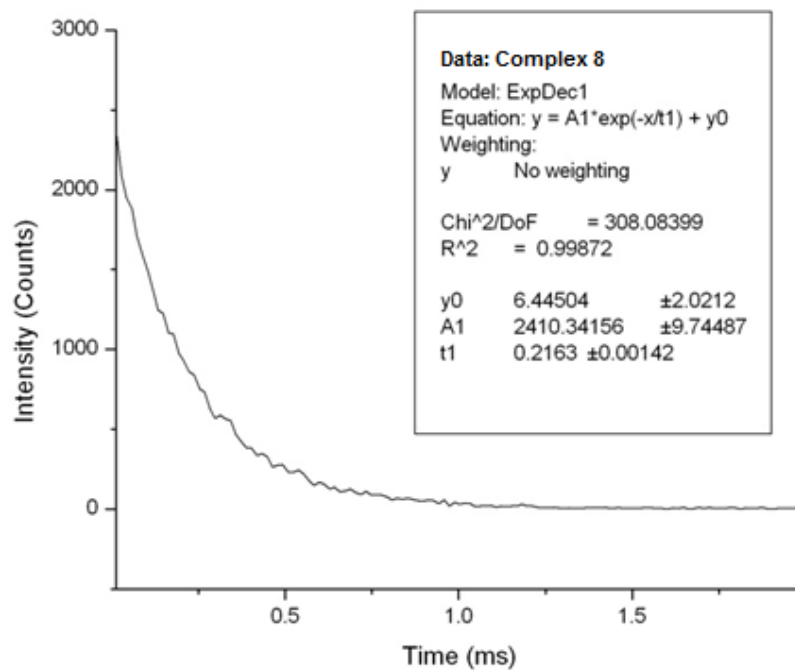
**Graph 7.** *Lifetime curve of trinuclear copper complex 8 which possess 1-ethynylpyrene as alkynyl ligand.*

Appendix 2: Lifetime curves of mononuclear copper (I) complexes
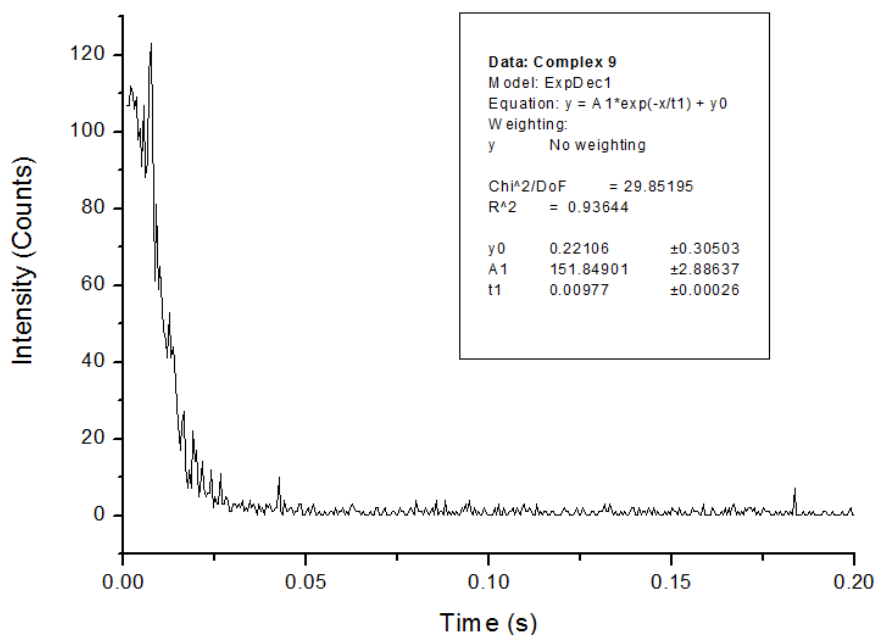
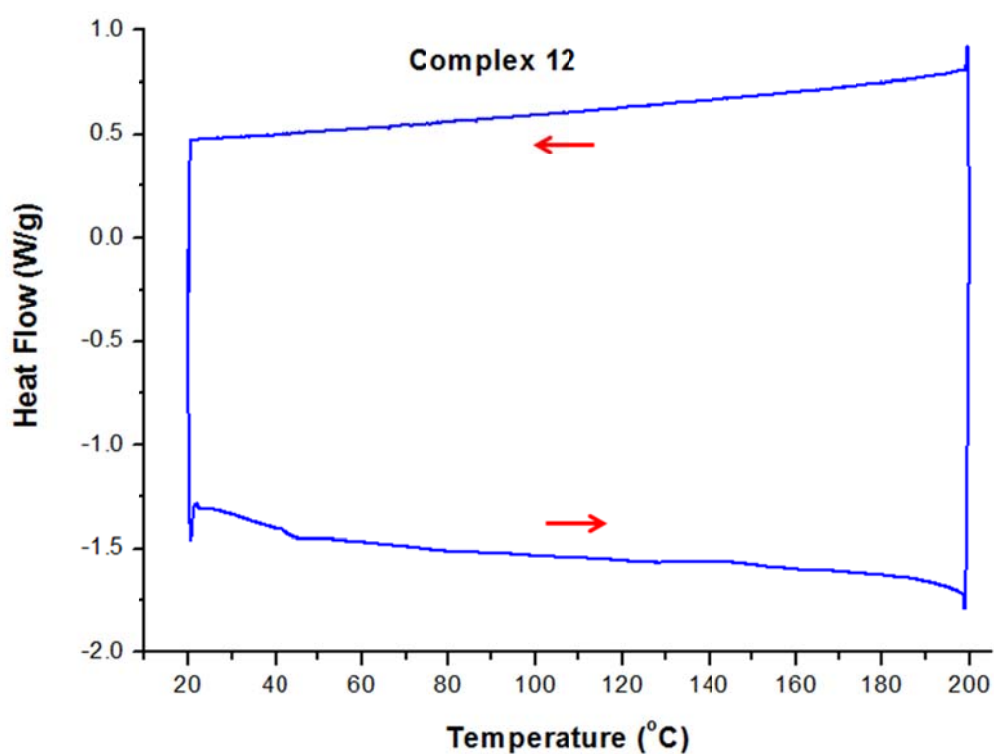**Graph 1.** *Lifetime curve of mononuclear copper complex 9 which possess 2,2'-bipyridyl as pyridine ligand and bis-(diphenylphosphinophenyl)ether as phosphine ligand.*
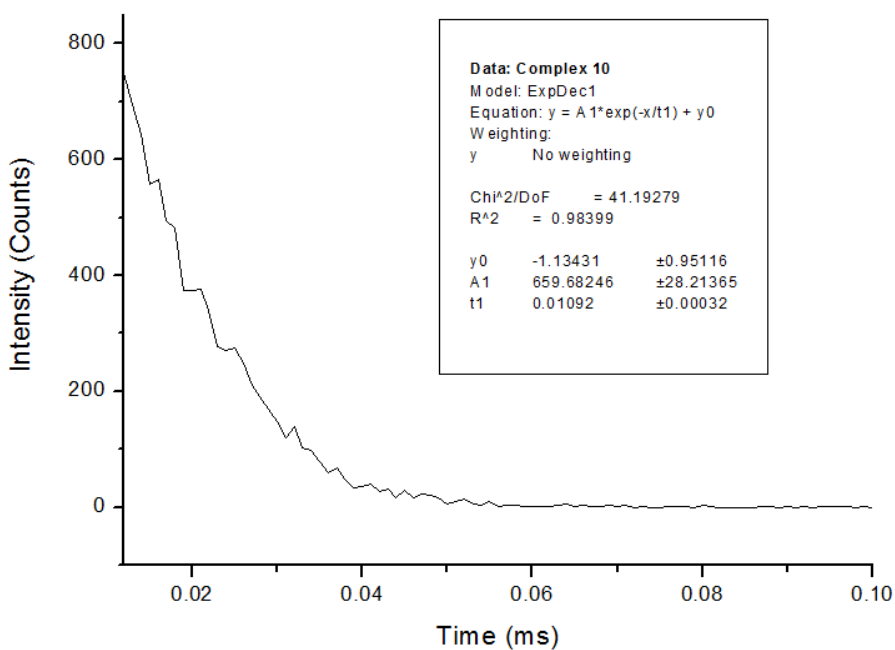
Graph 2. *Lifetime curve of mononuclear copper complex 10 which possess 4,4'-dimethyl-2,2'-bipyridyl as pyridine ligand and bis-(diphenylphosphinophenyl)ether as phosphine ligand.*
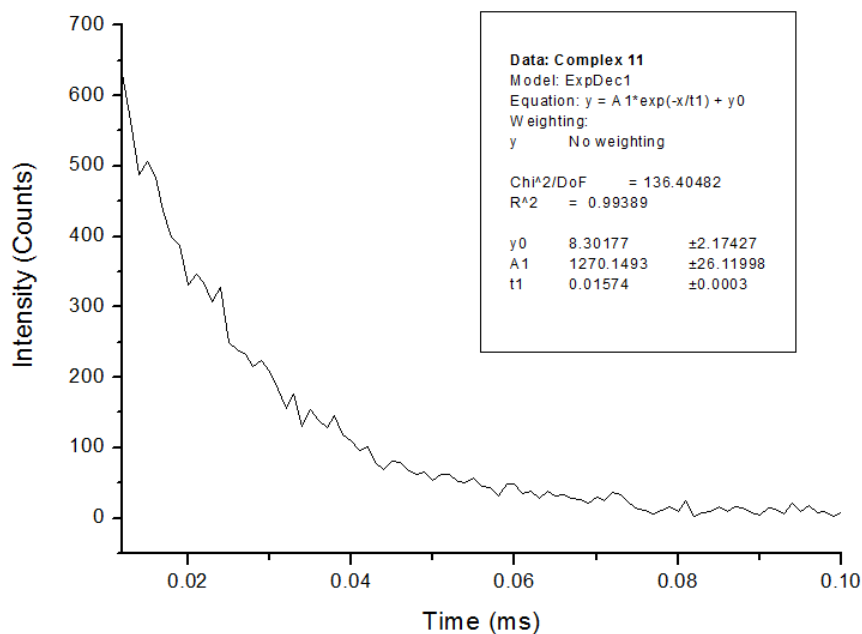
Graph 3. *Lifetime curve of mononuclear copper complex 11 which possess 6,6'-dimethyl-2,2'-bipyridyl as pyridine ligand and bis-(diphenylphosphinophenyl)ether as phosphine ligand.*
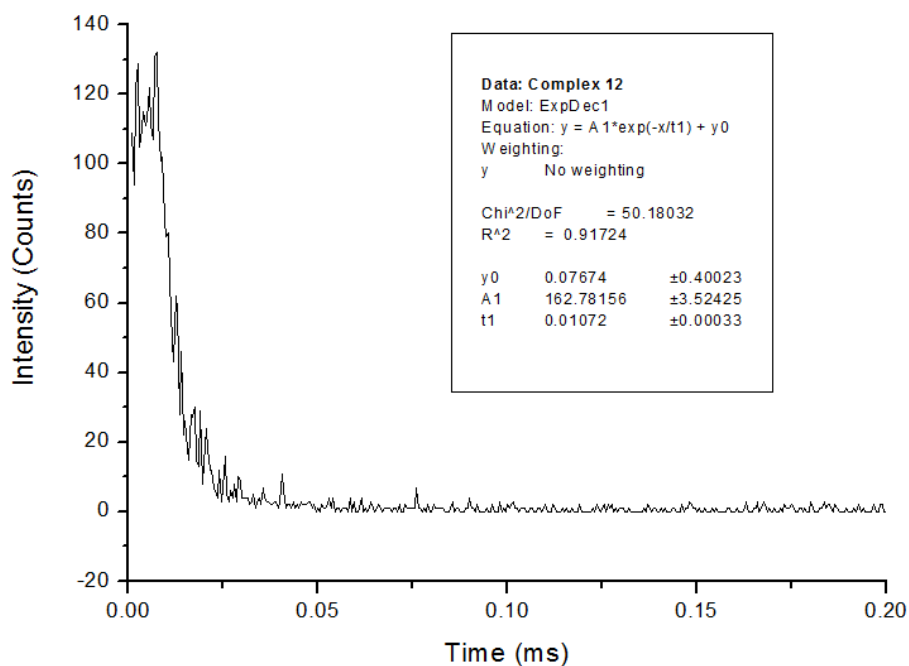
Graph 4. *Lifetime curve of mononuclear copper complex 12 which possess 2,2'-bipyridyl as pyridine ligand and triphenylphosphino as phosphine ligand.*
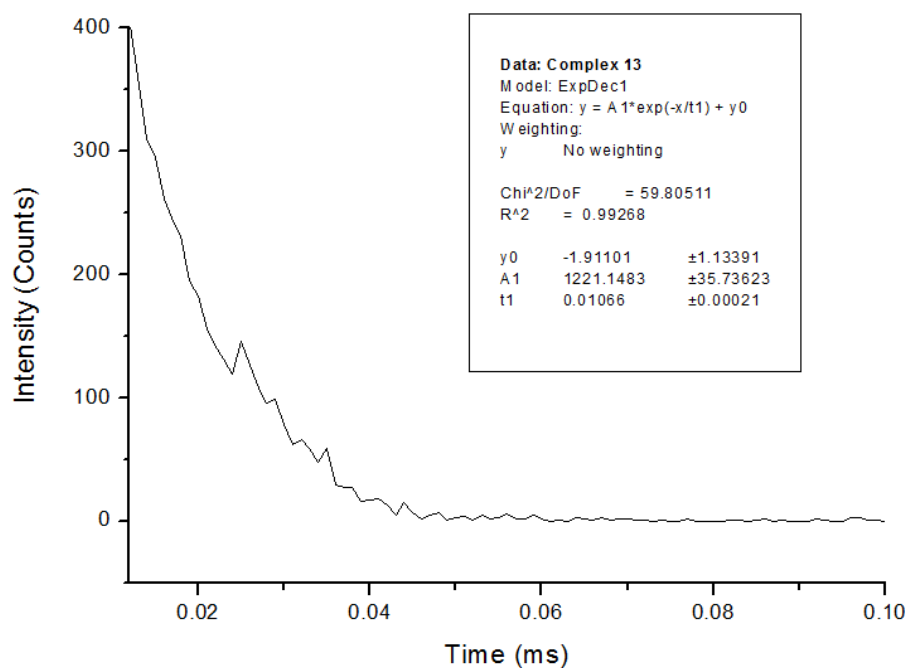
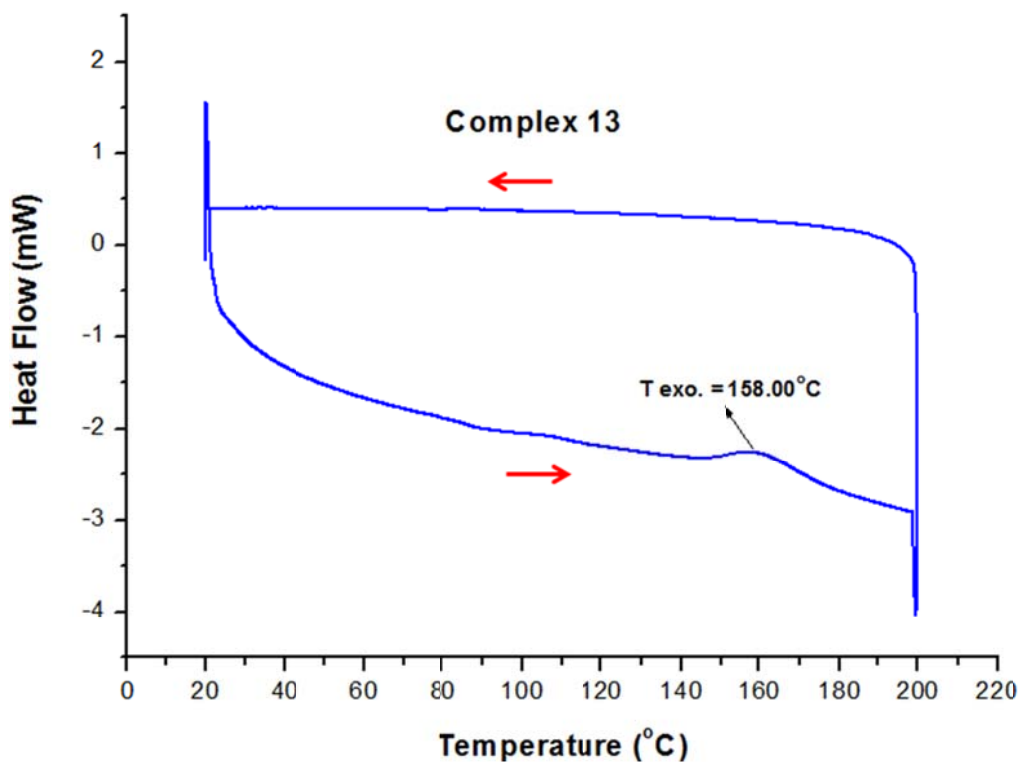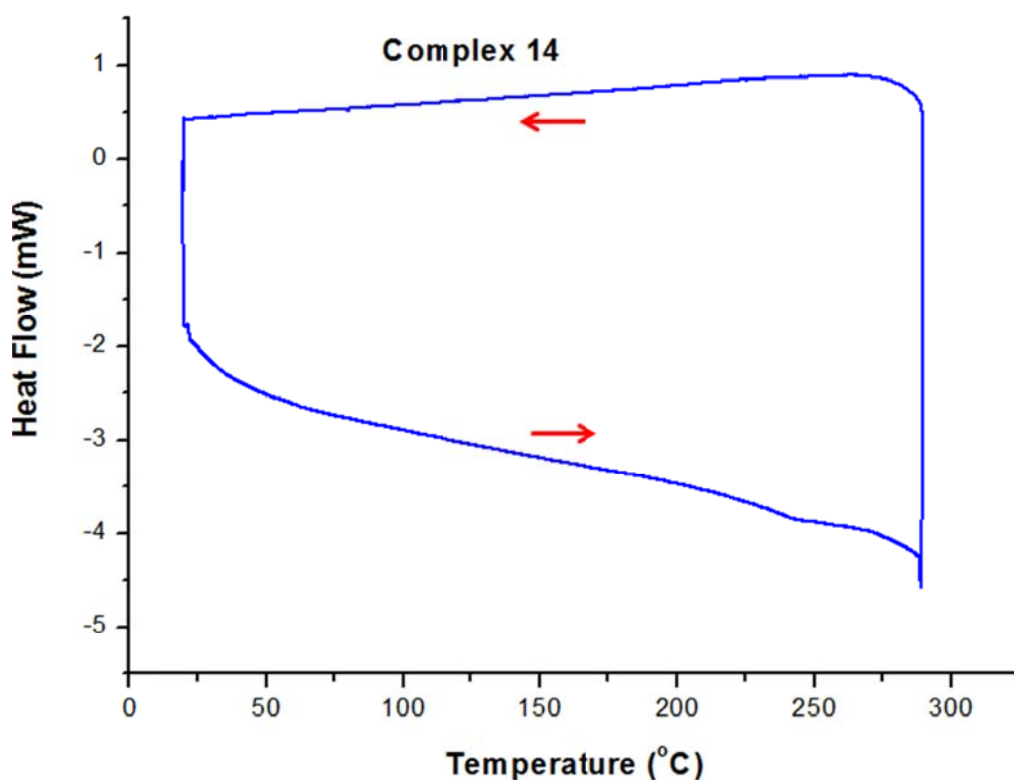**Graph 5.** *Lifetime curve of mononuclear copper complex 13 which possess 4,4'-dimethyl-2,2'-bipyridyl as pyridine ligand and triphenylphosphino as phosphine ligand.*
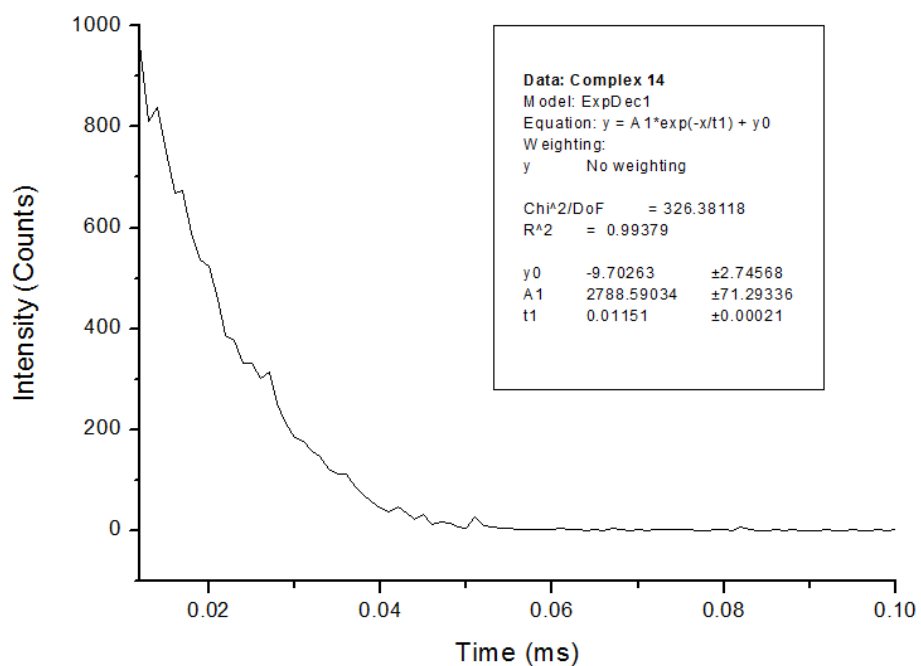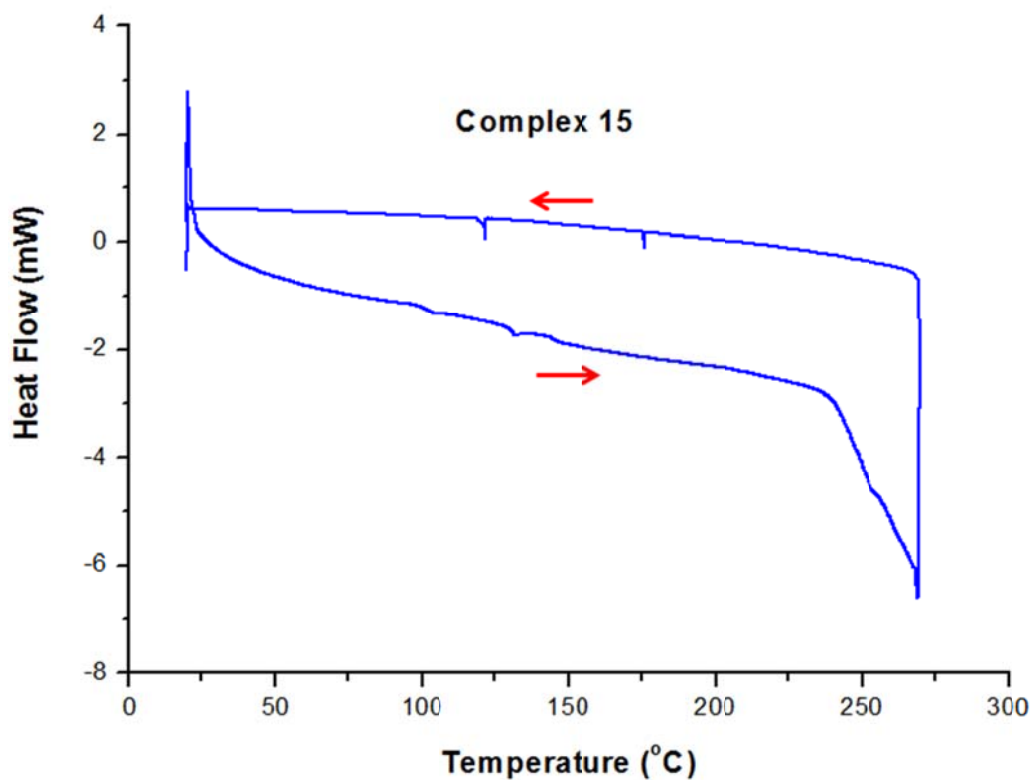

Graph 6. *Lifetime curve of mononuclear copper complex 14 which possess 2,2'-bipyridyl as pyridine ligand and 9,9-dimethyl-4,5-bis(diphenylphosphino) xanthene as phosphine ligand.*
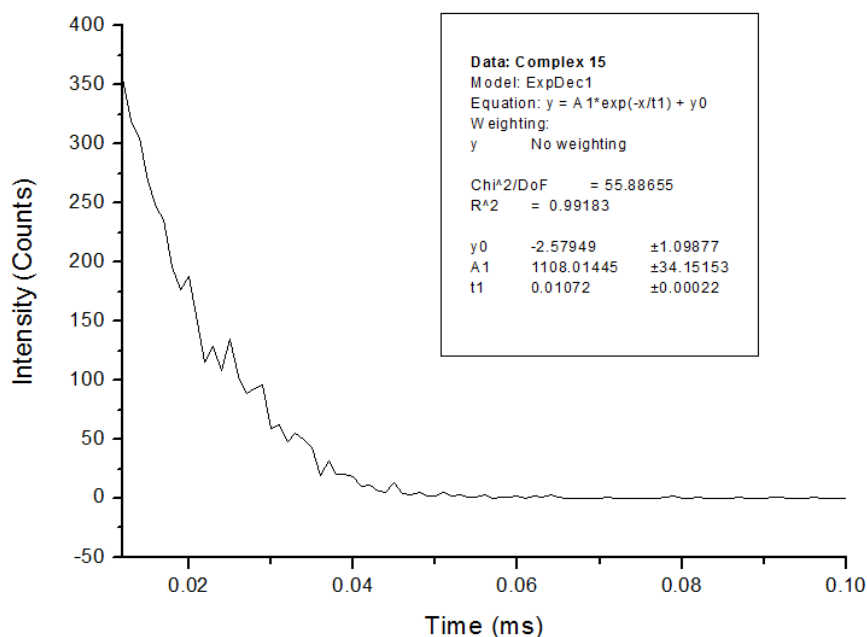
Graph 7. *Lifetime curve of mononuclear copper complex 15 which possess 4,4'-dimethyl-2,2'-bipyridyl as pyridine ligand and 9,9-dimethyl-4,5-bis(diphenylphosphino) xanthene as phosphine ligand.*
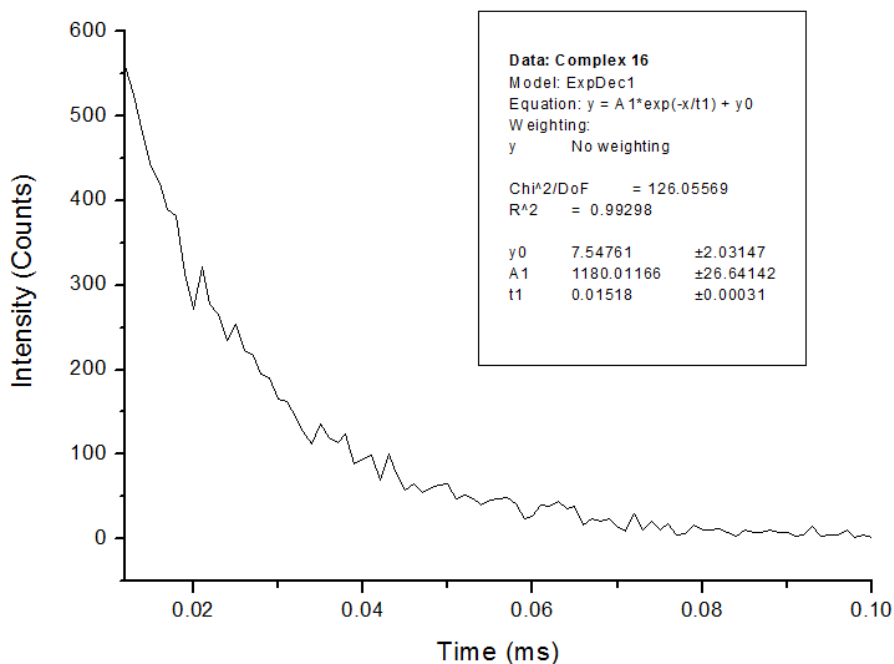
Graph 8. *Lifetime curves of mononuclear copper complex 16 which possess 6,6'-dimethyl-2,2'-bipyridyl as pyridine ligand and 9,9-dimethyl-4,5-bis(diphenylphosphino) xanthene as phosphine ligand.*

Appendix 3: Different scanning calorimetry graphs of trinuclear copper (I) complexes
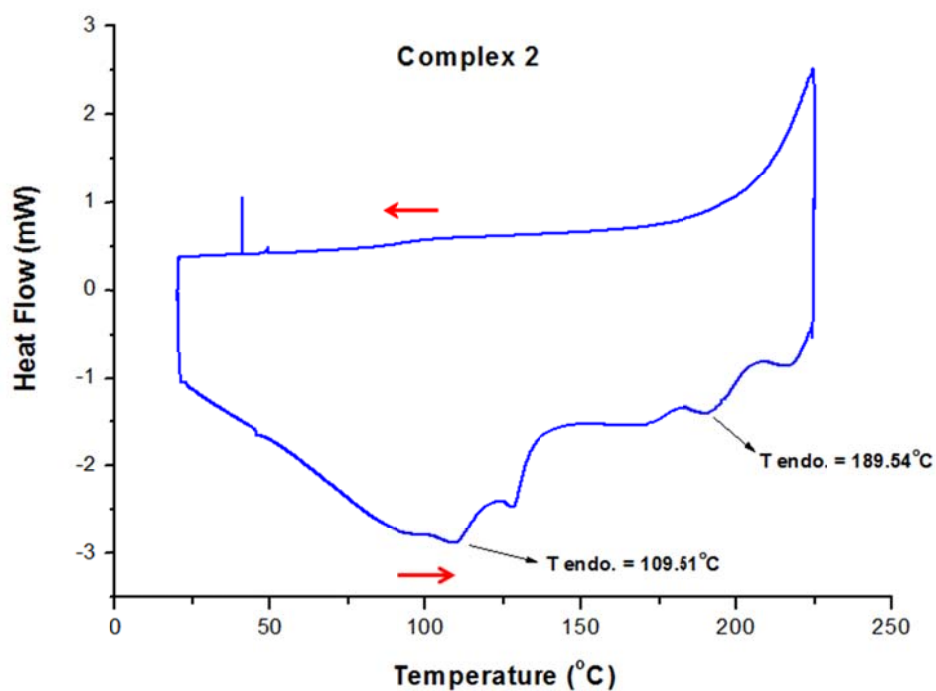
Graph1. *DSC curve of trinuclear copper complex 2 which possess 1-ethynyl-2,4-difluorobenzene as alkynyl ligand.*
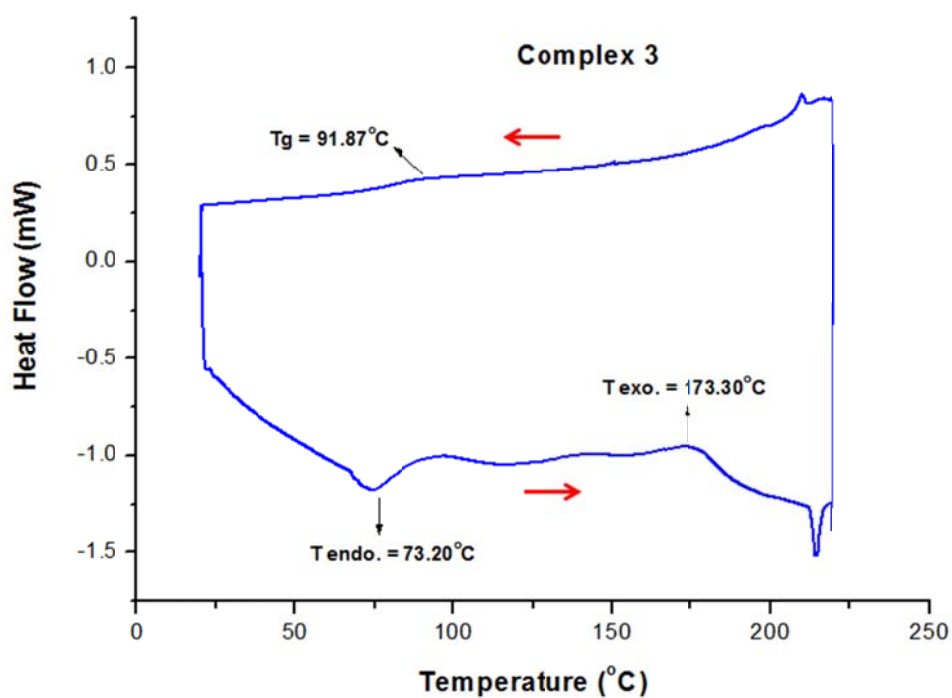
Graph 2. *DSC curve of trinuclear copper complex 3 which possess 1-ethynyl-3,5-difluorobenzene as alkynyl ligand.*
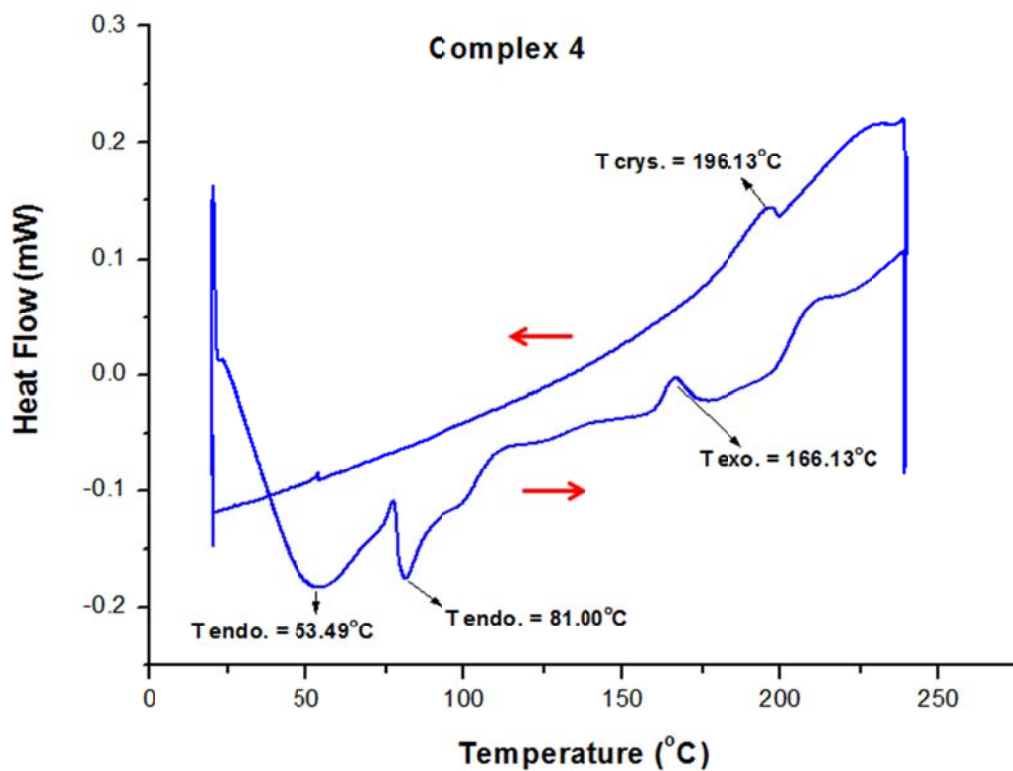
Graph 3. *DSC curve of trinuclear copper complex 4 which possess 1-ethynyl-3,5-bis(trifluoromethyl)benzene as alkynyl ligand.*

Graph 4. *DSC curve of trinuclear copper complex 5 which possess 1-ethynyl-α,α,α-4-(trifluoromethyl)benzene as alkynyl ligand.*

Graph 5. *DSC curve of trinuclear copper complex 6 which possess 9-ethynylphenanthrene as alkynyl ligand.*

Graph 6. *DSC curve of trinuclear copper complex 7 which possess 2-ethynyl-6-metoxynaphthalene as alkynyl ligand.*

Graph 7. *DSC curve of trinuclear copper complex 8 which possess 1-ethynylpyrene as alkynyl ligand.*

Appendix 4: Different scanning calorimetry graphs of mononuclear copper (I) complexes
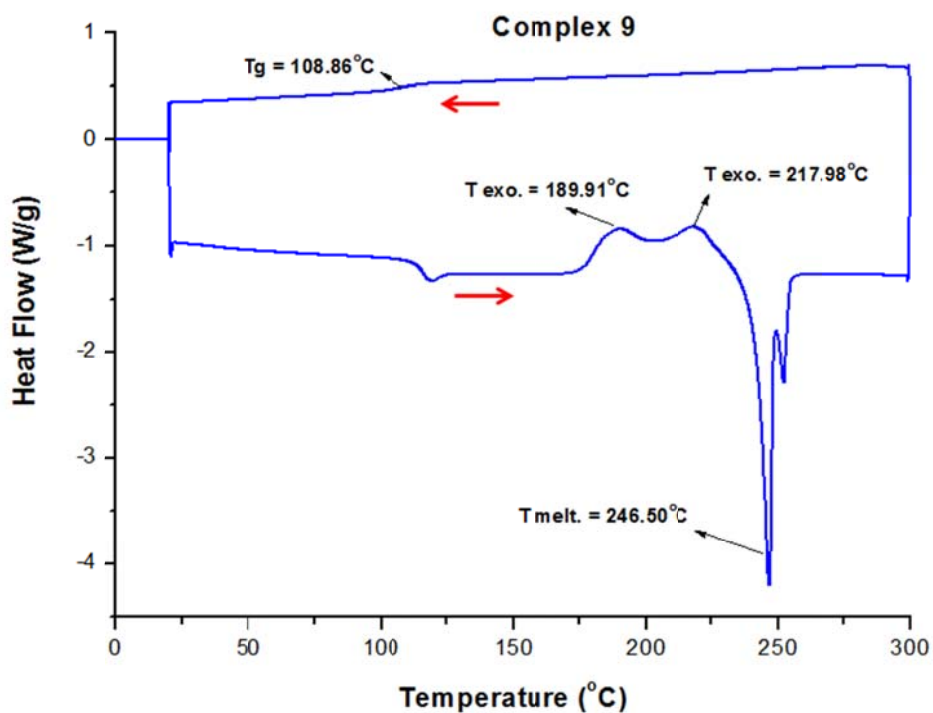
Graph 1. *DSC curve of mononuclear copper complex 9 which possess 2,2'-bipyridyl as pyridine ligand and bis-(diphenylphosphinophenyl)ether as phosphine ligand.*
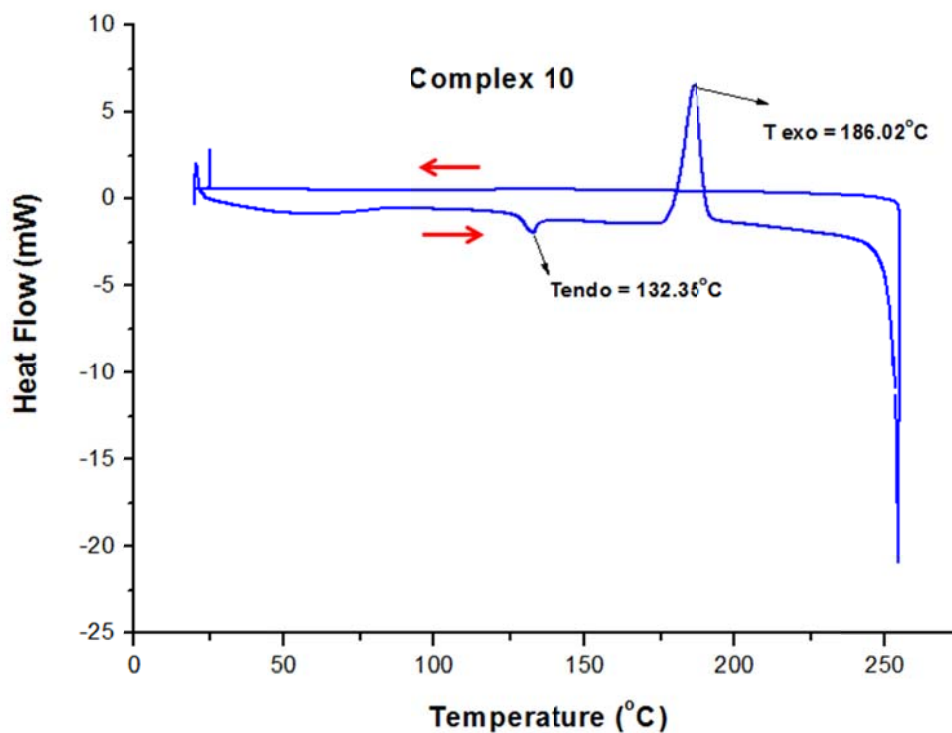
Graph 2. *DSC curve of mononuclear copper complex 10 which possess 4,4'-dimethyl-2,2'-bipyridyl as pyridine ligand and bis-(diphenylphosphinophenyl)ether as phosphine ligand.*
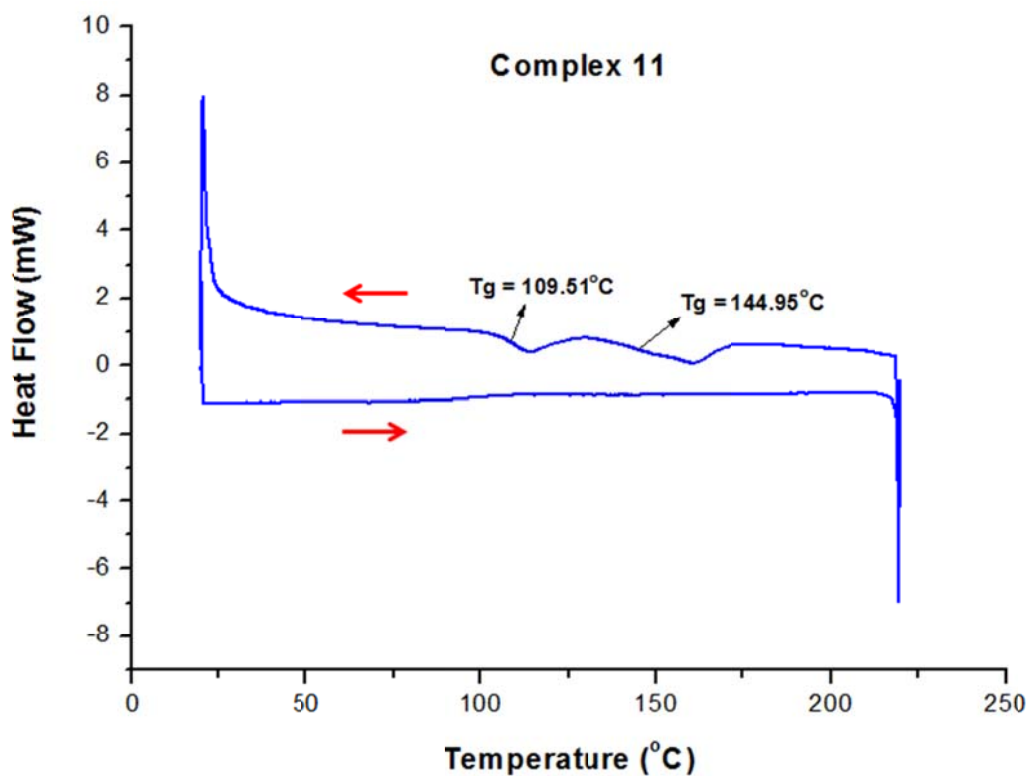
Graph 3. *DSC curve of mononuclear copper complex 11 which possess 6,6'-dimethyl-2,2'-bipyridyl as pyridine ligand and bis-(diphenylphosphinophenyl)ether as phosphine ligand.*


Graph 4. *DSC curve of mononuclear copper complex 12 which possess 2,2'-bipyridyl as pyridine ligand and triphenylphosphino as phosphine ligand.*

Graph 5. *DSC curve of mononuclear copper complex 13 which possess 4,4'-dimethyl-2,2'-bipyridyl as pyridine ligand and triphenylphosphino as phosphine ligand.*

Graph 6. *DSC curve of mononuclear copper complex 14 which possess 2,2'-bipyridyl as pyridine ligand and 9,9-dimethyl-4,5-bis(diphenylphosphino) xanthene as phosphine ligand.*

Graph 7. *DSC curve of mononuclear copper complex 15 which possess 4,4'-dimethyl-2,2'-bipyridyl as pyridine ligand and 9,9-dimethyl-4,5-bis(diphenylphosphino) xanthene as phosphine ligand.*
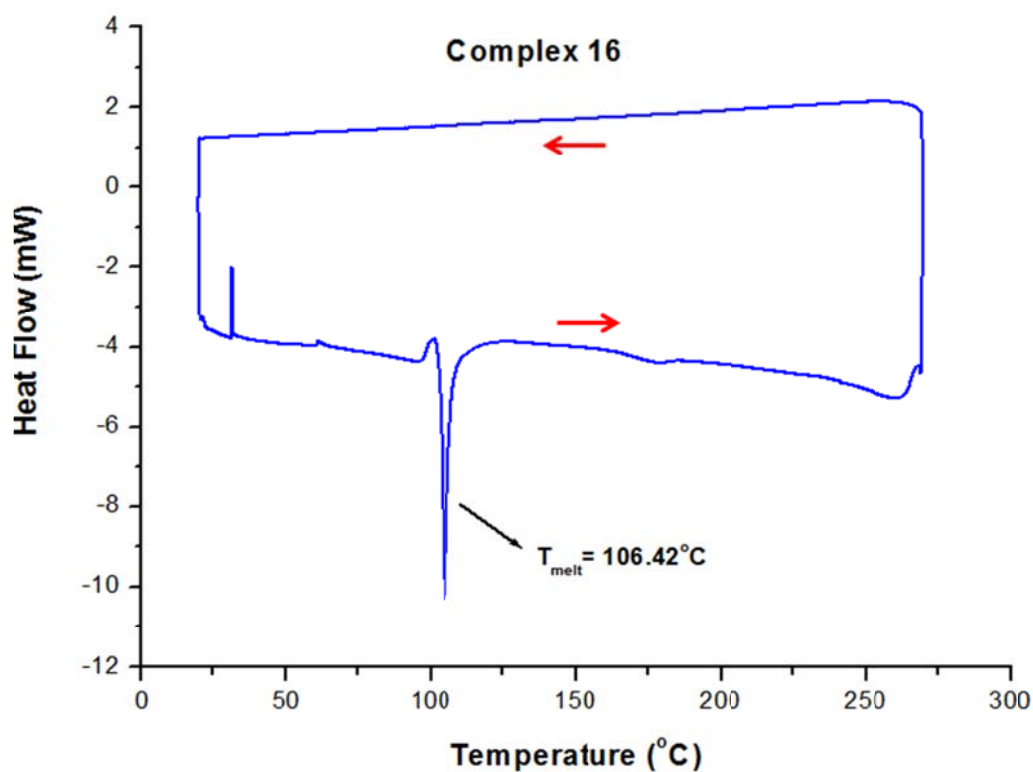
Graph 8. *DSC curves of mononuclear copper complex 16 which possess 6,6'-dimethyl-2,2'-bipyridyl as pyridine ligand and 9,9-dimethyl-4,5-bis(diphenylphosphino) xanthene as phosphine ligand.*

Appendix 5: Cyclic Voltammetry graphs of trinuclear copper (I) complexes
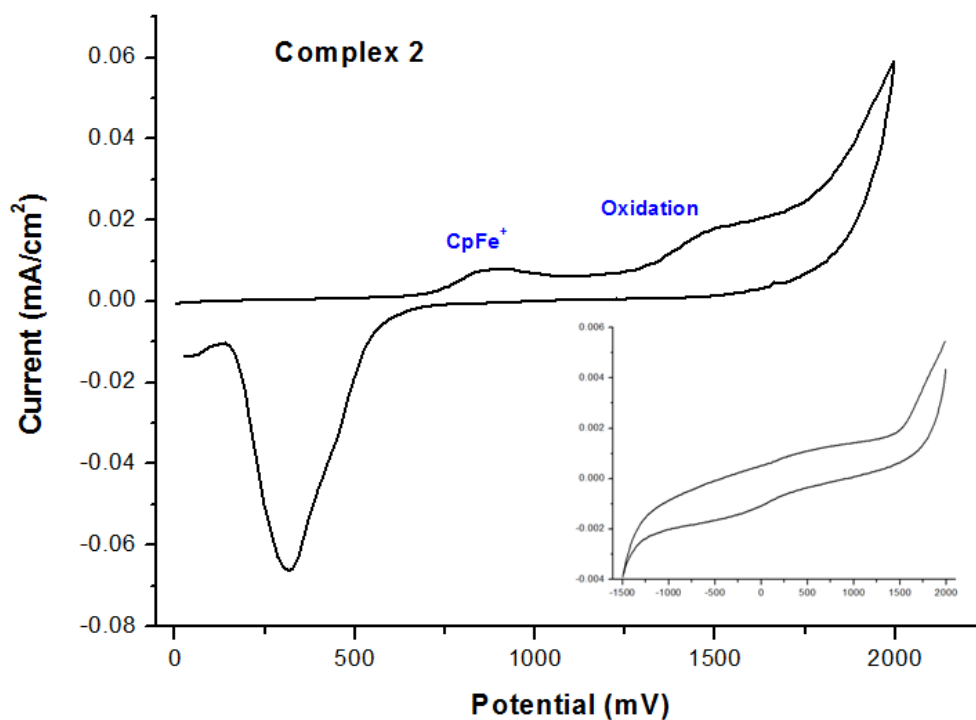
Graph 1. *Cyclic voltammetry curves of trinuclear copper complex 2 which possess 1-ethynyl-2,4-difluorobenzene as alkynyl ligand.*
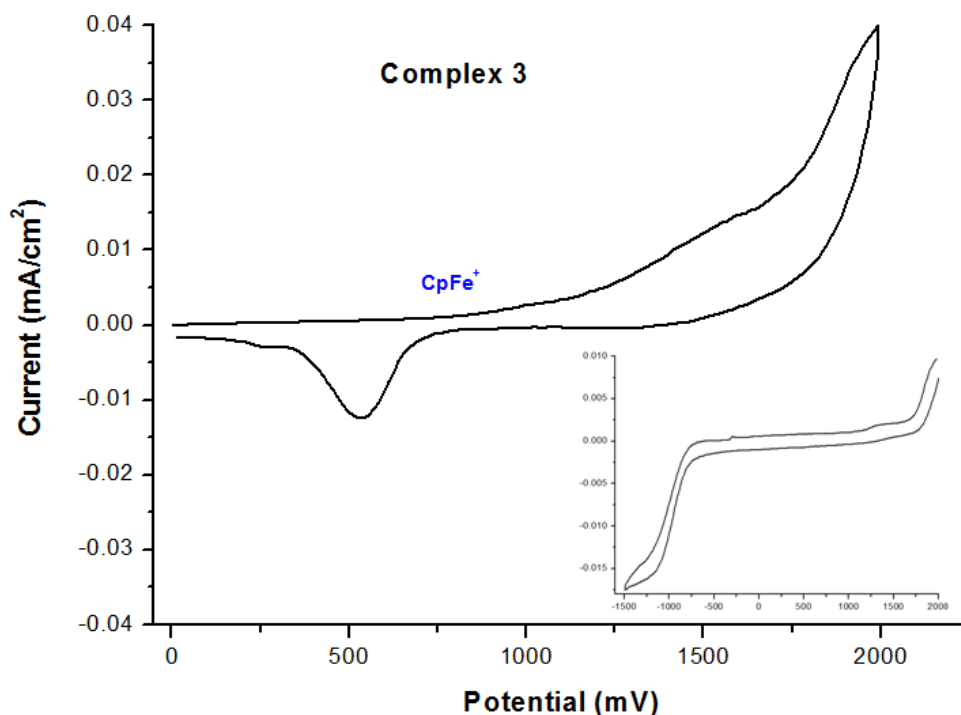
Graph 2. *Cyclic voltammetry curves of trinuclear copper complex 3 which possess 1-ethynyl-3,5-difluorobenzene as alkynyl ligand.*
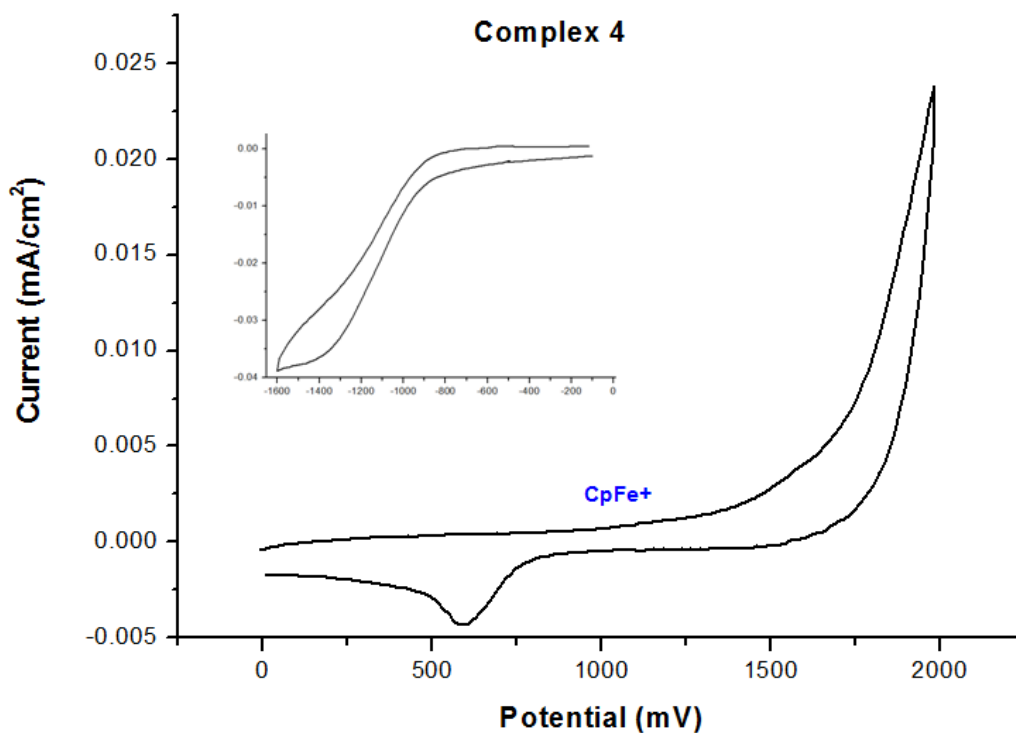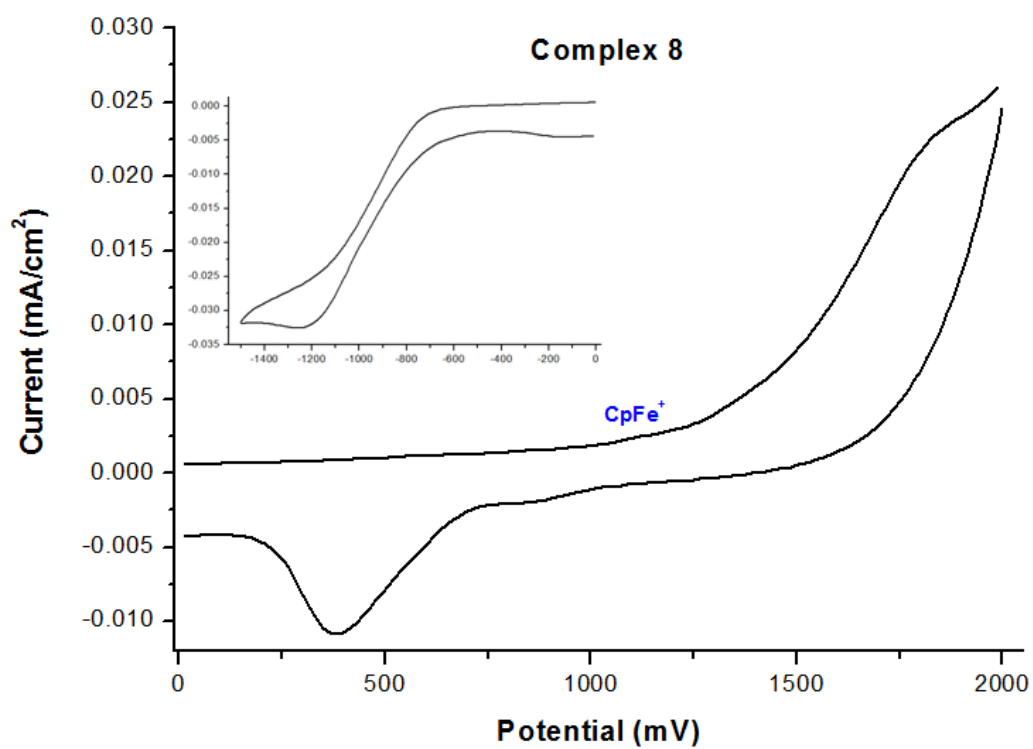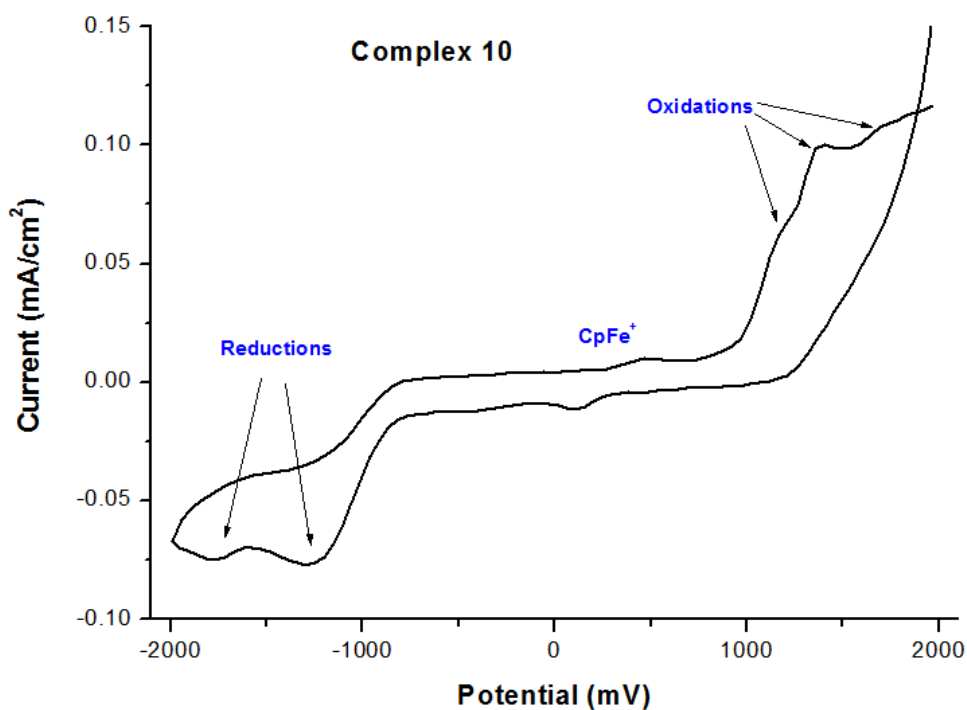
Graph 3. *Cyclic voltammetry curves of trinuclear copper complex 4 which possess 1-ethynyl-3,5-bis(trifluoromethyl)benzene as alkynyl ligand.*
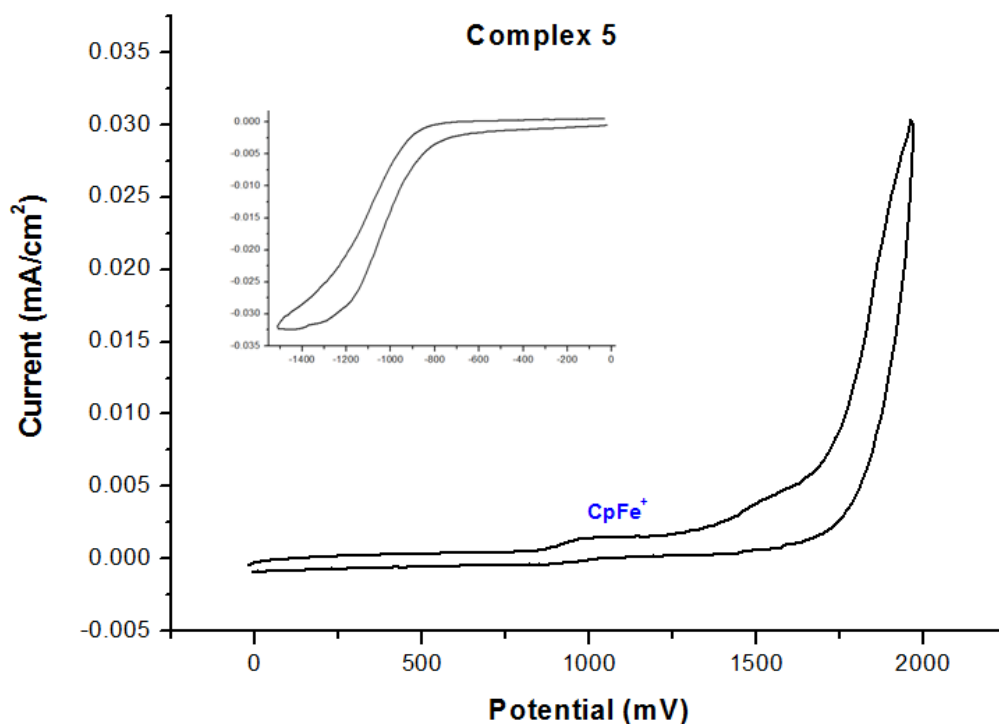
Graph 4. *Cyclic voltammetry curves of trinuclear copper complex 5 which possess 1-ethynyl-α,α,α-4-(trifluoromethyl)benzene as alkynyl ligand.*
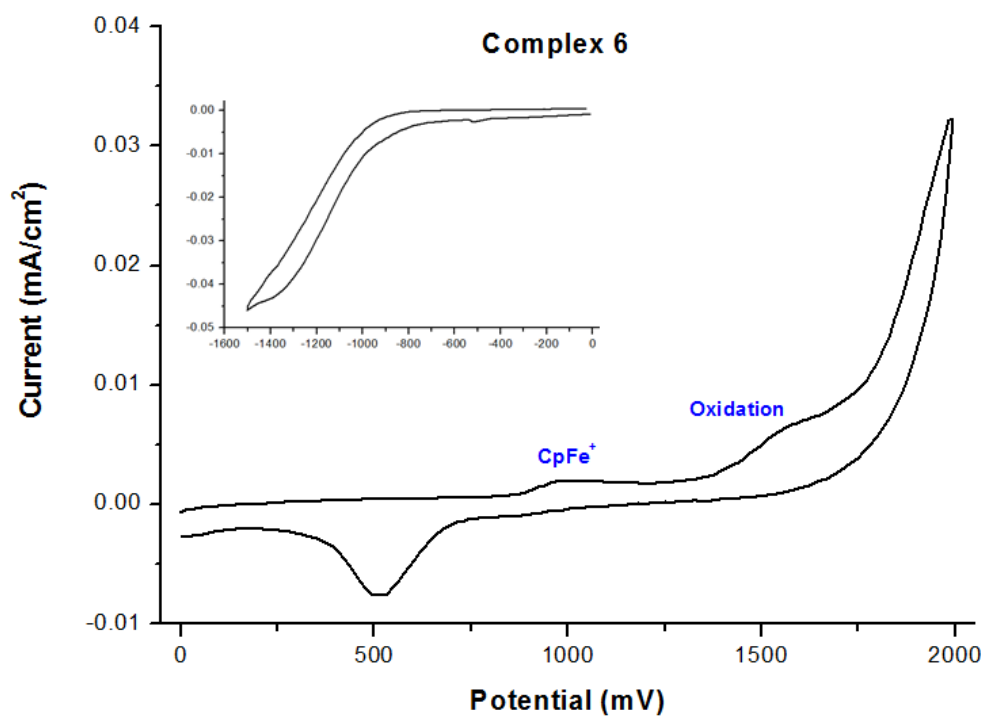
Graph 5. *Cyclic voltammetry curves of trinuclear copper complex 6 which possess 9-ethynylphenanthrene as alkynyl ligand.*
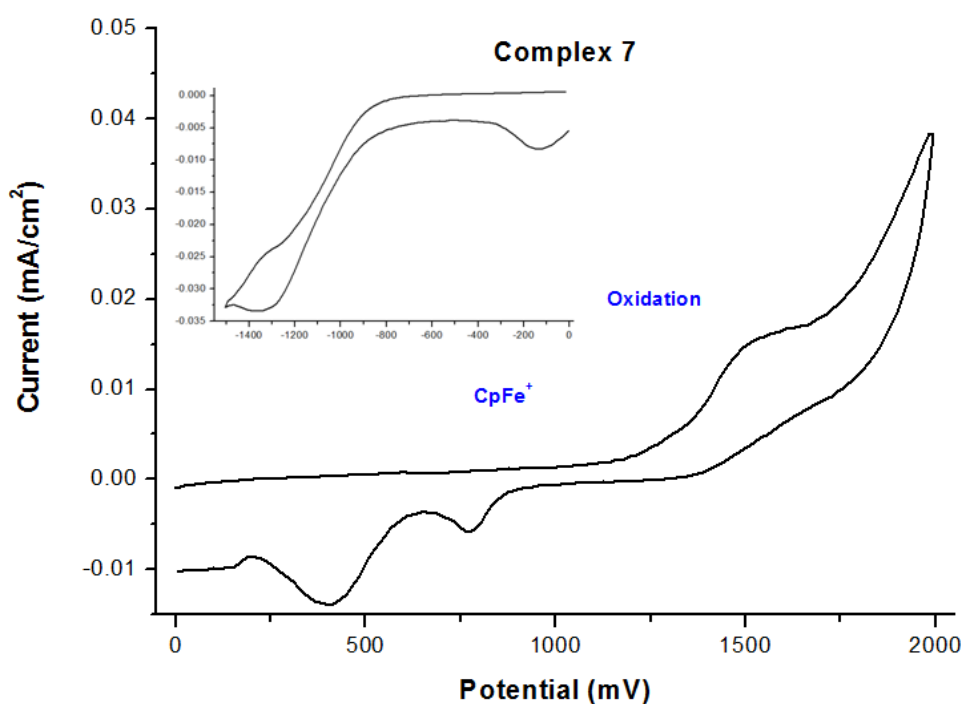
Graph 6. *Cyclic Voltammetry curves of trinuclear copper complex 7 which possess 2-ethynyl-6-metoxynaphthalene as alkynyl ligand.*

**Graph 7.** *Cyclic voltammetry curves of trinuclear copper complex 8 which possess 1-ethynylpyrene as alkynyl ligand.*

Appendix 6: Cyclic Voltammetry graphs of mononuclear copper (I) complexes
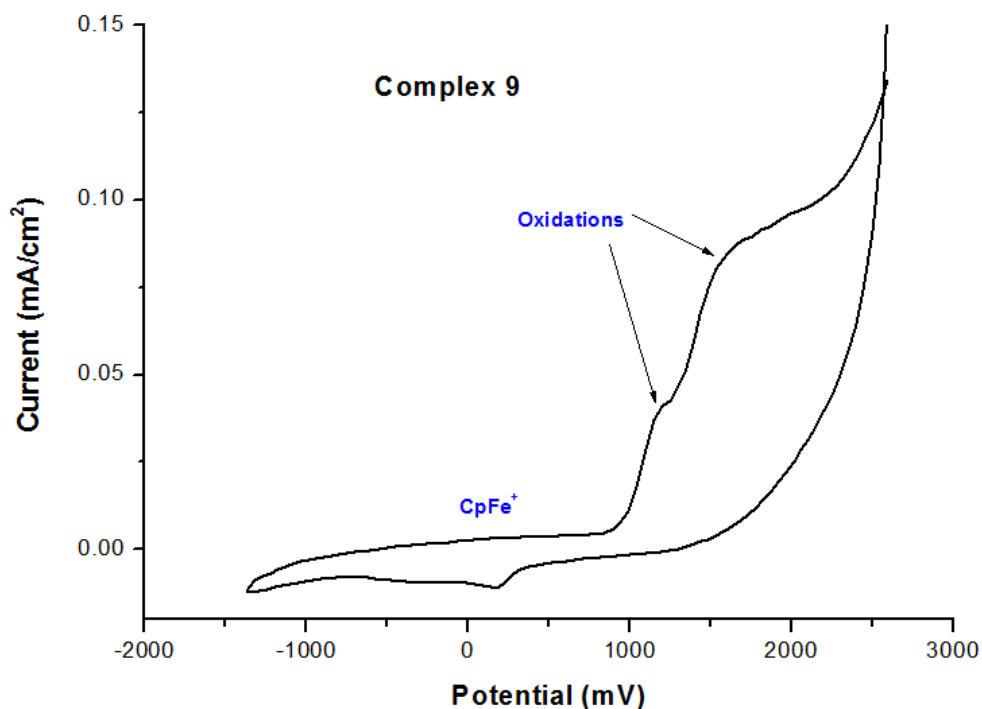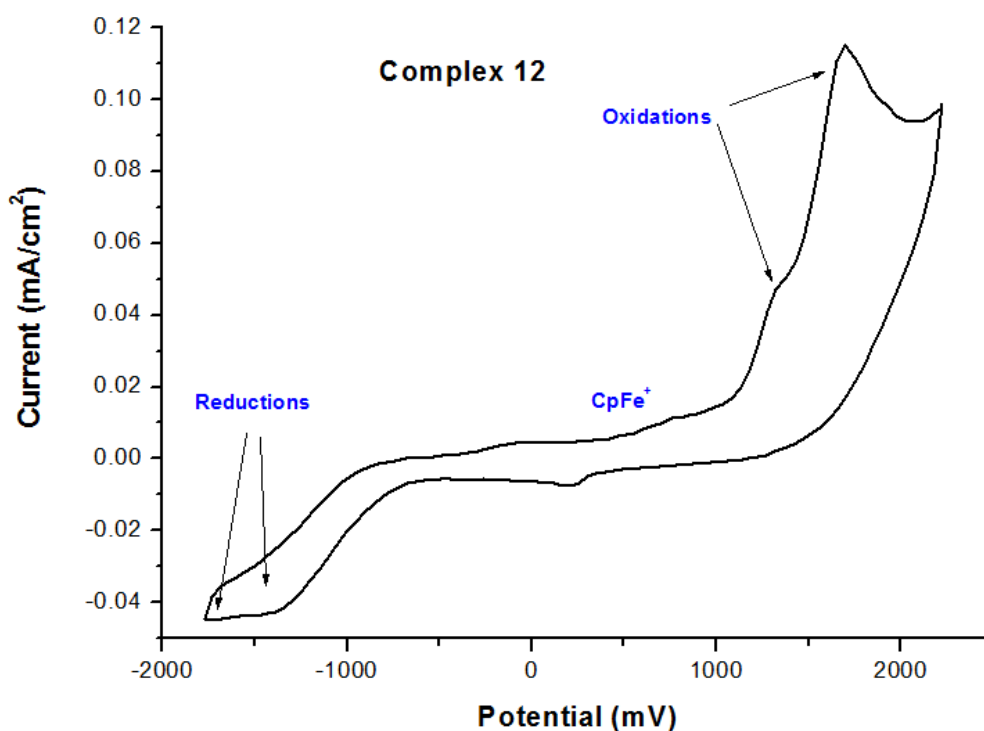
Graph 1. *Cyclic voltammetry curve of mononuclear copper complex 9 which possess 2,2'-bipyridyl as pyridine ligand and bis-(diphenylphosphinophenyl)ether as phosphine ligand.*
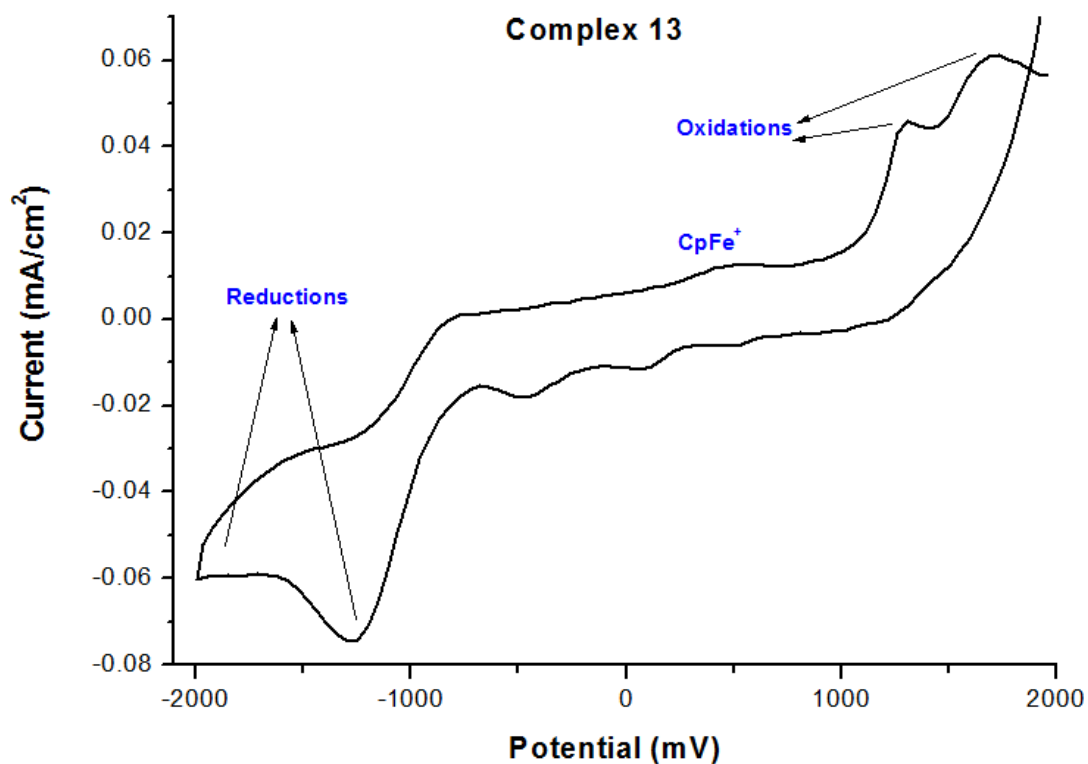

Graph 2. *Cyclic voltammetry curve of mononuclear copper complex 10 which possess 4,4'-dimethyl-2,2'-bipyridyl as pyridine ligand and bis-(diphenylphosphinophenyl)ether as phosphine ligand.*
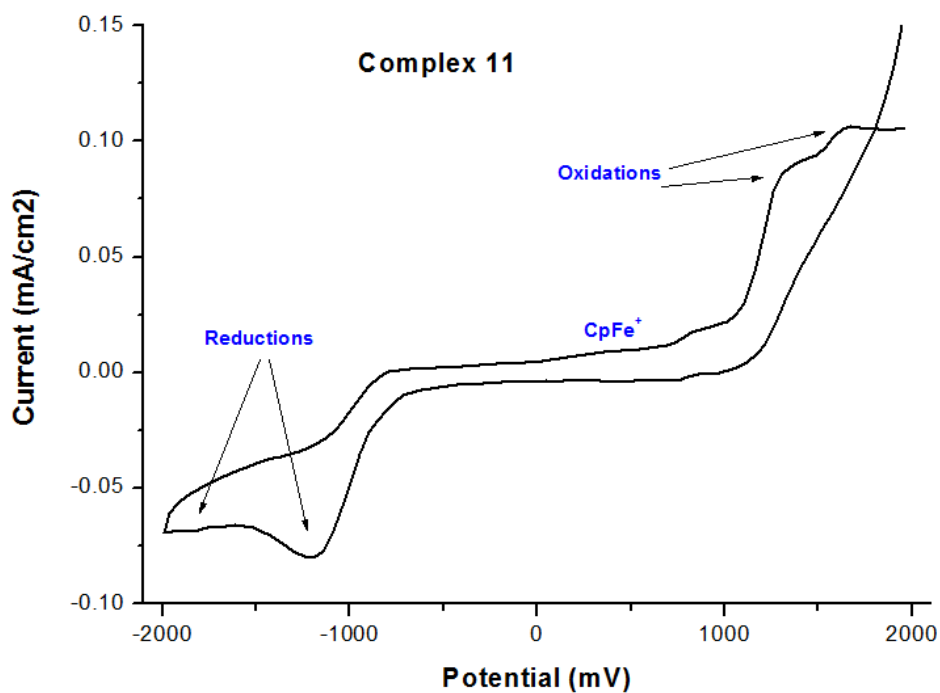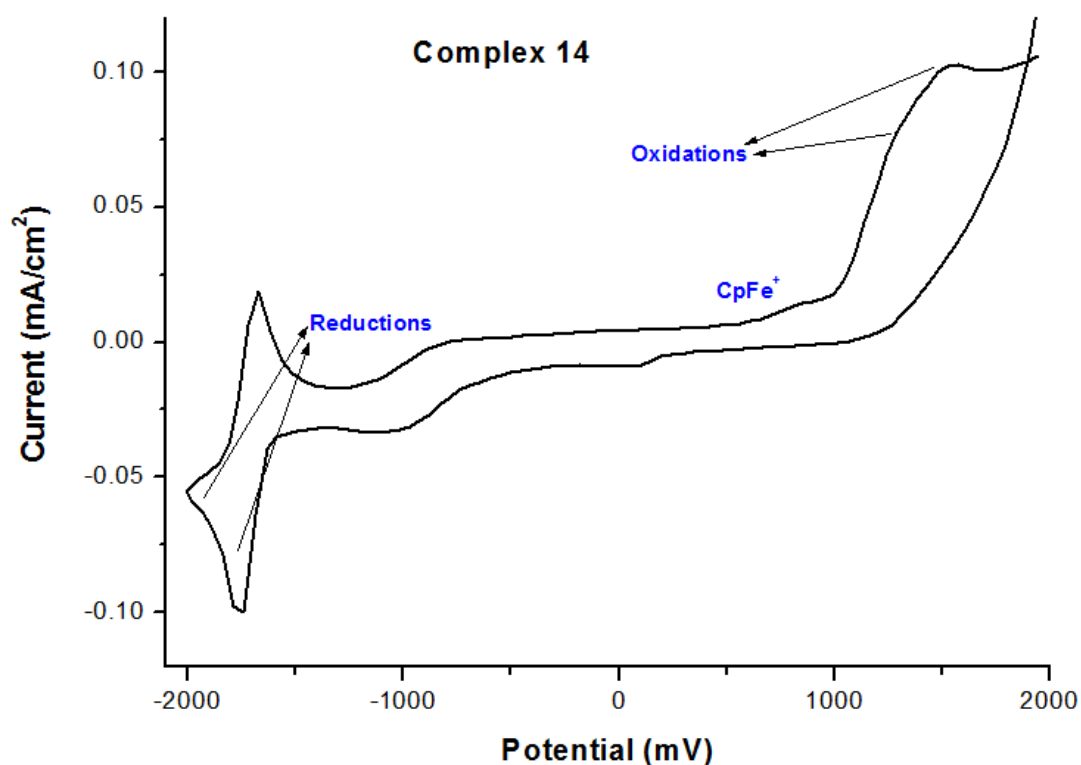
Graph 3. *Cyclic voltammetry curve of mononuclear copper complex 11 which possess 6,6'-dimethyl-2,2'-bipyridyl as pyridine ligand and bis-(diphenylphosphinophenyl)ether as phosphine ligand.*
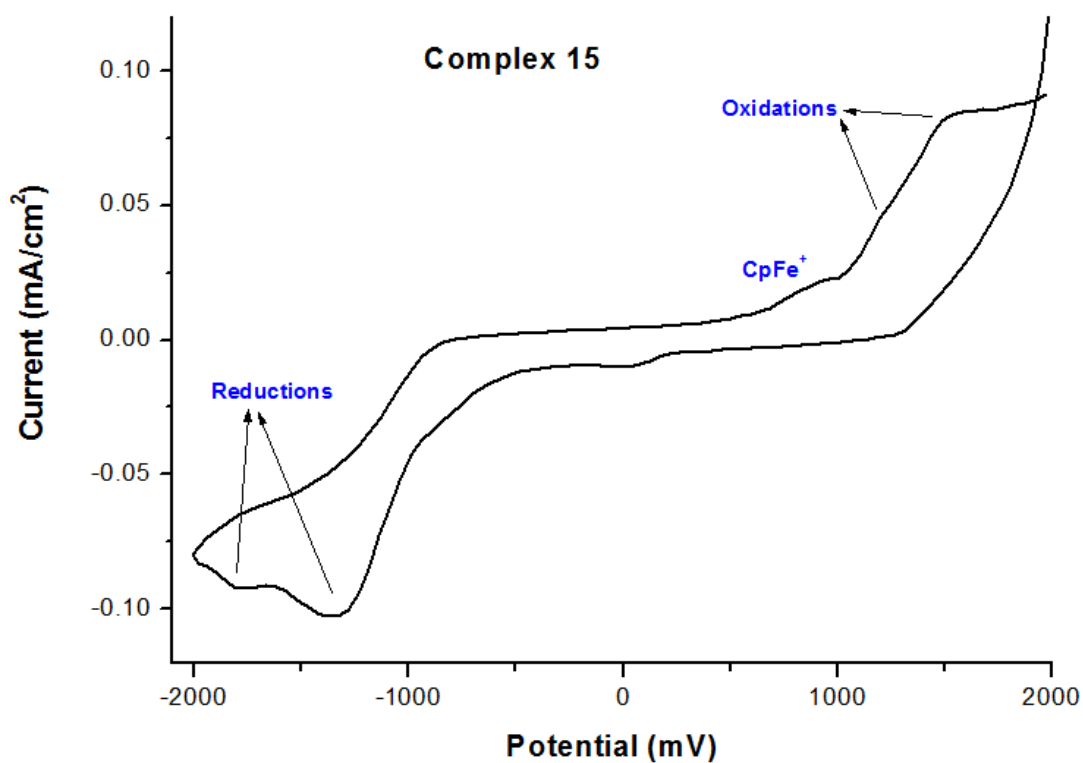

Graph 4. *Cyclic voltammetry curve of mononuclear copper complex 12 which possess 2,2'-bipyridyl as pyridine ligand and triphenylphosphino as phosphine ligand.*
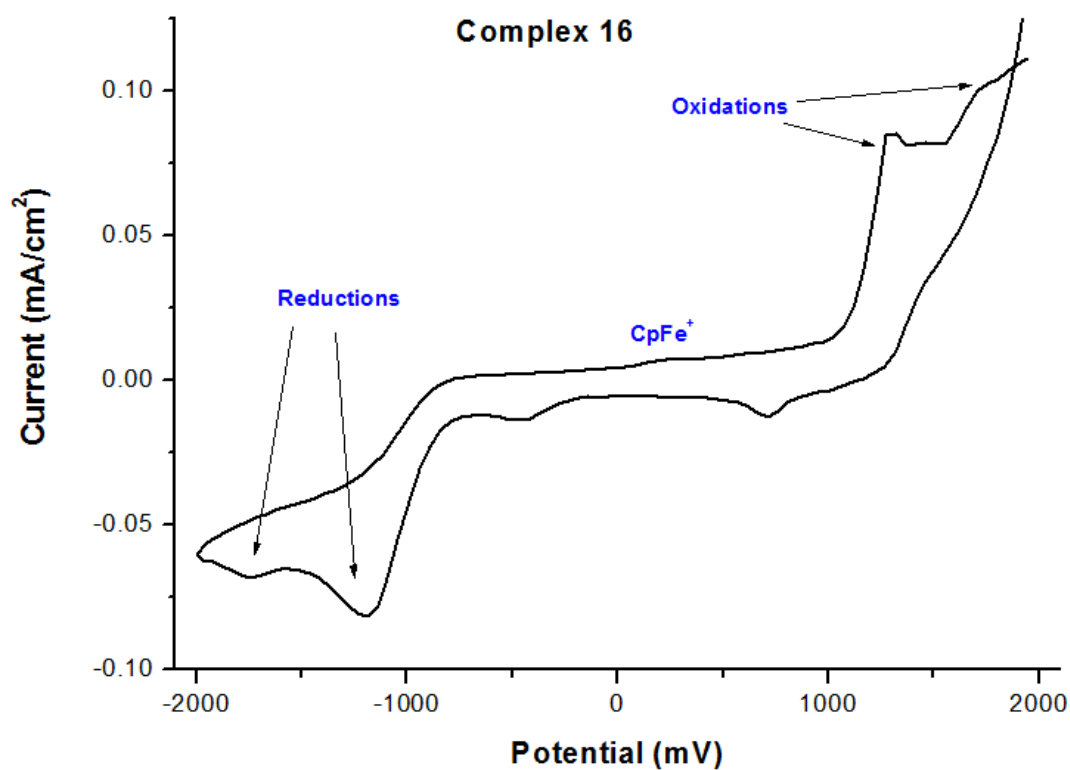
Graph 5. *Cyclic voltammetry curve of mononuclear copper complex 13 which possess 4,4'-dimethyl-2,2'-bipyridyl as pyridine ligand and triphenylphosphino as phosphine ligand.*

Graph 6. *Cyclic voltammetry curve of mononuclear copper complex 14 which possess 2,2'-bipyridyl as pyridine ligand and 9,9-dimethyl-4,5-bis(diphenylphosphino) xanthene as phosphine ligand.*

Graph 7. *Cyclic voltammetry curve of mononuclear copper complex 15 which possess 4,4'-dimethyl-2,2'-bipyridyl as pyridine ligand and 9,9-dimethyl-4,5-bis(diphenylphosphino) xanthene as phosphine ligand.*

Graph 8. *Cyclic voltammetry curve of mononuclear copper complex 16 which possess 6,6'-dimethyl-2,2'-bipyridyl as pyridine ligand and 9,9-dimethyl-4,5-bis(diphenylphosphino) xanthene as phosphine ligand.*

Appendix 7: Publications

Due to publisher copyright restrictions the publications from this thesis are excluded.